Distribution Agreement

In presenting this thesis or dissertation as a partial fulfillment of the requirements for an advanced degree from Emory University, I hereby grant to Emory University and its agents the non-exclusive license to archive, make accessible, and display my thesis or dissertation in whole or in part in all forms of media, now or hereafter known, including display on the world wide web. I understand that I may select some access restrictions as part of the online submission of this thesis or dissertation. I retain all ownership rights to the copyright of the thesis or dissertation. I also retain the right to use in future works (such as articles or books) all or part of this thesis or dissertation.

Signature:

_____ _____

Ashlyn Johnson Date

A Multi-Omic Approach to Define Molecular Changes in Human Tauopathy

By
Ashlyn Johnson
Doctor of Philosophy

Graduate Division of Biological and Biomedical Science
Neuroscience

_____
Chadwick M. Hales, M.D., Ph.D.
Advisor

_____
Ranjita Betarbet, Ph.D.
Committee Member

_____
Thomas Kukar, Ph.D.
Committee Member

_____
Steven Sloan, M.D., Ph.D.
Committee Member

_____
James Zheng, Ph.D.
Committee Member

Accepted:

_____
Kimberly Jacob Arriola, Ph.D, MPH
Dean of the James T. Laney School of Graduate Studies

_____
Date

A Multi-Omic Approach to Define Molecular Changes in Human Tauopathy

By

Ashlyn Johnson
B.S. Biological Sciences, North Carolina State University, 2017

Advisor: Chadwick M. Hales, M.D., Ph.D.

An abstract of
A dissertation submitted to the Faculty of the
James T. Laney School of Graduate Studies of Emory University
in partial fulfillment of the requirements for the degree of
Doctor of Philosophy
in Graduate Division of Biological and Biomedical Science
Neuroscience
2023

Abstract

A Multi-Omic Approach to Define Molecular Changes in Human Tauopathy

By Ashlyn Johnson

Tauopathies are a heterogeneous class of disorders united in their common pathology: the deleterious accumulation of tau protein. As a major underlying cause of dementia, tauopathies pose a global health threat and research is urgently required to identify new therapeutic solutions. With this dissertation, I aimed to define how tauopathy impacts the human brain on a molecular level. I begin by describing the biology of tau and summarizing the characteristic pathology, genetics, and clinical presentations of major tauopathies. I describe potential opportunities and challenges for targeting tau therapeutically and summarize important transcriptomic and proteomic studies of tauopathy, including prior work from our laboratory. I then use quantitative proteomics to identify the impact of tauopathy on the human grey and white matter proteome. I find that much of the grey and white matter proteome is shared, but they exhibit distinct expression profiles. Using a consensus weighted gene correlation network analysis (WGCNA), I identify unique and shared disease-associated changes in microglia and endothelia across grey and white matter. I then create a WGCNA network out of white:grey protein ratios and find a disease associated increase in mitochondrial proteins in white matter and decrease in grey matter. Next, I use a targeted transcriptomic approach to profile glial transcripts in human Alzheimer's disease (AD) and frontotemporal dementia with tau pathology (FTD-tau). I find that glial related pathway scores including astrocytes, microglia, and oligodendrocytes are increased in FTD-tau. Finally, I discuss the advantages of systems biology approaches to defining molecular changes in human neurodegeneration and conclude that the results of this dissertation collectively demonstrated the importance of characterizing grey/white matter and glial changes in tauopathy.

A Multi-Omic Approach to Define Molecular Changes in Human Tauopathy

By

Ashlyn Johnson
B.S. Biological Sciences, North Carolina State University, 2017

Advisor: Chadwick Hales, M.D., Ph.D.

A dissertation submitted to the Faculty of the
James T. Laney School of Graduate Studies of Emory University
in partial fulfillment of the requirements for the degree of
Doctor of Philosophy
in Graduate Division of Biological and Biomedical Science
Neuroscience
2023

Acknowledgements

At the risk of being cliché, Isaac Newton once said, “If I have seen further, it is by standing on the shoulders of Giants.” That is to say, no scientist works alone and I have many people to thank. Thank you to all past and present members of the Hales lab. They each made graduate school better through kindness, humor, and support. Thank you to James Webster who worked many hours side by side with me and trained me on various projects. Thank you to my committee members Drs. Betarbet, Kukar, Sloan, and Zheng, whose feedback and support throughout the years have been invaluable. Thank you to Dr. Eric Dammer who was an incredible resource and mentor in proteomic data analysis and Duc Duong for running the proteomic experiments. Thank you to Dr. Zachary McEachin for teaching me to isolate RNA and Dr. Cheyenne Hurst for assistance with getting consensus network code. I am immensely grateful for the funding to do this work and to the patients and families that chose to donate their brains for scientific research.

Thank you to my mentor, Dr. Chad Hales. Chad has been the best mentor I could have asked for. He is an awesome scientist and physician and dedicated to making a positive impact on the field of neurodegenerative disease. Perhaps most importantly, he is kind and patient and made my PhD journey a good one.

Thank you to my undergraduate mentor, Dr. John Meitzen. Without his support I wouldn’t have made it to graduate school in the first place.

I am grateful for the Emory Neuroscience Graduate Program and my cohort. They have been great friends and colleagues I’m so thankful I got to do graduate school with these brilliant scientists. I’m so proud to know all of them!

Graduate school was hard but the support and love from my friends helped me through. Friends from back home in Greensboro, from undergrad at NC State, and from here in Atlanta have all supported me with their kindness, humor, great times, and belief in me when I didn’t believe in myself. They’ve all showed up for me in so many ways and I hope I can do the same through their big milestones and challenges as well.

I am grateful for my family, including my grandparents, aunts and uncles, cousins, and my future in-laws. You’ve each been incredible forces of support but also role models for hard work, perseverance, and dedication. I wouldn’t be who I am today without you. I’d like to honor Jerry Cox and Rebecca Johnson whose experiences with neurodegenerative disease inspired my studies.

Finally, this thesis is dedicated to four people. 1) My sister and oldest friend, Lauren. She never fails to keep me humble and I know that she has always had my back. 2 and 3) My parents, Ray and Crystal. They have loved and supported me unconditionally my whole life, and they’ve taught me the value of working hard, both for myself and for others. They are incredibly kind and generous people that never made me feel like my goals were out of reach.

4) My partner, future wife, and fellow neuroscientist, Dr. Michelle Sequeira. We met when interviewing for the program. Since then, we’ve shared so many late nights and weekends working on our PhD together. She never entertained my jokes about quitting grad school because she has always believed in me. There aren’t enough words in the English language, and unfortunately, I’m not fluent in any others, to express how grateful I am that we could study neuroscience together and how grateful I am for her kindness, patience, guidance, and support in getting me to the finish line. Thank you, and I love you so, so much.

Finally, thank you to my son (dog) Marvel who literally wrote this dissertation with me, critiqued my work, and participated in existential crises. He has been both a source of joy and stress and a reason to go outside while working on my PhD.

TABLE OF CONTENTS

List of Tables and Figures

CHAPTER 1: AN OVERVIEW OF TAUOPATHY

1.1 CONTEXT, AUTHOR'S CONTRIBUTION, AND ACKNOWLEDGMENT OF RE-PRODUCTION

The following chapter reviews the characteristics of human tauopathy with an emphasis on frontotemporal dementia, the biology of tau, and existing and prospective clinical therapies that target tau. I also review known transcriptomic and proteomic changes in tauopathy which served as motivating work for the studies outlined in this dissertation. This chapter includes text and figures from Gutierrez-Quiceno L, Dammer EB, Johnson AG, et al. (2021) A proteomic network approach resolves state-specific molecular phenotypes in chronic traumatic encephalopathy. *Mol. Neurodegener.* The dissertation author specifically contributed to the western blots, densitometric analysis, immunostaining, and careful review and editing of the manuscript.

1.2 ABSTRACT

Tauopathies are a class of disorders characterized by abnormal accumulation of tau protein. Here, we first review the biology of tau protein. We then summarize the defining pathology, clinical symptoms, and current therapies of major tauopathies including Alzheimer's disease, frontotemporal dementia, progressive supranuclear palsy, corticobasal degeneration, and chronic traumatic encephalopathy. We then highlight prospective therapies that target tau biology. Finally, we discuss previous literature regarding transcriptomic and proteomic changes in human tauopathy and highlight known proteomic and transcriptomic differences in grey and white matter.

1.3 PHYSIOLOGY AND PATHOPHYSIOLOGY OF TAU

In 1975, Murray Weingarten and Marc Kischner discovered a protein that was necessary for the assembly of 6S tubulin into 36S rings and microtubules, which they named tau (Weingarten et al., 1975). Ten years later, tau was identified as the main component of neurofibrillary tangles in Alzheimer's disease (AD) (Brion et al., 1985; Grundke-Iqbal et al., 1986; Kosik et al., 1986;

Wood et al., 1986). In the decades since, research has centered on both the basic biology of tau and its role in neurodegenerative processes.

The gene for human tau, microtubule associated protein tau (*MAPT*), is located on chromosome 17q21 (Neve et al., 1986). There are four main regions of the tau protein: the amino-terminal region, the proline-rich region, the microtubule binding domain, and the carboxy-terminal region (Brandt et al., 2020). The 6 isoforms differ by the presence of zero, one, or two amino-terminal inserts and three or four repeats in the microtubule binding domain (Goedert et al., 1989). Functionally, the amino-terminal region protrudes from the surface of the microtubule, interacting with other proteins such as Annexin A2 and A6 and components of the plasma membrane (Hirokawa et al., 1988; Brandt et al., 1995; Gauthier-Kemper et al., 2018; Hernández et al., 2020). The proline-rich domain is important for the association of tau with actin and is the most abundantly phosphorylated region of tau (He et al., 2009; Wegmann et al., 2021). The microtubule binding domain consisting of three or four 31-residue repeats, binds to microtubules, and is the site of most pathogenic missense *MAPT* mutations (Kadavath et al., 2015; Strang et al., 2019). The carboxy-terminal region inhibits tau polymer formation (Abraha et al., 2000).

The tau transcript is comprised of 16 exons which yield six major protein isoforms of tau through alternative splicing of exon 10. Absence of exon 10 results in tau isoforms with three microtubule binding domain repeats (3R tau) while the presence of exon 10 results in isoforms with four repeats (4R tau). In development, 3R tau is most prominent. In the healthy adult brain, 3R and 4R tau are expressed at an approximately equal ratio which can be altered in neurodegenerative tauopathy (Boyarko and Hook, 2021). Expression of tau is most abundant in neurons, specifically axons, but is also expressed at lower levels in astrocytes and oligodendrocytes (Binder et al., 1985; Forrest et al., 2023).

Tau is an intrinsically disordered protein (Jeganathan et al., 2008) yet aggregates into paired helical filaments and neurofibrillary tangles in neurodegenerative disease states (Kidd, 1963; Wang and Mandelkow, 2016). One major factor that influences tau's propensity to aggregate is the presence of post-translational modifications (Alquezar et al., 2020). Modifications such as phosphorylation, acetylation, and nitration all weaken the interaction of tau with microtubules by making tau increasingly negatively charged, thus creating a pool of tau that is now more likely to self-assemble due to its modifications (Alquezar et al., 2020). Further, these post-translational modifications can either promote or inhibit tau aggregation depending on the site and type of modification (Wegmann et al., 2021).

How tau misfolds and propagates its altered conformation to other tau within the same cell and across other cells in a prion-like manner is an active area of study (Frost et al., 2009). Several mechanisms of tau release/secretion and uptake have been demonstrated (Brunello et al., 2020). Tau may be released from cells through a variety of pathways including via ectosomes, exosomes, and directly through the plasma membrane (Brunello et al., 2020; Merezhko et al., 2020). Methods of tau uptake or internalization include clathrin-mediated endocytosis, macropinocytosis, and membrane fusion (Zhao et al., 2021). Additionally, tunneling nanotubes provide a direct channel of transport of tau from one cell to another (Zhang et al., 2021). Inhibiting tau uptake or clearing extracellular tau could serve as a therapeutic strategy to mitigate propagation of tau aggregation.

1.4 SUBCLASSIFICATION OF HUMAN TAUOPATHIES

Tauopathies are a heterogeneous class of disorders united in their common pathology: the deleterious accumulation of tau protein. The regional, cellular, and subcellular distributions of pathological tau accumulations and the resulting clinical symptoms thereof are variable. In 2019, the global cost of dementia (direct medical costs, direct social sector costs, informal care costs)

was estimated to be $1313.4 billion (Wimo et al., 2023). As a major underlying cause of dementia, tauopathies pose a global health threat and research is urgently required to identify new therapeutic solutions. Here, I will review examples of tauopathy, outlining their historical context, defining pathology, genetic links, clinical presentation, and existing therapies.

1.4.1 Alzheimer's Disease

In 1907, Alois Alzheimer and Oskar Fischer used Bielschowsky silver staining to describe neuritic plaques (Fischer Priv.-Doz. Dr., 1907) and the co-occurrence of these plaques with neurofibrillary tangles (Alzheimer, 1907) in human brain from patients with presenile (Alzheimer) and senile (Fischer) dementia (Goedert, 2009). These pathological observations are now known as the defining pathology of AD: extracellular plaques comprised of amyloid beta (Aβ) and intracellular neurofibrillary tangles comprised of hyperphosphorylated tau.

AD is the most common cause of dementia, affecting an estimated 6.7 Americans over the age of 65 as of 2023 (Rajan et al., 2021; Alzheimer's Association, 2023). The prevalence of AD is higher in women than men and in non-Hispanic Black and Hispanic older adults than their White counterparts (Alzheimer's Association, 2023).The majority of AD cases are late-onset (after the age of 65) and sporadic, arising from an interaction between genetic risk factors and environmental exposure. Only 5-10% of AD cases are early onset (before the age of 65) and only 10% of early onset AD cases can be attributed to autosomal dominant mutations in genes such as amyloid precursor protein (APP), presenilin 1 (PSEN1) and presenilin 2 (PSEN2) (Wingo et al., 2012; Barber et al., 2017; Reitz et al., 2020). Other genetic variants are associated with AD risk, though not explicitly causal. For example, the strongest genetic risk factor for late onset AD is the ε4 allele of apolipoprotein E (APOE) (Strittmatter et al., 1993; Wightman et al., 2021). To date, genome wide association studies (GWAS) have identified 101 independent AD-associated variants across 81

genome-wide significant loci (Andrews et al., 2023).

The amyloid cascade hypothesis has been a major focus in defining AD pathophysiology and therapeutic strategies. Supported by discoveries that genetic mutations in APP, PSEN1 and PSEN2 lead to overproduction and oligomerization of toxic Aβ42 and deposition of diffuse plaques, the amyloid hypothesis posits that the deposition of Aβ is a main contributor to AD and that deposition of tau, neurodegeneration, and the other pathological characteristics of AD are downstream consequences of this abnormal accumulation (Hardy and Higgins, 1992; Hardy, 2006). This deposition of amyloid initiates neuroinflammation and synaptic damage which ultimately leads to a change in kinase and phosphatase activity which triggers tau pathology. These processes then culminate in neuron dysfunction and death (Tcw and Goate, 2017). Recently, a large-scale imaging study identified amyloid in 24% of the cognitively normal elderly group that was sampled (Jansen et al., 2022), calling into question what factors outside of amyloid deposition may trigger the transition from normal cognition to cognitive impairment in subjects with amyloid pathology. Additional investigation of the asymptomatic phase of AD will shed light on other processes that may contribute to the clinical phenotype of AD.

The most common form of AD, late-onset, typically presents as an amnestic disorder in which a progressive decline in episodic memory is the key clinical feature. There are also impairments in executive function, language, and visuospatial function along with neuropsychiatric symptoms (Rabinovici, 2019). Early-onset amnestic AD is characterized by a diagnosis before age 65 and a more aggressive course of disease compared to its late-onset counterpart. Other atypical variants include visuospatial variant (posterior cortical atrophy), language variant (logopenic variant primary progressive aphasia), and behavioral/dysexecutive variants (Polsinelli and Apostolova, 2022). Notably, the clinical presentations of these atypical variants of AD overlap

with the clinical presentations of frontotemporal dementia (discussed below), thus biomarker testing and careful consideration of differential diagnoses is important for delineating between the two (Chaudhry et al., 2020; Giebel et al., 2021).

Clinically, AD progression can be conceptualized as a continuum beginning with preclinical AD in which there are no symptoms but biological changes in the brain (Jack et al., 2013). Next, patients enter a period of mild cognitive impairment (MCI) in which they experience mild symptoms with little interference in daily life. Then, patients experience a progression of dementia from mild to moderate to severe in which symptoms progressively interfere with participating in daily activities (Aisen et al., 2017; Alzheimer's Association, 2023). AD progression can also be characterized neuropathologically. There are several neuropathological staging schemes for AD including Braak staging, Consortium to Establish a Registry for Alzheimer's Disease (CERAD) scoring, and Thal phases which characterize the progression and burden of tau (Braak) and amyloid (CERAD and Thal) pathology. These schemes also provide conceptual framework for understanding the progression of AD.

Braak and Braak established six neuropathological hierarchical stages as part of the diagnostic criteria for AD (Braak and Braak, 1991; Braak et al., 2006; Hyman et al., 2012; Montine et al., 2012; Macedo et al., 2023). Importantly, Braak stages characterize the progression of neurofibrillary tau pathology in AD. Neurofibrillary tangles develop in the transentorhinal region (stage I) and then extend into the entorhinal region (stage II), neocortex of the fusiform and lingual gyri (stage III), and neocortical association areas (stage IV). Neocortical pathology then extends in the direction of the frontal, superolateral, and occipital cortices, reaching the peristriate region (stage V). Finally, pathology reaches the secondary and primary neocortical areas and the striate region (stage VI). With each increase in Braak stage number, the density and severity of lesions present

in prior stages become more severe (Braak and Braak, 1991; Braak et al., 2006; Hyman et al., 2012; Montine et al., 2012; Macedo et al., 2023).

CERAD scores quantify neuritic plaque density in the cortex. Scores range from 0 to 3 where 0 represents an absence of neuritic plaques and 3 represents more than 20 neuritic plaques per square millimeter (Mirra et al., 1991; Doher et al., 2023). Thal phase scoring, similar to Braak staging, evaluates the distribution of amyloid plaques. Beginning with an absence of amyloid plaques (0), then deposition in the neocortex (1), allocortex (2), subcortical regions including striatum (3), brainstem (4) and then finally cerebellum (5) (Thal et al., 2002; Doher et al., 2023). Neuropathologists will use Braak, CERAD, and Thal scores together to evaluate the probability that AD pathology is responsible for the clinical symptoms (Hyman et al., 2012; Montine et al., 2012).

Though there is no cure for AD, there are several therapeutic options. The two main classes of drugs used to reduce AD symptoms include cholinesterase inhibitors and N-methyl D-aspartate (NMDA) receptor antagonists. Early loss of cholinergic neurons in the basal forebrain leading to dysfunction in cholinergic neurotransmission is a classic feature of AD (Chen et al., 2022). Cholinesterase inhibitors prevent the breakdown of acetylcholine to address the deficit in cholinergic neurotransmission (Marucci et al., 2021). Neuronal excitotoxicity is a component of AD pathogenesis, thus NMDA receptor antagonists are used to prevent glutamate binding (Witt et al., 2004) although the putative mechanism for this class remains unknown. Recently, two disease-modifying therapies for AD were approved by the United States Food and Drug Administration (FDA): aducanumab (Budd Haeberlein et al., 2022) and lecanemab (van Dyck et al., 2023). Both are monoclonal antibodies that target Aβ and were shown to affect the rate of cognitive decline, but there is concern over the tradeoff between the relatively intense course of treatment, potential for side

effects and cost with the relatively small effect on the rate of cognitive decline (Cummings et al., 2022; Reardon, 2023). In July 2023, a third amyloid monoclonal, donanemab, was submitted for FDA approval due to strong phase three clinical trial results in which AD progression was slowed by up to 60% in patients with MCI (Sims et al., 2023).

1.4.2 Frontotemporal Dementia

The first description of the disorder now known as frontotemporal dementia (FTD) was provided by Arnold Pick in 1892 in which he described a patient with a progressive decline in language abilities (Pick, 1892). Alois Alzheimer used silver staining to identify neuronal cytoplasmic inclusions which were later deemed Pick bodies (Alzheimer, 1911; Olney et al., 2017). Today, FTD is a clinical diagnosis for the symptoms that arise from frontotemporal lobar degeneration (FTLD) which is associated with a variety of protein pathologies. FTD is the second most common cause of dementia in persons under the age of 65 after AD and affects over 50,000 people in the United States alone (Knopman and Roberts, 2011).

There are three primary clinical variants of FTD: behavioral variant (bvFTD), semantic variant primary progressive apahasia (svPPA), and nonfluent/agrammatic primary progressive aphasia (nfvPPA) (Olney et al., 2017). Diagnostic criteria for bvFTD includes a progressive decline in behavior or cognition and at least three of the following: behavioral disinhibition, apathy, loss of sympathy or empathy, stereotyped or ritualistic behaviors, dietary changes, and deficits in executive function but not episodic memory or visuospatial skills (Rascovsky et al., 2011). Diagnostic criteria for svPPA include impairments in confrontation naming and single-word comprehension and at least three of the following: decreased object knowledge, dyslexia or dysgraphia, retention of repetition, and retention of speech production. Finally, diagnostic criteria for nfvPPA include agrammatism and/or speech apraxia and at least two of the following: difficulty

understanding complex sentences, spared understanding of single words and spared object knowledge (Gorno-Tempini et al., 2011). The behavioral variant is the most common clinical presentation, accounting for around half of the cases (Woollacott and Rohrer, 2016).

The neuropathology FTLD is heterogeneous. Abnormal deposition of tau and TAR DNA-binding protein (TDP-43) are the two major neuropathologies of FTLD, each individually contributing to 45% of cases. An additional 5% of cases exhibit fused in sarcoma (FUS) pathology, while the remaining 5% demonstrate accumulation of other proteins such as ubiquitin and p62 (Younes and Miller, 2020). Atrophy of the frontal and anterior temporal lobes are gross pathological hallmarks of FTLD and protein deposits can be localized to the cytoplasm and/or nucleus of neurons and/or glia (Cairns et al., 2007; Snowden et al., 2007).

There is a significant genetic component to FTD, with nearly 30% of patients demonstrating a family history of disease (Rohrer et al., 2009; Wood et al., 2013; Greaves and Rohrer, 2019). Autosomal dominant mutations in microtubule-associated protein tau (*MAPT*), progranulin (*GRN*), and chromosome 9 open reading frame 72 (*C9orf72*) are the most common causes of genetic FTD. *MAPT* mutations lead to tau pathology while mutations in *GRN* and *C9orf72* lead to TDP-43 pathology. There are less common autosomal dominant mutations in genes such as *VCP*, *CHMP2B*, *TARDBP*, and *FUS*, as well as other genetic risk factors that also lead to FTD (Sirkis et al., 2019; Sawyer et al., 2022).

For the purposes of this dissertation, there is a focus on frontotemporal dementia with tau pathology (noted as FTD-tau or FTD-MAPT) in chapters 2 and 3. Progressive supranuclear palsy (PSP) and corticobasal degeneration (CBD) are sometimes considered part of the FTLD tau spectrum, but in this dissertation will be considered as separate tauopathies and discussed in sections below. Pick's disease is a sporadic form of FTD-tau in which spherical inclusions of 3R tau form

within neurons along with ramified astrocytes and oligodendroglial coiled inclusions. Most patients with Pick's disease present clinically with bvFTD (Irwin et al., 2016). Frontotemporal dementia with parkinsonism linked to chromosome 17 (FTDP-17) is caused by mutations in *MAPT*. 3R tau, 4R tau, or a combination thereof accumulates in neuron and glia, resulting in deficits in behavior, language, memory, and movement (Ghetti et al., 2015). *MAPT* mutations were first implicated in FTDP-17 in 1998 (Hutton et al., 1998; Poorkaj et al., 1998; Spillantini et al., 1998). Today, over 50 *MAPT* mutations have been identified (Strang et al., 2019).

There are no disease modifying therapies for FTD and current treatment strategies focus on managing symptoms. Anti-depressants and anti-psychotics can be helpful in managing the behavioral symptoms of FTD. Physical and occupational therapies are also recommended to prevent falls and aid daily activities while speech therapy is also recommended for FTD patients experiencing aphasia (Tsai and Boxer, 2014).

1.4.3 Progressive Supranuclear Palsy

PSP was first described in 1964 by John Steele, Clifford Richardson, and Jerzy Olszewski where patients presented with downward gaze, postural instability, motor abnormalities, and dementia. Post-mortem examination of their brains revealed neural loss and gliosis in many subcortical and brainstem regions and neurofibrillary tangles with an absence of senile plaques (Steele et al., 1964). PSP is characterized by deposits of hyperphosphorylated straight and tubular tau filaments comprised of 4R tau in neurons and glia, including tufted astrocytes and oligodendroglial coiled bodies. These depositions primarily impact the brainstem, subthalamic nucleus, and basal ganglia (Kovacs et al., 2020). However, the regional deposition of tau varies and is reflective of the varied clinical phenotypes of PSP. For example, behavioral and speech abnormalities are associated with more cortical tau pathology while motor symptoms are associated with less cortical

tau pathology (Robinson et al., 2020).

Most PSP cases are sporadic with no family history of the disease. In rare instances, PSP can be associated with mutations in *MAPT.* GWAS studies have identified several variants that increase risk for PSP including the H1 and H1c haplotype of *MAPT* and single nucleotide polymorphisms (SNPs) in several genes including myelin-associated oligodendrocyte basic protein (*MOBP*) and CXC motif chemokine receptor 4 (*CXCR4*) (Pittman, 2005; Yokoyama et al., 2017). Current treatments of PSP only manage symptoms and do not modify the disease. Pharmacologic therapies targeting motor symptoms and mood are common (Coughlin and Litvan, 2020).

1.4.4 Corticobasal Degeneration

First deemed corticodentatonigral degeneration, the disorder now known as CBD was first described in 1967 by Jean Rebeiz, Edwin Kolodny, and Edward Richardson (Rebeiz et al., 1967). In this initial publication, the authors described three patients with muscular and motor abnormalities including apraxia but relatively intact cognition. Upon death, pathological examination revealed atrophy in the frontal and parietal regions, enlarged ventricles, neuronal loss (especially in the substantia nigra), astrogliosis, and swollen neuronal cell bodies (Rebeiz et al., 1967). Over twenty years later, three patients presented with clinical symptoms similar to PSP and pathology similar to Pick's disease. Pathological findings included frontoparietal atrophy, neuronal loss and gliosis in the cortex, basal ganglia, and other brain stem regions, and inclusions in the substantia nigra similar to those in PSP and Pick's disease. Given the distribution of neuronal loss and inclusions in the cortex and the basal ganglia, the name of the disorder was simplified to corticobasal degeneration (Gibb et al., 1989).

Like PSP, CBD is a 4R tauopathy. Staining reveals diffuse granular cytoplasmic tau as well as spherical cytoplasmic bodies within neurons (ballooned neurons), oligodendroglial coiled

bodies, and astrocytic plaques (Saranza et al., 2019). The astrocytic plaques are characteristic of CBD and distinguish it from PSP (Dickson et al., 2002; Kovacs, 2015). Like PSP, most cases of CBD are sporadic. Some mutations in *MAPT* have been associated with CBD including N296N (Spillantini et al., 2000), G389R (Rossi et al., 2008), p.N410H (Kouri et al., 2014), and P301S (Bugiani et al., 1999). CBD and PSP share some common genetic risk factors including H1 haplotypes and SNPs around *MOBP* and *CXCR4* (Houlden et al., 2001; Yokoyama et al., 2017). While there are no disease-modifying treatments for CBD, current treatments target symptoms such as levodopa for Parkinsonism, botulinum toxin for dystonia, and clonazepam for myoclonus (Kompoliti et al., 1998; Cordivari et al., 2001; Constantinides et al., 2019).

1.4.5 Chronic Traumatic Encephalopathy

Our understanding of chronic traumatic encephalopathy (CTE) has evolved substantially over the last century (Lindsley, 2017). In 1928, Harrison Martland theorized that up to fifty percent of boxers (the less skilled ones) go on to develop a condition called "Punch Drunk" due to repeated concussions from multiple blows to the head, leading to gliosis and degenerative processes. These boxers developed symptoms including motor impairments, tremors, and personality changes (Martland, 1928). Punch Drunk was renamed dementia pugilistica in 1937 (Millspaugh, 1937) and finally defined as a medical diagnosis and termed chronic traumatic encephalopathy in 1957 (Critchley, 1957). Though initially described in boxers, CTE has been diagnosed in athletes and military members who have suffered repetitive head injury. From 2005 to 2010, Bennet Omalu reported the autopsy results of three National Football League (NFL) players whose pathological findings were indicative of CTE including neuronal loss, diffuse amyloid plaques, and neurofibrillary tangles and threads throughout the cortex (Omalu et al., 2005, 2006, 2010). These reports raised widespread concern over the long-term consequences of repetitive head injury for athletes,

both amateur and professional. In 2017, post-mortem pathological investigation of a convenience sample of over 200 American football players revealed that 87% of cases met the neuropathological criteria for a CTE diagnosis (Mez et al., 2017).

The criteria for pathological CTE diagnosis include aggregates of phosphorylated tau in neurons in cortical sulci near blood vessels in deeper cortical layers. Phosphorylated tau aggregates may also be present in glia, particularly astrocytes (Bieniek et al., 2021). Similar to Braak staging in AD, pathologists can categorize the severity of CTE pathology into four progressive pathological stages (McKee et al., 2013). Briefly, stage I (CTE I) is characterized by perivascular phosphorylated tau, neurofibrillary, and astrocytic tangles at the depths of sulci with very sparse pathology outside of these pathological focal points. Stage II (CTE II) is defined by spread of phosphorylated tau from pathological focal points to outer layers of nearby cortex. Stage III (CTE III) exhibits more widespread phosphorylated tau pathology throughout the cortex, large concentrations of neuronal and astrocytic tau pathology at the depths of sulci, and tau pathology in various subcortical and brainstem regions. Stage IV (CTE IV) demonstrates widespread phosphorylated tau throughout most of the cortex, marked astrocytic tau pathology, and neuronal loss in the cortex and some subcortical regions.

The clinical presentation of CTE includes a variety of changes in cognition, behavior, mood, and motor skills (Montenigro et al., 2015). Cognitive symptoms such as deficits in memory, executive control, and attention progress slowly to dementia in over two-thirds of cases (McKee et al., 2013; Montenigro et al., 2014). Behavioral changes can include increased violent behavior, impulsivity, and delusions. Mood changes can include depression, anxiety, and suicidal ideation. Motor changes can include ataxia, Parkinsonism, and tremors (Montenigro et al., 2015). While diagnosis of CTE cannot be confirmed until autopsy, proposed criteria for clinical diagnosis

include a history of multiple head impacts, exclusion of other neurological disorders that may account for symptoms, persistence of symptoms of at least twelve months, at least one core clinical feature and two supportive features of traumatic encephalopathy syndrome (Montenigro et al., 2014).

The greatest risk factor for and precipitating event of CTE is repetitive brain injury. However, given the variation of pathology between individuals, there are likely other factors that contribute to the risk for developing CTE and disease progression, including genetic variants. The minor allele of *TMEM106B* was associated with decreased phosphorylated tau and neuroinflammation and increased synaptic protein density (Cherry et al., 2018a). *APOEε4* was associated with CTE stage and phosphorylated tau burden (Atherton et al., 2022). Though there are no disease-modifying treatments for CTE, prevention of TBI is an important measure for prevention of CTE. Current pharmacological treatments for CTE are off-label and include memory impairment medications used for AD, stimulants, dopamine agonists, and antidepressant and anxiety medications (Pierre et al., 2021).

1.5 PROSPECTIVE THERAPEUTIC STRATEGIES FOR TARGETING TAU

The lack of disease modifying therapies for most tauopathies presents a daunting challenge for medical providers. Investigation into therapeutic strategies for targeting tau are needed to address this gap in therapy. The principles of tau biology provide windows of opportunity for therapeutic strategies. For example, tau in disease can be overexpressed, post-translationally modified, mutated, and/or aggregated, all of which are pathological mechanisms that can serve as therapeutic targets (Congdon et al., 2023). The current landscape of tau-targeting therapies was thoroughly reviewed by Congdon et al. (2023) and briefly summarized below:

Tau anti-sense oligonucleotides (ASOs) are one method of targeting tau overexpression (Scoles et al., 2019). Tau ASO $MAPT_{Rx}$ decreased phosphorylated tau and inflammatory markers in the CSF in Phase I testing and is in Phase II clinical trials for patients with MCI or mild AD (Mummery et al., 2023). Tau ASO NIO752 is in two Phase I clinical trials for patients with PSP and MCI or early AD. Kinase inhibitors are one way to target hyperphosphorylation. Lithium chloride is an inhibitor of glycogen synthase kinase 3β, a tau kinase (Fu et al., 2010). A Phase II trial assessing the efficacy of lithium chloride for treating bvFTD was completed in 2022 but results have yet to be reported. Another very active line of therapeutic research is that of tau immunotherapy. E2814 is an antibody that binds to extracellular tau and is currently in Phase III testing alongside anti-amyloid antibodies in patients with autosomal dominant early-onset AD (Roberts et al., 2020). Several vaccines that target tau phosphorylation sites and tau fragments are also undergoing clinical testing in patients with AD and FTD (Hickman et al., 2011; Kontsekova et al., 2014; Novak et al., 2017).

While there is certainly promise for tau-targeting therapies, there are notable challenges. There has been success in using monoclonal antibodies to target amyloid (Sims et al., 2023; van Dyck et al., 2023), but several anti-tau therapies failed in clinical trials. Monoclonal antibodies targeting the amino terminus of tau all failed to meet endpoints or demonstrate a slowing effect on cognitive decline. Discouragingly, the amino-terminal targeting antibody Gosuranemab exacerbated cognitive decline in early AD patients (Imbimbo et al., 2023). Further research into the basic science of tau and the specific molecular changes in tauopathy may provide further insight into the best strategies for targeting tau for therapeutics.

1.6 MOLECULAR CHANGES IN TAUOPATHY

Advances in transcriptomic and proteomic approaches have led to the generation of many

hypotheses and systems-level insights into the molecular underpinnings of tauopathy. There is an abundance of transcriptomic and proteomic investigations of human AD, including studies of post-mortem brain and biofluids, creating opportunities for meta-analyses (Rehiman et al., 2020; Wan et al., 2020; Noori et al., 2021; Shokhirev and Johnson, 2022; Viejo et al., 2022). Work from the Emory proteomics core has leveraged proteomic profiling of post-mortem human AD brain to identify AD-associated changes in the matrisome (Dammer et al., 2022; Johnson et al., 2022), glial energy metabolism (Johnson et al., 2020), proteostasis (Dammer et al., 2022), disease-associated-microglia (Rangaraju et al., 2018), and other pathways (Rayaprolu et al., 2021). Importantly, these works all leveraged systems biology, or integrative approaches including weighted gene correlation network analysis (WGCNA) and enrichment analyses to generate pathway level insights.

Transcriptomic and proteomic studies of FTD-tau human brain are less common than those of AD but have been used to identify dysregulated processes and pathways including calcium signaling (Minaya et al., 2023), oxidative phosphorylation (Bridel et al., 2023), RNA processing, oligodendrocyte and axons (Miedema et al., 2022), as well as increased abundance of astrocytic and endothelial cell proteins (Bridel et al., 2023). Omic studies of human CTE brain are even less common but they have identified changes in oligodendrocytes and astrocytes in CTE white matter (Chancellor et al., 2021), a decrease in phosphatases (Seo et al., 2017), a decrease in axonal guidance signaling proteins (Bi et al., 2019), and an increase in RNA processing proteins and oxidative stress in astrocytes (Cherry et al., 2018b). Collectively, these high-throughput studies of molecular changes in tauopathy demonstrate immense utility for hypothesis generation and systems-level insights.

Previously, we used quantitative proteomics on samples from human dorsolateral prefrontal cortex and temporal cortex to examine proteomic changes in tauopathy, with a focus on the

stages of CTE and FTD-tau (Gutierrez-Quiceno et al., 2021). Most FTD-tau samples were derived from patients with mutations in *MAPT*. Three key findings were: 1) early enrichment of immunoglobulins in CTE, particularly in CTE II, 2) FTD-tau samples demonstrated exaggerated proteomic changes when compared to control and CTE, and 3) an enrichment of astrocytic proteins in FTD-tau that exceeded that of other tauopathies.

The enrichment of astrocytic proteins in FTD-tau was demonstrated both computationally and biochemically. WGCNA modules in which FTD-tau eigenprotein values were significantly increased were also enriched with astrocytic proteins (Figure 1.1A, Figure 1.1B). The Digital Sorting Algorithm (Zhong et al., 2013), a cellular deconvolution method, demonstrated a significant increase in the relative abundance of astrocytes in FTD-tau that was higher than controls, all stages of CTE, and asymptomatic AD and AD cases from an external dataset (Johnson et al., 2018) (Figure 1.1.C).

To validate these findings, we performed protein blotting for astrocytic proteins glial fibrillary acidic protein (GFAP) (Figure 1.2A), hepatic and glial cell adhesion molecule (HEPACAM) (Figure 1.2B), and megalencephalic leukoencephalopathy with subcortical cysts 1 (MLC1) (Figure 1.2C). All of which were significantly enriched in FTD-tau relative to control. HEPCAM and MLC1 were enriched in FTD-tau relative to AD and CTE IV. Positive immunostaining for GFAP was noted in all groups (control, AD, FTD-MAPT, and CTE IV) (Figure 1.2.D). However, in FTD-MAPT tissues, astrocytes stained with GFAP were predominantly surrounding vasculature which was distinct from the other tauopathies examined. Likewise, positive staining for MLC1 was concentrated near perivascular astrocytes and was much darker in FTD-MAPT than AD and CTE IV. Limitations of this study included the lack of broad proteomic coverage of multiple tauopathies, including AD, and more importantly, that the samples were greatly

biased toward grey matter highlighting the need for studies that investigate both grey and white matter as in Chapter 2 of this dissertation. The marked enrichment of astrocytic proteins in FTD-tau, especially over that of other tauopathies, was a major motivation for Chapter 3 of this dissertation.

1.7 A NEED FOR INCLUDING WHITE MATTER IN STUDIES OF TAUOPATHIES

The transcriptomic and proteomic studies reviewed previously were performed with primarily grey matter samples. The brain is comprised of both grey and white matter which exhibit distinct cellular and subcellular compositions. Grey matter is enriched with neuronal cell bodies while white matter is enriched with axons (Fields, 2010). Tauopathies exhibit grey and white matter tau pathology in a disease-specific manner (Vega et al., 2021; Coughlin et al., 2022). Yet, grey and white matter are most often studied in isolation.

There are few omics-based studies that directly compare grey and white matter in non-pathological contexts. Proteomic comparison of grey and white matter samples from 8 subjects free from pathology demonstrated a largely shared proteome in grey and white matter samples. Differential expression and pathway analysis identified an upregulation of proteins associated with cell signaling, biomolecule and energy metabolism, and protein trafficking in grey matter and an upregulation of proteins associated with cellular development and post-translational modifications in white matter (Alexander-Kaufman et al., 2007). Transcriptional comparison of grey and white matter superior frontal gyrus from three subjects free from pathology and neurodegeneration demonstrated distinct expression profiles. Synaptic genes were upregulated in grey matter while axonal genes and long intergenic non-coding RNAs were upregulated in white matter (Mills et al., 2013). Notably, these studies had small samples sizes and were limited by the technology that was available at the time.

Many disease-oriented studies that include both grey and white matter are focused on multiple sclerosis (MS). Such transcriptomic studies of MS have identified disease-associated changes in CD56 bright natural killer cells and downregulation of white matter specific genes in both grey and white matter lesions and tissue-specific changes in mast cells and grey matter-specific genes (Satoh and Kino, 2015; Chai et al., 2022). Transcriptomic profiling of microglia isolated from control and MS grey and white matter demonstrated tissue and disease-specific expression: increased interferon genes in grey matter and NF-κB genes in white matter; increased lipid metabolism genes in white matter MS and increased glycolysis and iron homeostasis genes in grey matter MS (van der Poel et al., 2019). Proteomic studies of grey and white matter MS samples are less common but have identified diverging patterns of mitochondrial protein expression between grey and white matter, across MS disease progression (Rai et al., 2021). Collectively, these studies demonstrate the value of including both grey and white matter in transcriptomic and proteomic studies of neurological disease. This value and the paucity white matter proteomic studies of human tauopathy were major motivations for Chapter 3 of this dissertation.

1.8 OVERVIEW OF THE DISSERTATION

With this dissertation, I aimed to define how tauopathy impacts the human brain on a molecular level.

In Chapter 2, I use a multi-network proteomic approach to identify and compare grey and white matter DLPFC proteomic changes in human tauopathy. With an expanded sample of human tauopathies (AD, FTD-Tau, PSP, CBD, and CTE I-IV), I identified tissue-specific and disease-specific proteomic changes in microglial, endothelial, and mitochondrial processes. The dataset generated in this study will be an asset to others, and future investigations motivated by my findings could reveal new biomarker and therapeutic opportunities.

In Chapter 3 I use a targeted approach to measure transcripts related to glial biology in human control, AD, and FTD-tau DLPFC. My goal was to understand how glia in FTD-tau may differ from those in AD and control. I identified an increase in glial-related pathway scores and decrease in neuron-related pathway scores in FTD-tau samples. AD samples had intermediate pathway scores compared to control and FTD-tau, suggesting that FTD-tau may represent a more extreme form of tauopathy with increased contributions from glial processes. Comparison of this transcriptomic dataset with a previously published proteomic dataset (Gutierrez-Quiceno et al., 2021) revealed findings not identified in the prior dataset and demonstrated the utility of multi-omic approaches to understanding tauopathy.

Finally, in Chapter 4, I summarize the findings of my dissertation, evaluate limitations, and make recommendations for future studies. Specifically, I speculate on the utility of the ratio network approach for other scientific questions, suggest methods that are more suited for evaluating cell-type specific contributions to tauopathy, and reflect on the translational potential of this work as an extension of systems biology approaches.

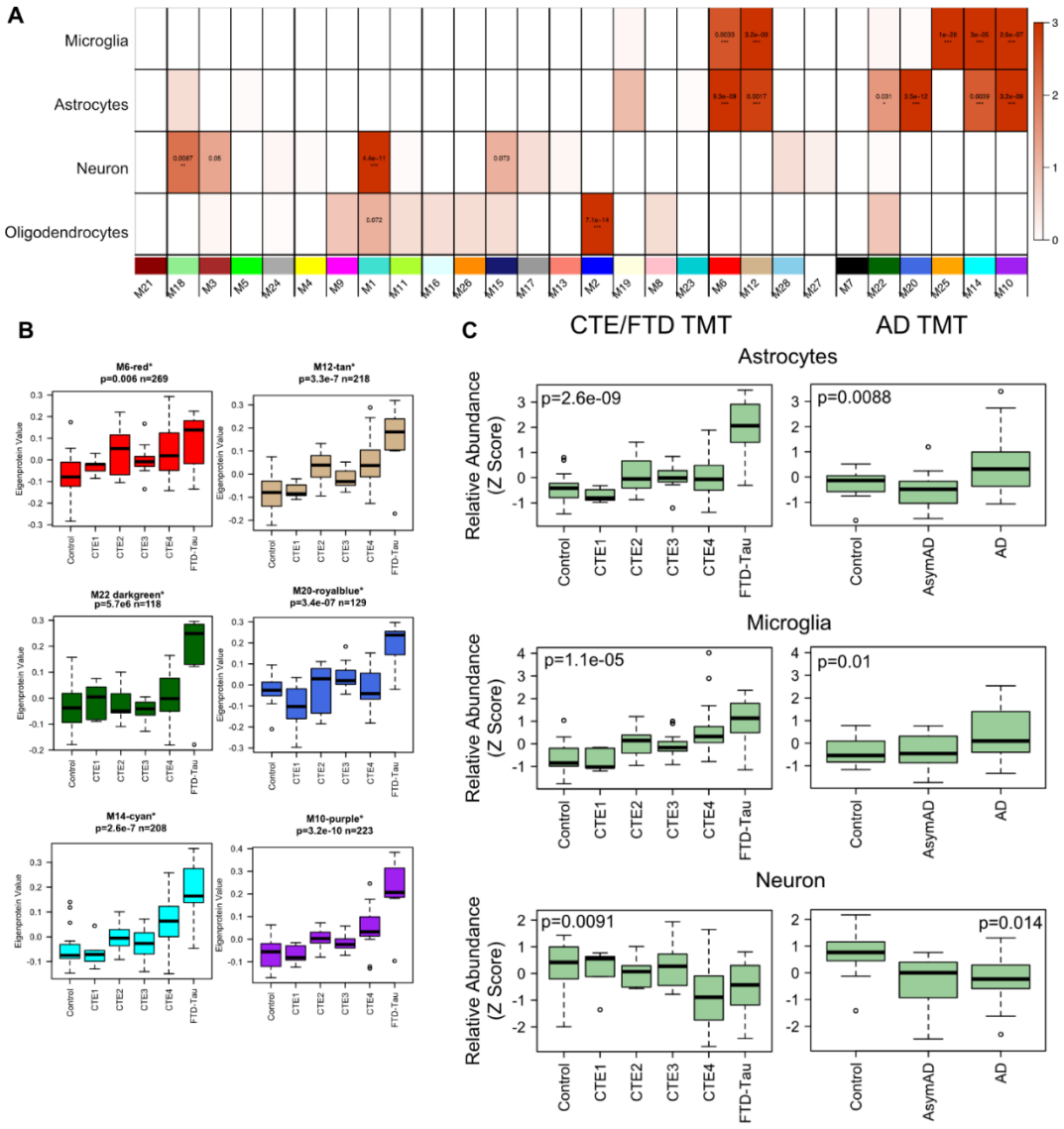

Figure 1.1 Quantitative proteomics and WGCNA demonstrate an enrichment of astrocytic proteins in FTD-Tau samples. (A) Enrichment of cell type specific proteins within WGNCA modules, determined by Fisher's Exact Test and Benjamini-Hochberg False Discovery Rate (FDR) p-value adjustment. (B) Boxplots of eigenprotein values for astrocyte-enriched modules. (C) Relative abundance of cell-type specific proteins as determined by DSA. Left panel is from dataset generated in (Gutierrez-Quiceno et al., 2021) and the right panel is from the dataset generated in (Johnson et al., 2018).

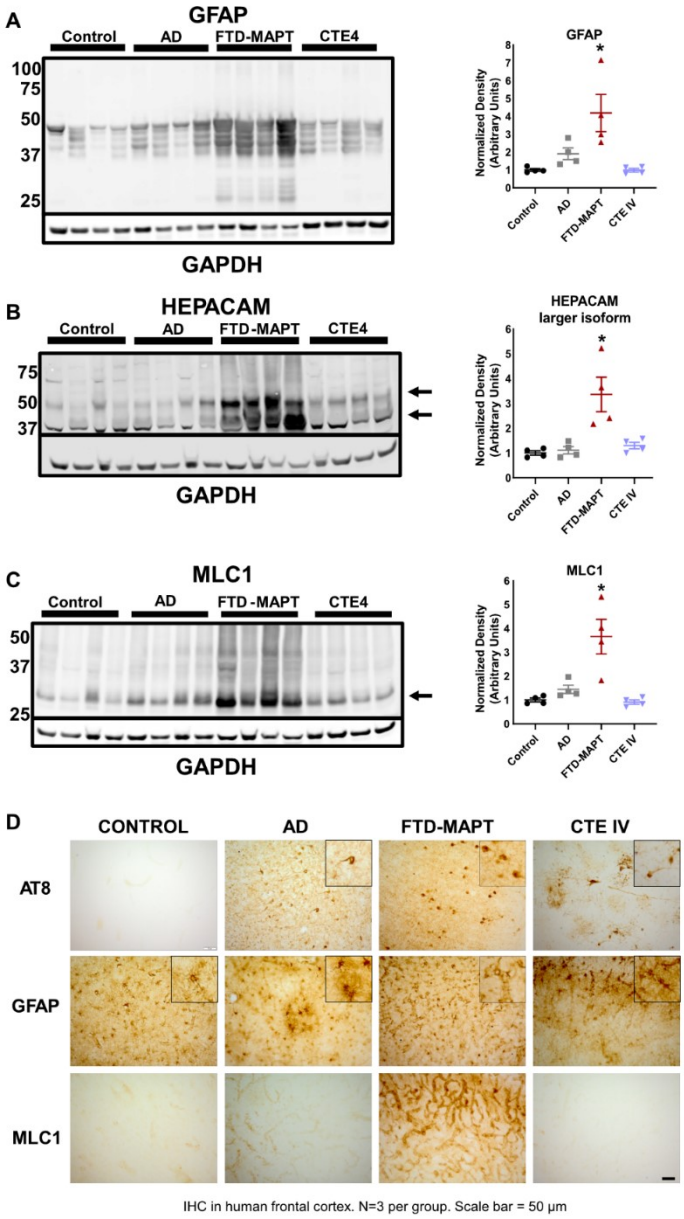

Figure 1.2 Western blotting and IHC for astrocytic proteins demonstrates enrichment of astrocytes in FTD-Tau tissues. (A-C) Protein blots and densitometry for three astrocytic proteins. * designates p-value < .05. GFAP: FTD-MAPT was significant compared to control and CTE IV. HEPACAM and MLC1: FTD-MAPT was significant compared to control, AD, and CTE IV.

CHAPTER 2: CONSENSUS AND RATIO PROTEOMIC NETWORKS OF GREY AND WHITE MATTER REVEAL TISSUE-SPECIFIC CHANGES IN HUMAN TAUOPATHY

2.1 CONTEXT, AUTHOR'S CONTRIBUTION, AND ACKNOWLEDGMENT OF RE-PRODUCTION

This chapter describes a proteomic comparison of grey and white matter in control and tauopathy. The dissertation author contributed to design and execution of bioinformatic analyses, interpretation of results, and writing the manuscript under the guidance of Dr. Chad Hales. Dr. Eric Dammer provided guidance and support in bioinformatic analysis. Dr. Chad Hales and James Webster generated samples for proteomic analysis and Duc Duong and Dr. Nicholas Seyfried facilitated sample processing and proteomic measurements.

2.2 ABSTRACT

Objective

To identify the impact of tauopathy on the human grey and white matter proteome.

Method

We applied tandem mass tagged labeling and mass spectrometry, consensus, and ratio weighted gene correlation network analysis (WGCNA) to grey and white matter sampled from post-mortem human dorsolateral prefrontal cortex. The sampled tissues included control as well as Alzheimer's disease, corticobasal degeneration, progressive supranuclear palsy, frontotemporal degeneration with tau pathology, and chronic traumatic encephalopathy.

Results

Only eight proteins were unique to grey matter while six were unique to white matter. Comparison of the grey and white matter proteome revealed an enrichment of microglial proteins in the white matter. Consensus WGCNA sorted over 6700 protein isoforms into 46 consensus modules across the grey and white matter proteomic networks. Consensus network modules demonstrated unique and shared disease-associated microglial and endothelial protein changes. Ratio WGCNA sorted

over 6500 protein ratios (white:grey) into 33 modules. Modules associated with mitochondrial proteins and processes demonstrated higher white:grey ratios in diseased tissues relative to control, driven by mitochondrial protein downregulation in grey and upregulation in white.

Interpretation

The dataset is an important resource for understanding proteomic changes in human tauopathy grey and white matter. The identification of unique and shared disease-associated changes across grey and white matter emphasizes the utility of examining both tissue types. These results indicate that microglia, endothelial, and mitochondrial changes in white matter warrant future study to define their contributions to tauopathy.

2.3 INTRODUCTION

Tauopathies are neurodegenerative diseases characterized by abnormal accumulation and hyperphosphorylation of tau. As a major underlying cause of dementia, tauopathies like Alzheimer's disease (AD), frontotemporal degeneration (FTD-tau), corticobasal degeneration (CBD), progressive supranuclear palsy (PSP), and chronic traumatic encephalopathy (CTE), represent a global public health concern. Tau accumulation can vary by cell type and region, and symptoms can include changes in memory, personality, executive function, language, and motor skills (Musa et al., 2020; Chung et al., 2021; Zhang et al., 2022). Given this heterogeneity, studies that include multiple tauopathies may provide clarity on the variable nature of tauopathy.

Advances in proteomic profiling and bioinformatics have deepened our understanding of how the brain changes in neurodegenerative disease. Mitochondrial dysfunction (Johnson et al., 2020; Swarup et al., 2020), glial reactivity (Johnson et al., 2020; Miedema et al., 2022), the spliceosome (Hales et al., 2016; Bishof et al., 2018), and the matrisome (Dammer et al., 2022) are just a few of the processes and pathways that proteomic studies have further implicated in neurodegenerative

disease. These studies have primarily used tissue from grey matter (GM), the area of the brain concentrated with neuronal cell bodies. However, tau-mediated neurodegeneration also impacts white matter (WM), the area of the brain in which axons are concentrated. White matter degeneration is associated with tau deposition in AD and tau accumulates in WM in a disease-specific manner. Thus, proteomic studies that include WM may provide a more complete understanding of how tauopathy impacts the brain.

With this work, we aimed to identify and compare how the GM and WM proteomes change in tauopathy. We dissected GM and WM from human dorsolateral prefrontal cortex (DLPFC) and employed tandem mass tagged (TMT) labelling and mass spectrometry. Using differential expression, clustering, cellular deconvolution, and weighted gene correlation network analyses (WGCNA), we defined GM and WM tissue-specific, disease-associated proteomic changes in human tauopathy.

2.4 MATERIALS AND METHODS

2.4.1 Collection of human postmortem brain

Human brain tissues were obtained and processed as previously described(Gutierrez-Quiceno et al., 2021). Briefly, tissues were obtained from the Emory Goizueta Alzheimer's Disease Research Center Neuropathology Brain Bank in Atlanta, Georgia and from the Veteran's Affairs-Boston University Concussion Legacy Foundation Brain Bank in Boston Massachusetts. Samples of fresh frozen dorsolateral prefrontal cortex (DLPFC) were used for the present study. Specimens were selected for this study based on demographics and neuropathological diagnosis (Tables 2.1, 2.2). FTD-tau samples were comprised of seven cases with a familial mutation in the tau gene and two sporadic cases with Pick's pathology.

2.4.2 Preparation of brain homogenates

Approximately 100 mg of GM and WM were dissected with a razor blade from fresh frozen DLPFC. Clean razor blades were used for each sample to avoid cross contamination. Each ~100 mg tissue piece was individually homogenized in 500 uL of urea lysis buffer (8M urea, 100 mM NaHPO4, pH 8.5), including 5 uL (100x stock) HALT protease and phosphatase inhibitor cocktail (Pierce). All homogenization was performed using a Bullet Blender (Next Advance) according to manufacturer protocols. Briefly, each tissue piece was added to Urea lysis buffer in a 1.5 mL Rino tube (Next Advance) harboring 750 mg stainless steel beads (0.9-2 mm in diameter) and blended twice for 5 minute intervals in the cold room (4°C). Protein supernatants were transferred to 1.5 mL Eppendorf tubes and sonicated (Sonic Dismembrator, Fisher Scientific) 3 times for 5 s with 15 s intervals of rest at 30% amplitude to disrupt nucleic acids and subsequently vortexed. Protein concentration was determined by the bicinchoninic acid (BCA) method, and samples were frozen in aliquots at −80°C. Protein homogenates (100 ug) were diluted with 50 mM NH4HCO3 to a final concentration of less than 2M urea and then treated with 1 mM dithiothreitol (DTT) at 25°C for 30 minutes, followed by 5 mM iodoacetimide (IAA) at 25°C for 30 minutes in the dark. Protein was digested with 1:100 (w/w) lysyl endopeptidase (Wako) at 25°C for 2 hours and further digested overnight with 1:50 (w/w) trypsin (Promega) at 25°C. Resulting peptides were desalted with a Sep-Pak C18 column (Waters) and dried under vacuum.

2.4.3 Tandem Mass Tag (TMT) Labeling

All samples were labeled using the TMT 11-plex kit (ThermoFisher 90406) according to manufacturer's protocol. Each sample (containing 100 μg of peptides) was re-suspended in 100 mM TEAB buffer (100 μL). The TMT labeling reagents were equilibrated to room temperature, and anhydrous ACN (256 μL) was added to each reagent channel. Each channel was gently

vortexed for 5 min, and then 41 µL from each TMT channel was transferred to the peptide solutions and allowed to incubate for 1 h at room temperature. The reaction was quenched with 5% (vol/vol) hydroxylamine (8 µl) (Pierce). All channels for each batch were then combined and dried by SpeedVac (LabConco) to approximately 150 µL and diluted with 1 mL of 0.1% (vol/vol) TFA, then acidified to a final concentration of 1% (vol/vol) FA and 0.1% (vol/vol) TFA. Peptides were desalted with a 200 mg C18 Sep-Pak column (Waters). Each Sep-Pak column was activated with 3 mL of methanol, washed with 3 mL of 50% (vol/vol) ACN, and equilibrated with 2×3 mL of 0.1% TFA. The samples were then loaded and each column was washed with 2×3 mL 0.1% (vol/vol) TFA, followed by 2 mL of 1% (vol/vol) FA. Elution was performed with 2 volumes of 1.5 mL 50% (vol/vol) ACN. The eluates were then dried to completeness.

2.4.4 High pH Fractionation

Dried samples were re-suspended in high pH loading buffer (0.07% vol/vol NH4OH, 0.045% vol/vol FA, 2% vol/vol ACN) and loaded onto an Agilent ZORBAX 300 Extend-C18 column (2.1mm x 150 mm with 3.5 µm beads). An Agilent 1100 HPLC system was used to carry out the fractionation. Solvent A consisted of 0.0175% (vol/vol) NH4OH, 0.01125% (vol/vol) FA, and 2% (vol/vol) ACN; solvent B consisted of 0.0175% (vol/vol) NH4OH, 0.01125% (vol/vol) FA, and 90% (vol/vol) ACN. The sample elution was performed over a 58.6 min gradient with a flow rate of 0.4 mL/min. The gradient consisted of 100% solvent A for 2 min, then 0% to 12% solvent B over 6 min, then 12% to 40 % over 28 min, then 40% to 44% over 4 min, then 44% to 60% over 5 min, and then held constant at 60% solvent B for 13.6 min. A total of 96 individual equal volume fractions were collected across the gradient and subsequently pooled by concatenation into 24 fractions and dried to completeness using a vacuum centrifugation.

2.4.5 Liquid Chromatography Tandem Mass Spectrometry

Each of the 24 high-pH peptide fractions was resuspended in loading buffer (0.1% FA, 0.03% TFA, 1% ACN). Peptide eluents were separated on a self-packed C18 (1.9 µm Dr. Maisch, Germany) fused silica column (50 cm × 75µM internal diameter (ID), New Objective, Woburn, MA) by a Dionex Ultimate U3000 RSLCnano (Thermo Scientific) and monitored on an Orbitrap Fusion mass spectrometer (Thermo Scientific). Elution was performed over gradients of 100 and 120 minutes at a rate of 300 nL/min and 250 nL/min with buffer B ranging from 7% to 40% (buffer A: 0.1% FA in water, buffer B: 0.1 % FA in 80% ACN). Mass spectrometry was performed in positive ion mode using data-dependent acquisition with 3 second top speed cycles. Each cycle consisted of one full MS scan followed by as many MS/MS events that could fit within the given 3 second cycle time limit. MS scans were collected at a resolution of 120,000 (400-1600 m/z range, 4x10^5 AGC, 50 ms maximum ion injection time, FAIMS CV of -45 and -65). Only precursors with charge states between 2+ and 5+ were selected for MS/MS. All higher energy collision-induced dissociation (HCD) MS/MS spectra were acquired at a resolution of 60,000 (1.6 m/z isolation width, 35% collision energy, 5x10^4 AGC target, 50 ms maximum ion time). Dynamic exclusion was set to exclude previously sequenced peaks for 20 seconds within a 10-ppm isolation window.

2.4.6 Proteomic Data Analysis

All raw files were searched using Thermo's Proteome Discoverer suite (version 2.3.0.522) with Sequest HT. The spectra were searched against a human uniprot database downloaded April 2015 (90293 target sequences). Search parameters included 20ppm precursor mass window, 0.05 Da product mass window, dynamic modifications methione (+15.995 Da), deamidated asparagine and glutamine (+0.984 Da), phosphorylated serine, threonine and tyrosine (+79.966 Da), and static

modifications for carbamidomethyl cysteines(+57.021 Da) and N-terminal and Lysine-tagged TMT (+229.26340 Da). Percolator was used filter PSMs to 0.1%. Peptides were grouped using strict parsimony and only razor and unique peptides were used for protein level quantitation. Reporter ions were quantified from MS2 scans using an integration tolerance of 20 ppm with the most confident centroid setting. Only unique and razor (i.e., parsimonious) peptides were considered for quantification.MS/MS spectra were identified using the UniprotKB Human proteome database. Peptides were assembled into proteins to determine abundances based on extracted ion intensities and gene symbol redundancy was managed as previously described (Gutierrez-Quiceno et al., 2021). Data was normalized using global internal standard (GIS) samples.

The Tunable Approach for Median Polish of Ratio (TAMPOR) (Dammer et al., 2023) method was applied to remove variability due to batch and remove proteins with greater than 50% missingness. Next, the data from GM and WM samples were split into two matrices. WGCNA network connectivity outliers were eliminated ($|Z.k| > 3$ SD from mean). If a sample was removed from the GM matrix, then it was also removed from the WM matrix, and vice-versa. Nonparametric bootstrap regression removed any residual covariance due to TMT batch according to a linear mixed model that also included (protected) diagnosis/CTE stage. The variancePartition package in R (Hoffman and Schadt, 2016) was used to visualize the decrease in covariance due to TMT batch after TAMPOR and bootstrap regression (Supplemental Figure 2.1). Due to the low covariance attributed to age, sex, and post-mortem interval (PMI) and the prevalence of young, male, samples with longer PMIs in the CTE samples, we elected to not regress for these factors (Supplemental Figure 2.1). The GM and WM matrices were joined and proteins with more than 50% missingness were removed. The resulting data matrix was the basis for downstream analyses.

WGCNA analyses were used to identify clusters or modules of proteins with highly correlated expression patterns. To prepare the data for consensus WGCNA (cWGCNA) analysis, the data were again split into two separate matrices (GM and WM) and proteins absent in both matrices were removed. The power at which approximate scale free topology was determined at the elbow of the curve of power vs R-squared approaching an asymptote, ideally with $R^2 = 0.8$ and with overall connectivity reduced to around 100; this power was 9.0. We then used the blockwiseConsensusModules function with the following parameters: deepsplit = 4, minModuleSize = 20, mergeCutHeight = 0.07, TOMDenom = "mean, corType = "bicor", networkType = "signed", pamStage = TRUE, pamRespectsDendro = TRUE, and reassignThresh = 0.05.

In parallel, ratios of WM to GM protein abundances were calculated as input for a WGCNA analysis. Similar to the data preparation for the cWGCNA analysis, batch corrected and regressed data were split into individual GM and WM matrices. For each pair of samples (one GM and one WM sample per subject), the GM abundance was subtracted from the WM abundance to create a WM:GM ratio. The power at which approximate scale free topology was determined at the elbow of the curve of power vs R-squared approaching an asymptote, ideally with $R^2 = 0.8$ and with overall connectivity reduced to around 100; this power was 8.5. We then used the blockwiseModules function with the same parameters as was used for cWGCNA analysis. Additional cleanup was used to ensure that resulting network modules members had an intramodule kME values of at least 0.28.

Cell subtype analysis with brain cell type proteome and transcriptome as the reference (Dammer, 2023), was used to identify cell type markers in the WGCNA modules (both consensus and ratio). This analysis was also modified to identify WGCNA modules enriched with mitochondrial markers generated from Human MitoCarta3.0(Rath et al., 2021) and tissue-specific

microglial markers(van der Poel et al., 2019). Gene ontology (GO) pathway analyses were performed using the GOparallel function (Dammer, 2022a). Briefly, hypergeometric overlap with Fisher Exact Test for enrichment were used to assess enrichment of WGCNA modules or lists of differentially abundant proteins with GO terms. GO terms were derived from lists maintained by the Bader Lab at the University of Toronto. The database was accessed on March 1st, 2023, and those GO terms were used for all GO analyses in this work. Redundant GO terms were pruned using the ontologyIndex package (Greene et al., 2017).

Differential abundance was calculated with two approaches. 1) To compare GM and WM protein abundance within each disease group: The GM abundance was subtracted from the WM abundance for each pair of samples (one GM and one WM sample per subject) to calculate the mean of the differences, with paired T-tests and Benjamini-Hochberg FDR adjustment of p-values for multiple tests to determine statistical significance. For each protein, a sample pair was removed from the paired analysis if one of the samples was missing data. If there were not more than two pairs of samples, then that protein was also removed from the analysis. 2) To compare protein abundances between disease groups to control within GM or WM: Average control protein abundance was subtracted from average disease protein abundance, with one-way ANOVA plus Tukey's honestly significant difference (Tukey HSD) to determine statistical significance, using the parANOVA function (Dammer, 2022b).

K-Means analysis was performed on both the samples and the proteins. For clustering of samples, we specified the number of clusters as 2 based on *a priori* knowledge that the samples were derived from GM and WM. For clustering of the proteins, we reduced the dataset to proteins with no missing data (n = 4700) and used the within cluster sums of squares method within the fviz_nbclust function in the factoextra R package(Kassambra and Mundt, 2020) to determine to

optimal number of clusters as 4. We used a random seed of 1969 and set centers equal to 4 and nstart equal to 25 in the kmeans function in the stats R package(R Core Team, 2023).

Cell type deconvolution was performed using the EnsDeconv R package (Cai et al., 2022). TAMPOR and batch-regressed non-log2 transformed data were the input. The parameters for deconvolution were set with the get_params function: data_type = “singlecell-rna”, data_name = names(testdata$ref_list), n_markers = 50, Marker.Method = c("t", "wilcox", "combined", "none", "regression"), TNormalization = "none", CNormalization = "none", and dmeths = c("DCQ","CIBERSORT","ICeDT","FARDEEP","EPIC","hspe").

The shiny R package was used to create an interactive app for exploration of this dataset. The app can be accessed at ashlyngjohnson.github.io/greywhiteproteome. Scripts used for data analysis can be found at https://github.com/ashlyngjohnson/grey_white_tauopathy.

2.5 RESULTS

2.5.1 Cell-type specific proteins are differentially expressed in GM and WM DLPFC proteomes.

Our prior work leveraged TMT labeling and LC-MS/MS to compare the proteomes of control and tauopathy DLPFC and temporal lobe cortex (Gutierrez-Quiceno et al., 2021). However, these and other proteomic studies of neurodegeneration have been biased toward GM, though WM changes are known components of disease pathogenesis (Holleran et al., 2017; Chancellor et al., 2021; Vega et al., 2021; Coughlin et al., 2022; Alosco et al., 2023). Thus, we aimed to identify and compare GM and WM proteomic alterations in human tauopathy to more fully understand tau-mediated neurodegeneration. We hypothesized that WM would share many changes with GM, while also demonstrating unique disease-associated changes. We dissected GM and WM from human control (n = 12), AD (n = 12), CBD (n = 4), PSP (n = 5), FTD-tau (n = 9), CTE I (n = 5),

CTE II (n = 5), CTE III (n = 5), CTE IV (n = 6) DLPFC. From a total of 126 samples (2 samples – GM and WM – per subject) across 14 TMT batches, LC-MS/MS identified over 9,000 high confidence unique protein isoforms.

We found that 89.3% of the proteome or 8,542 proteins were detected in at least one sample of both GM and WM (Figure 2.1A). 615 proteins were measured in at least one GM sample and zero samples of WM (Figure 2.1A). 412 proteins were measured in at least one WM sample and zero GM samples (Figure 2.1A). Interestingly, just 8 proteins (ARC, NSG2, CSMD2, LRFN2, LRRTM1, PCDH7, CDH9, KHDRBS2) were measured in all 63 GM samples and zero WM samples. Only 6 proteins (TMC7, SRCIN1, HHIP, GNG8, SLC27A6, GJB1) were measured in all 63 WM samples and zero GM samples (Figure 2.1B), all of which are enriched in oligodendroglial cell types at the transcript level (Zhang et al., 2014a, 2016).

After pre-processing to remove sample outliers and proteins with high missingness across samples, 122 samples (from 61 subjects) and 6,728 unique protein isoforms were selected for downstream analysis. We used a paired differential expression analysis to compare GM and WM. Proteins with an FDR p-value < 0.05 and a mean difference with an absolute value greater than or equal to 1 were differentially expressed. 462 proteins were upregulated in control GM while 278 were upregulated in control WM (Figure 2.1C). As expected, cell type analysis demonstrated enrichment of neuronal proteins in upregulated GM proteins and enrichment of oligodendrocyte proteins in the upregulated WM proteins. Microglial proteins were enriched in upregulated WM proteins, but not upregulated GM proteins (Figure 2.1D). This pattern of differential expression and cell type enrichment was similar for GM vs WM comparisons in all other disease groups (Supplemental Figures 2.2, 2.3). Interestingly, endothelial proteins were significantly enriched in WM FTD-tau samples but not other WM samples (Supplemental Figure 2.3A).

Given the enrichment of microglial proteins in WM, we compared our results with an existing transcriptome of human microglia derived from occipital cortex and corpus callosum from control and subjects with multiple sclerosis (MS) (van der Poel et al., 2019). With a similar analysis (van der Poel et al., 2019), we restricted the comparison to proteins with an absolute mean difference greater than or equal to 2. Upregulated WM proteins across all GM vs WM comparisons in our dataset were enriched for upregulated WM-specific microglial markers identified in the comparison dataset (van der Poel et al., 2019) (Supplemental Figure 2.3B). Cellular deconvolution analysis identified a higher proportion of microglia in WM than GM and endothelia in FTD-tau WM than all of other groups. The deconvolution results also aligned well with GM and WM differential expression and cell type analyses, further demonstrating the strength of this approach and dataset. (Supplemental Figure 2.4).

We then used k-means clustering analysis on the 122 samples, specifying the number of clusters, k, as 2, given our *a priori* knowledge that the samples were derived from either GM or WM. Reassuringly, the GM and WM samples formed two distinct clusters. Further hierarchical clustering of the samples within their respective k-means clusters showed that the FTD-tau samples were most similar to one another. We also used k-means clustering analysis (k = 4) on proteins with no missingness across all samples (n = 4700) (Figure 2.2A). Cluster 1 (n = 1,526 proteins) was significantly enriched with microglial proteins with a trending enrichment in endothelial proteins (Figure 2.2B) whose top gene ontologies were associated with inflammation-associated terms such as Wound Healing and Acute-Phase Response (Figure 2.2C). Notably, the FTD-tau samples had increased expression of Cluster 1 proteins, particularly in WM (Figure 2.2A). Cluster 2 was enriched for oligodendroglial proteins while Cluster 3 was enriched for neuronal proteins (Figure 2.2B). Top GO terms for Cluster 2 were associated with cytoskeleton and myelin while top GO

terms for Clusters 3 and 4 were associated with mitochondria and translation, respectively (Supplemental File 2.1). Differential expression, cell type and cellular deconvolution, and k-means analyses collectively demonstrated an enrichment of microglial proteins in WM and endothelial proteins in FTD-tau WM.

2.5.2 Consensus WGCNA reveals unique disease-associated endothelial and microglial protein changes in WM.

WGCNA is an unsupervised systems biology approach to characterize proteomic changes based on protein expression profiles through pairwise correlations of proteins. Modules consist of proteins whose expression profiles are highly correlated and often biologically related in function. We previously applied WGCNA in a cohort of GM-matter biased samples and identified an enrichment of astrocytic proteins in FTD-tau and stage-specific molecular phenotypes in CTE (Gutierrez-Quiceno et al., 2021). Given the notable difference in protein expression and cell type enrichment between the GM and WM tissues (Figures 2.1, 2.2), we treated the GM and WM samples as separate networks and used cWGCNA to identify shared or consensus modules between the two networks. We identified 46 consensus modules across the GM and WM proteomes (Figure 2.3A). Inter-module correlation was well preserved across both networks (Figures 2.3B,C) with a mean preservation for each eigenprotein of 0.82 (Figure 2.3D). M22, a heterogeneous module was the most preserved while M11, a module of actin-related and tRNA aminoacylation proteins was the least preserved (Figure 2.3D).

Enrichment of microglial proteins in WM and endothelial proteins in FTD-tau WM identified in our differential expression analyses drove us to examine consensus modules that may reflect these findings. After identifying consensus modules enriched for cell-type specific proteins (Figure 2.4A), cluster-specific proteins from our k-means analysis (Figure 2.4B), and GO terms

associated with microglial and endothelial processes (Supplemental File 2.2), we identified four consensus modules of interest. Module 28 (M28) was enriched with Cluster 1 proteins as well as complement and blood-related proteins which are associated with microglial processes (Figure 2.4C). M28 eigenprotein values demonstrated WM disease-associated changes (one-way ANOVA, $p = 0.002$). PSP (T-test, $p = 0.00093$) and CTE III (T-test, $p = 0.021$) M28 eigenprotein values were significantly higher than control. Module 45 (M45) was enriched with endothelial proteins associated with the circulatory system (Figure 2.4D) and demonstrated WM disease-associated changes (one-way ANOVA, $p = 0.00051$). AD M45 eigenprotein values were significantly lower than control (T-test, $p = 0.044$) while FTD-tau M45 eigenprotein values were significantly higher (T-test, $p = 0.0061$). Module 19 (M19) was enriched with Cluster 1 and microglial proteins and demonstrated both GM (one-way ANOVA, $p = 0.0038$) and WM (one-way ANOVA, $p = 0.039$) matter disease-associated changes (Figure 2.4E). GM CBD (T-test, $p = 0.02$) and FTD-tau (T-test, $p = 0.00023$) M19 eigenprotein values were higher than control, while only FTD-tau (T-test, $p = 0.0015$) M19 eigenprotein values were higher than control in WM. Finally, Module 27 (M27) was enriched with endothelial and astrocytic proteins and demonstrated disease-associated changes in both GM (one-way ANOVA, $p = 3.7e\text{-}08$) and WM (one-way ANOVA, $p = 4.1e\text{-}06$) matter (Figure 2.4F). Specifically, AD (T-test, $p = 0.021$) and FTD-tau (T-test, $p = 6.5e\text{-}07$) M27 eigenprotein values were higher than control in GM, while CTE IV (T-test, $p = 0.0085$) and FTD-tau (T-test, $p = 1.8e\text{-}05$) M27 eigenprotein values were higher than control in WM. Enriched GO terms for M27 indicate that proteins in this module are involved in extracellular matrix and basement membrane processes. Collectively, these results demonstrate both unique and shared disease-associated microglial and endothelial protein changes across GM and WM.

2.5.3 WGCNA of WM:GM ratio reveals disease-associated alterations in mitochondrial proteins

Recently, grey to white matter signal ratio was identified as a novel metric of neurodegeneration and was associated with tau deposition (Putcha et al., 2023). To assess if the ratio of proteins across GM and WM were dysregulated in disease, we calculated a ratio by subtracting GM abundance from WM abundance. WGCNA of the resulting 6,573 ratios revealed 33 modules (Figure 2.5A). Module 1 (M1) proteins had the highest ratios, indicating higher expression in WM than GM (Figure 2.5B,C). Top GO terms were associated with myelin sheath and sphingolipid metabolism (Supplemental File 2.3). Module 2 (M2) proteins had the lowest ratios (Figure 2.5B,C), indicating higher expression in GM than WM. Top GO terms were associated with synaptic vesicles. Thus, the modules with the most extreme ratios were associated with the primary cellular components of GM and WM. Furthermore, disease associated changes in M1 eigenprotein values demonstrated a marked decrease of oligodendroglial proteins in AD (T-test, $p = 0.046$), CBD (T-test, $p = 0.035$), FTD-tau (T-test, $p = 1.4e-05$), and CTE IV (T-test, $p = 0.017$) relative to control (Figure 2.5C).

The ratio network approach revealed 6 mitochondria-associated modules which demonstrated elevated WM:GM ratios in one or more disease groups relative to control: modules (M) 21, 16, 9, 13, 14, and 30 (Supplemental File 2.5). Most of these modules were comprised of proteins involved in multiple Mitocarta-defined (Rath et al., 2021) mitochondrial pathways such as metabolism, central dogma, oxidative phosphorylation, and protein import, sorting and homeostasis. Notably, M13 was only enriched for mitochondrial central dogma proteins while M14 and M30 were enriched for mitochondrial metabolism and central dogma proteins (Figure 2.6A, B). An elevated WM:GM ratio may be driven by both a decrease in protein expression in GM and/or an increase

in WM. Thus, we examined differential expression patterns of all proteins in the 6 mitochondrial modules of interest and all mitochondrial proteins as defined in Mitocarta 3.0 (Rath et al., 2021), comparing each disease group to control (Figure 2.6C,D) . Indeed, most of these proteins were downregulated in GM and upregulated in WM. FTD-tau samples demonstrated the most differentially expressed proteins, mitochondrial and otherwise (Supplemental Figures 2.5, 2.6). Notably, this diverging pattern of mitochondrial expression in GM and WM in diseased tissues was not evident in the consensus network mitochondrial modules (Supplemental File 2.4). The ratio network approach identified reciprocal proteomic changes across GM and WM that were not readily detectible through conventional WGCNA.

2.6 DISCUSSION

Tauopathies and dementia are a global health concern, yet there is a paucity in research to define how tauopathy impacts WM. To better inform our understanding of disease, we used quantitative proteomics to identify and compare changes in GM and WM human tauopathy tissues. Initial comparison of GM and WM demonstrated that a majority of the proteome is shared, though there are select proteins that are tissue specific. Comparison of GM and WM demonstrated enrichment of microglial proteins in WM, which was validated in an orthogonal dataset(van der Poel et al., 2019). K-means clustering analysis and cWGCNA of GM and WM networks demonstrated tissue-specific, disease-associated changes in microglial and endothelial proteins. Ratio WGCNA identified a non-specific, disease-associated dysregulation of white:grey ratio in mitochondrial proteins. Together, our results highlight the value of examining both GM and WM to better understand the pathophysiology of tauopathy.

We identified eight (GM) and six (WM) proteins that were only detected in one tissue type. While this tissue-specificity of a select few proteins may be tool or technique dependent, they may

be useful as markers of GM or WM in tissue preparations. Comparison of GM and WM revealed an enrichment of microglial proteins in white matter, regardless of disease status, and an enrichment of endothelial proteins in FTD-tau WM. Enrichment of microglial proteins in WM may be driven by tissue-specific molecular profiles or tissue-specific differences in microglial density. Indeed, prior work has demonstrated higher density of microglia in WM regions compared to GM (Mittelbronn et al., 2001; Mizee et al., 2017). However, unique molecular signatures have also been attributed to microglia in WM in mice and humans in the contexts of aging (Hahn et al., 2023) and disease, including MS (van der Poel et al., 2019) and AD (Safaiyan et al., 2021). It is likely that both a difference in microglia cell count and molecular phenotype in WM drive our findings.

The results of our K-means clustering and cWGCNA analyses identified shared and unique disease-associated changes in microglial and endothelial pathways and processes, where FTD-tau samples were often the extreme. Prior work has also demonstrated increased astrocyte, microglia, and endothelial transcripts and proteins in FTD-tau relative to control and other tauopathies (Gutierrez-Quiceno et al., 2021; Johnson et al., 2021; Bridel et al., 2023; Hartnell et al., 2023). Proteins associated with microglia, innate immunity, the extracellular matrix, and the basement membrane were dysregulated in both GM and WM while proteins associated with complement, blood, and the circulatory system were dysregulated in WM. These WM-specific changes appear to be targeted to vasculature. WM vascularization is less dense than GM and vulnerable to chronic hypoperfusion (Pansieri et al., 2023). This difference in density could make the WM more vulnerable to disease-associated changes in vascular-associated proteins. Recent work demonstrated that capillaries in WM are wider than capillaries in GM, and this width increases in neurodegenerative disease(Hase et al., 2019), which may explain the unique WM increases in consensus modules M28 and M45.

Ratio WGCNA identified, in an unbiased manner, a dysregulation of mitochondrial proteins. Proteomic studies of predominantly GM samples previously demonstrated dysregulation (often a decrease) of mitochondrial proteins in neurodegenerative disease (Adav et al., 2019; Agrawal and Fox, 2019; Johnson et al., 2020; Swarup et al., 2020). For this study, mitochondrial protein dysregulation was driven by disease-associated downregulation in GM and upregulation in WM. Interestingly, mitochondrial protein expression in multiple sclerosis GM and WM lesions also demonstrated an opposite or reciprocal pattern of expression (Rai et al., 2021). It was postulated that mitochondrial proteins were decreased in GM lesions and increased in WM due to both neuronal loss and defective retrograde transport of damaged mitochondria back to the cell body (Rai et al., 2021). However, the increase in mitochondrial proteins in WM could also be explained by altered mitochondrial dynamics in glial cells, which comprise a larger proportion of the cells in WM than GM (Yu et al., 2018).

There are important limitations of this study to consider. Primarily, the sample size is low. The FTD-tau group predominantly consisted of samples from subjects with *MAPT* mutations which could lead to higher in-group homogeneity compared to other disease groups, driving significant findings. The dissection of GM and WM from each sample was performed by hand, which is less precise than other techniques such as laser-capture microdissection (Liao et al., 2004). Future studies may benefit from spatial biology as a more precise method of defining tissue/region-specific molecular changes (Hahn et al., 2023). Finally, there is potential for bias in selecting which findings to highlight from the many WGCNA modules that demonstrate tissue-specific and/or disease-specific changes. Our systems-based approach also yielded several prospective avenues of research outside the scope of the present manuscript including WM-specific, disease-associated

changes in collagen and extracellular matrix proteins (Supplemental Files 2.2, 2.4) and disease-associated WM:GM ratio changes in cytoskeletal proteins (Supplemental Files 2.3, 2.5)

This work provides improved understanding of GM and WM proteomic changes in tauopathy, both shared and distinct. This dataset is a resource for investigators to explore novel insights on GM and WM proteomic differences in control and tauopathy conditions. Studies that measure or modify WM microglia, endothelia, or mitochondria in neurodegenerative disease models may also reveal new biomarker and therapeutic opportunities. Future human brain proteomic studies will benefit from separating GM and WM to uncover unique and reciprocal disease-associated changes.

2.7 ACKNOWLEDGMENTS

We acknowledge the Goizueta Alzheimer's Disease Research Center [P30AG066511] and Dr. Ann McKee for their neuropathological services and sample repository. We are grateful for the individuals and families whose specimen donations supported this work. This study was supported in part by the Emory Integrated Proteomics Core (EIPC), which is subsidized by the Emory University School of Medicine and is one of the Emory Integrated Core Facilities. Additional support was provided by the Georgia Clinical & Translational Science Alliance of the National Institutes of Health under Award Number UL1TR002378. The content is solely the responsibility of the authors and does not necessarily reflect the official views of the National Institutes of Health. We thank Dr. Cheyenne Hurst for providing sample R scripts.

TABLES

Table 2.1. Demographics for all samples.

	Overall, N = 63	**Control**, N = 12	**AD**, N = 12	**CBD**, N = 4	**FTD**, N = 9	**PSP**, N = 5	**CTE I**, N = 5	**CTE II**, N = 5	**CTE III**, N = 5	**CTE IV**, N = 6	**p-value**[1]
PMI (hours), Median (IQR)	15 (7 – 42)	6 (6 – 8)	7 (6 – 13)	7 (4 – 12)	15 (7 – 18)	15 (11 – 23)	48 (24 – 48)	48 (36 – 48)	48 (48 – 72)	53 (48 – 68)	**<0.001**
Age at Death (years), Median (IQR)	65 (60 – 72)	60 (55 – 74)	68 (61 – 70)	67 (64 – 75)	64 (60 – 65)	75 (70 – 83)	30 (27 – 60)	70 (60 – 70)	60 (40 – 70)	73 (63 – 79)	0.12
Sex, n (%)											**0.032**
Female	17 (27)	6 (50)	6 (50)	0 (0)	4 (44)	1 (20)	0 (0)	0 (0)	0 (0)	0 (0)	
Male	46 (73)	6 (50)	6 (50)	4 (100)	5 (56)	4 (80)	5 (100)	5 (100)	5 (100)	6 (100)	

[1]Kruskal-Wallis rank sum test; Fisher's exact test

Table 2.2 Demographics after removal of outlier samples.

	Overall, N = 61	Control, N = 12	AD, N = 12	CBD, N = 4	FTD, N = 9	PSP, N = 4	CTE I, N = 4	CTE II, N = 5	CTE III, N = 5	CTE IV, N = 6	p-value[1]
PMI (hours), Median (IQR)	13 (7 – 37)	6 (6 – 8)	7 (6 – 13)	7 (4 – 12)	15 (7 – 18)	13 (11 – 27)	36 (24 – 48)	48 (36 – 48)	48 (48 – 72)	53 (48 – 68)	**<0.001**
Age at Death (years), Median (IQR)	65 (60 – 71)	60 (55 – 74)	68 (61 – 70)	67 (64 – 75)	64 (60 – 65)	73 (68 – 77)	45 (28 – 63)	70 (60 – 70)	60 (40 – 70)	73 (63 – 79)	0.33
Sex, n (%)											**0.042**
Female	17 (28)	6 (50)	6 (50)	0 (0)	4 (44)	1 (25)	0 (0)	0 (0)	0 (0)	0 (0)	
Male	44 (72)	6 (50)	6 (50)	4 (100)	5 (56)	3 (75)	4 (100)	5 (100)	5 (100)	6 (100)	

[1]Kruskal-Wallis rank sum test; Fisher's exact test

FIGURES

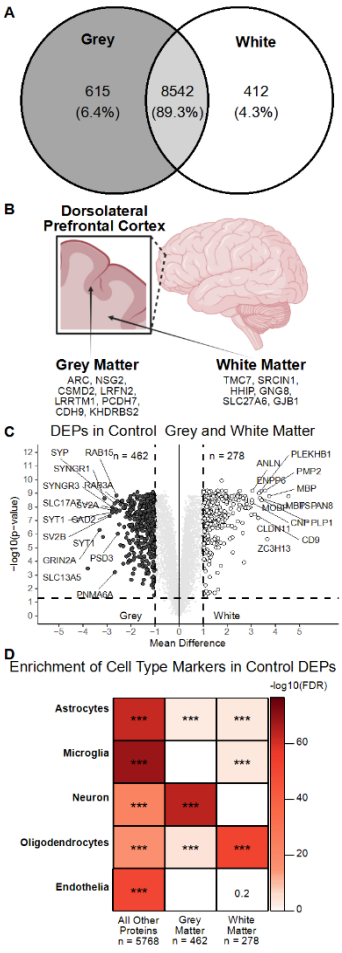

Figure 2.1. Comparison of GM and WM cell-type specific differential expression. (A) Overlap of proteins detected in GM and WM prior to removing sample outliers and proteins with high missingness. (B) Schematic demonstrating the dissection site and the unique proteins for GM and WM. Created with BioRender.com (C) Volcano plot demonstrating differentially expressed proteins in control GM and WM. Differentially expressed proteins had an absolute mean difference greater than one and a Benjamini-Hochberg FDR adjustment p-value of less than 0.05. (D) Heatmap of enrichment of cell type specific proteins in control GM and WM as determined by Fisher's Exact Test and Benjamini-Hochberg FDR p-value adjustment. * = p-value < .05, ** = p-value < .01, *** = p-value < .005.

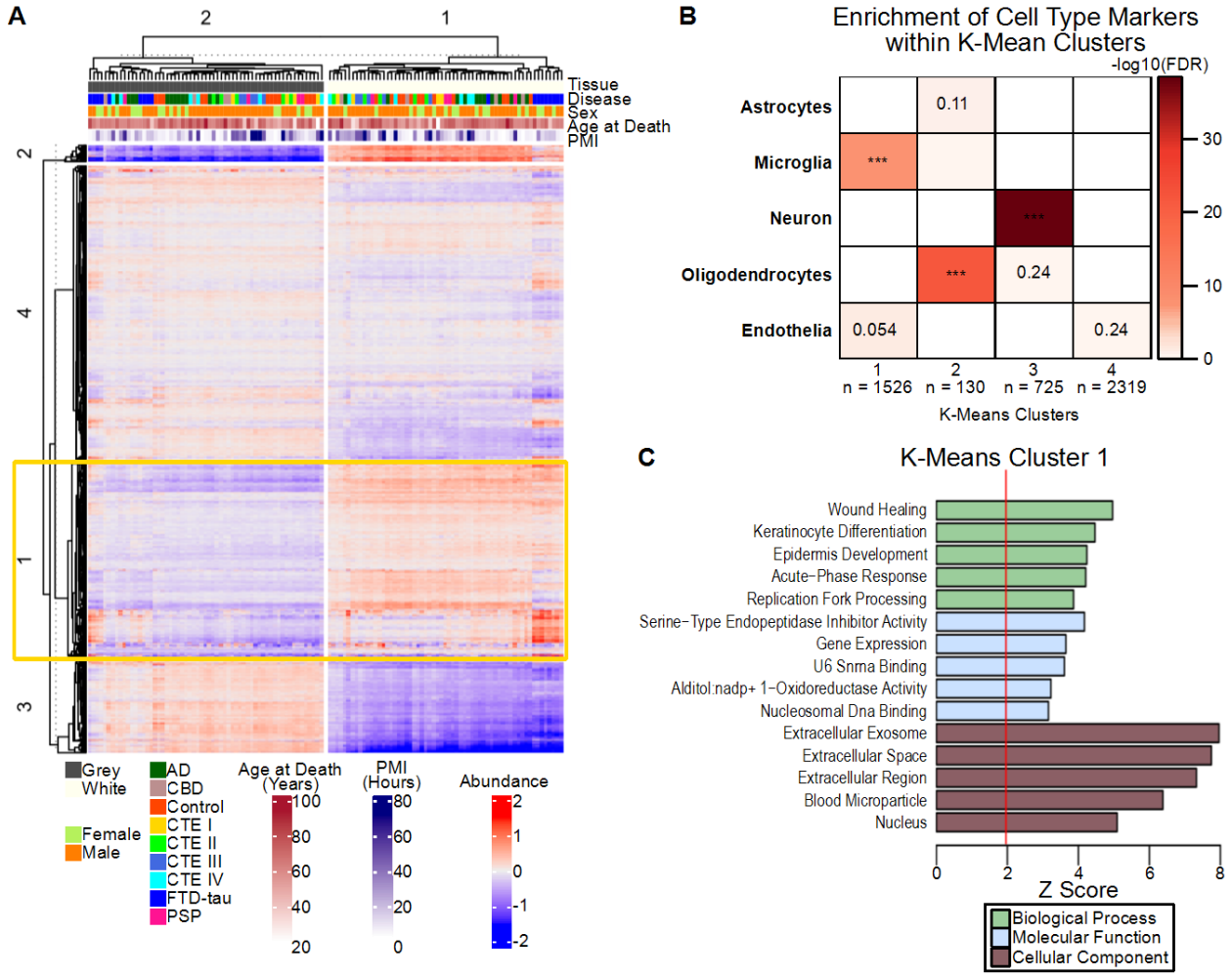

Figure 2.2 K-means clustering reveals cluster enriched with microglial and endothelial proteins. (A) Heatmap of protein abundance with k-means clusters of proteins (left) and samples (top). Cluster 1 is outlined in yellow. (B) Heatmap of enrichment of cell type specific proteins in each k-means clusters determined by Fisher's Exact Test and Benjamini-Hochberg FDR p-value adjustment. * = p-value < 0.05, ** = p-value < 0.01, *** = p-value < 0.005. (C) Top 5 (highest Z-score) gene ontology terms for each domain for k-means cluster 1.

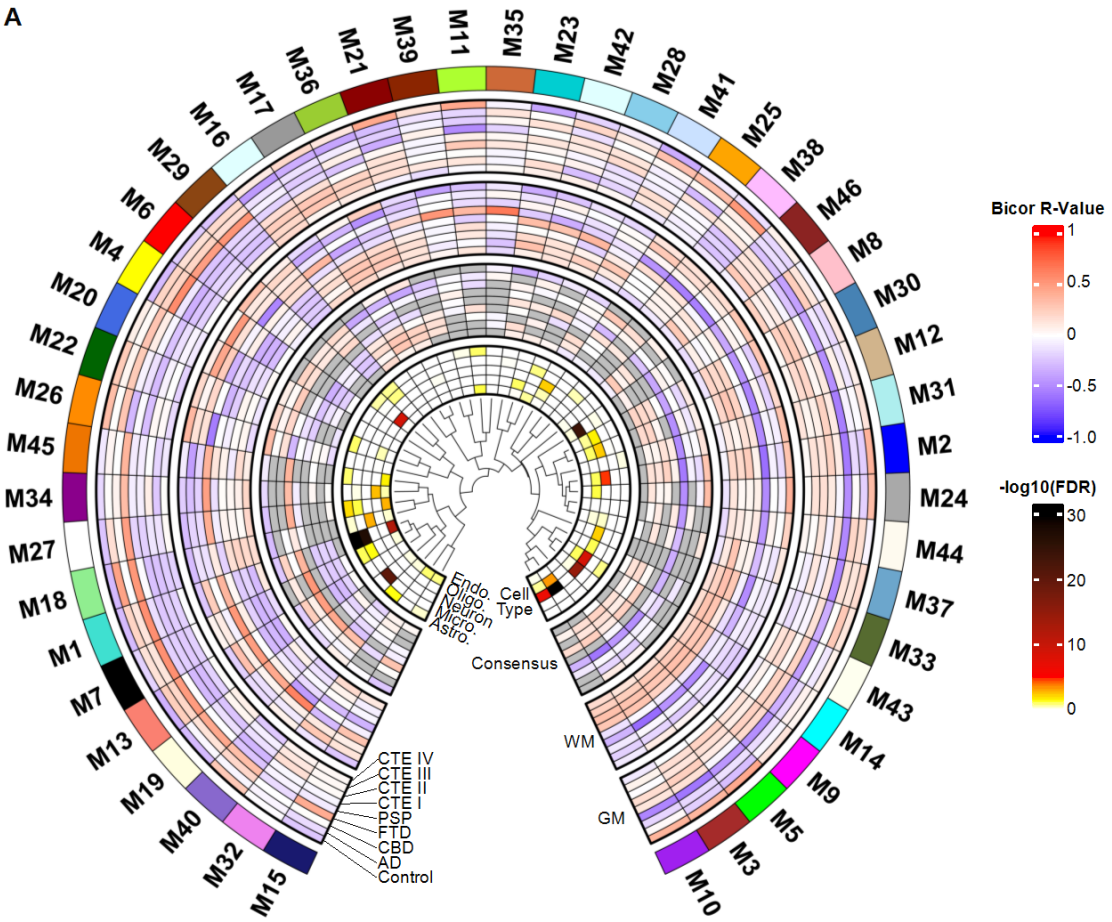

Module	Annotation
M15	Ribosome/Translation
M32	Translation
M40	
M19	Microglia/Immune System
M13	Gene Expression
M7	Nucleotide Metabolism
M1	Cell Adhesion/Integrin Signaling
M18	Neuron/GABA
M27	Extracellular Matrix/Basement Membrane
M34	Collagen
M45	Circulatory System
M26	

Module	Annotation
M22	
M20	Gene Expression
M4	Nucleosome/Regulation of Transcription
M6	
M29	
M16	Mitochondrial Gene Expression/Translation
M17	Mitochondrial Translation
M36	Mitochondrial Translation
M21	Mitochondria
M39	Mitochondria/Fatty Acid Oxidation
M11	Actin Dynamics/tRNA Aminoacylation

Module	Annotation
M35	
M23	Immunoglobulin
M42	Blood
M28	Complement/Blood
M41	Neuron/Potassium Ion Channels
M25	HSP90
M38	
M46	Translation
M8	Oligodendrocyte/Myelination
M30	Neuron/Ion Transport and Homeostasis
M12	

Module	Annotation
M31	Ubiquitination
M2	Microtubule Dynamics
M24	Dynactin Complex
M44	Cytoskeleton/Endoplasmic Reticulum
M37	Glycolysis
M33	
M43	RNA Splicing/Processing
M14	Neuron/Synapse/Development
M9	Neuron/Synapse
M5	Mitochondria/Oxidative Phosphorylation
M3	Neuron/Synapse
M10	Neuron/Synapse

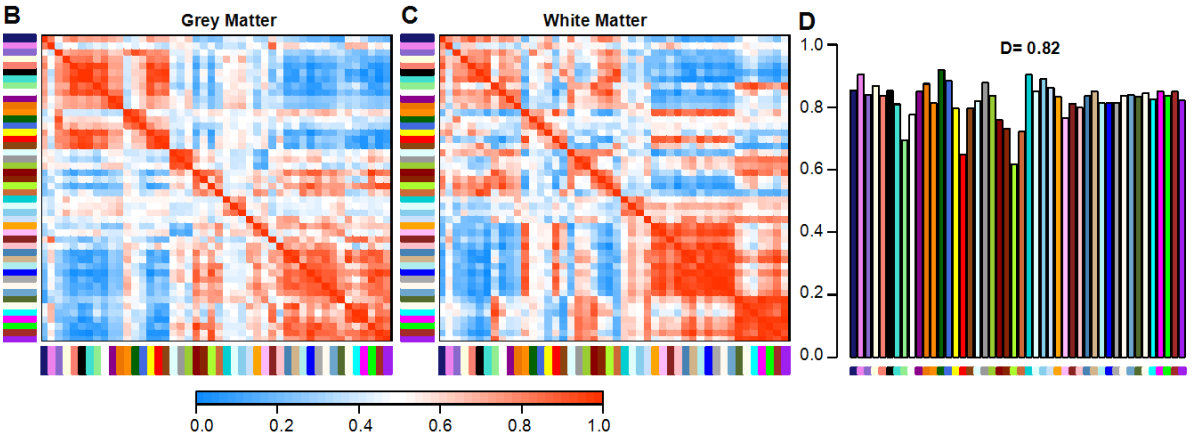

Figure 2.3. Consensus WGCNA network of human control and tauopathy GM and WM. (A) Diagram illustrating the association of each module with brain cell types and sample traits (disease group). The inner dendrogram illustrates module relatedness. The GM layer illustrates the bicorrelation of each module eigenprotein with each trait in the GM network. The WM layer illustrates the bicorrelation of each module eigenprotein with each trait in the WM network. The consensus correlation layer indicates a module's consensus correlation. If a module had a negative bicorrelation in GM and WM, then the consensus correlation was negative, and vice versa. If bicorrelations were opposite in GM and WM, then the cell is shaded grey as there is no consensus. The cell type layer indicates enrichment of each module for cell type specific proteins as determined by Fisher's Exact Test and Benjamini-Hochberg FDR p-value adjustment. The table below the diagram indicates each module's annotation. Modules were annotated based on the results of gene ontology and those with no clear ontology were not assigned an annotation. Heatmaps illustrating the adjacency or correlation of modules within the GM (C) and WM (C) networks. (D) Mean preservation of adjacency for each module eigengene to all other module eigengenes. Preservation is defined as one minus the absolute difference of the eigengene networks in the GM and WM datasets.

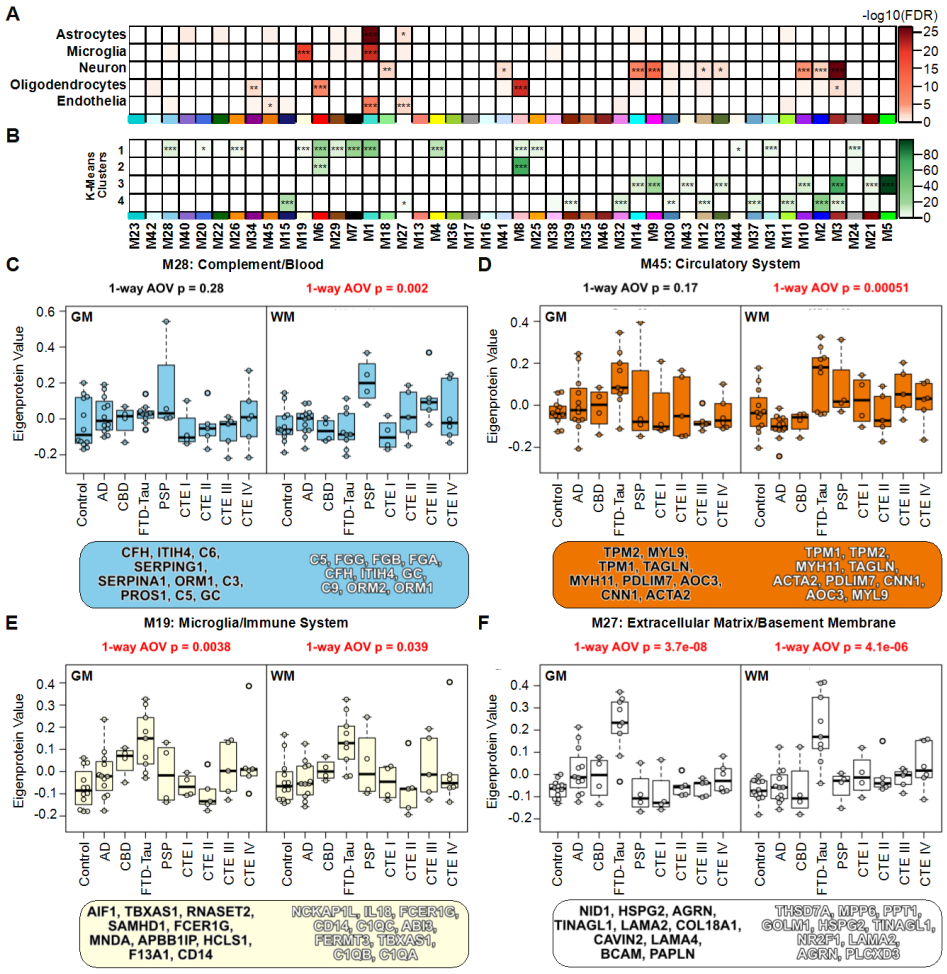

Figure 2.4. Consensus network reveals modules with unique and shared disease-associated changes. (A) Heatmap of enrichment of cell type specific proteins in in each consensus module as determined by Fisher's Exact Test and Benjamini-Hochberg FDR p-value adjustment. * = p-value < 0.05, ** = p-value < 0.01, *** = p-value < 0.005. (B) Heatmap of enrichment of k-means cluster proteins in in each consensus module as determined by Fisher's Exact Test and Benjamini-Hochberg FDR p-value adjustment. * = p-value < 0.05, ** = p-value < 0.01, *** = p-value < 0.005. (C) Boxplots of module eigenprotein values for (C) M28, (D) M45, (E) M19, and (F) M27 by disease group. Module hub proteins for each network are highlighted in black (GM) and white (WM) text in boxes below each boxplot.

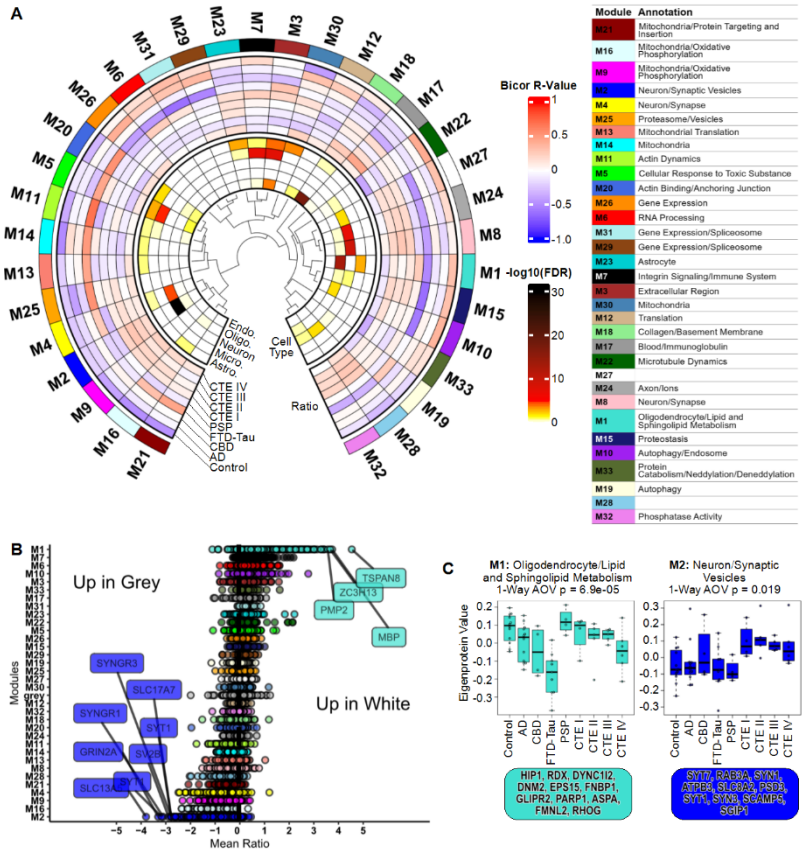

Figure 2.5. Ratio network modules with the most extreme white:grey ratios are associated with the primary cell types in GM and WM. (A) Diagram illustrating the association of each module with brain cell types and sample traits (disease group). The inner dendrogram illustrates module relatedness. The ratio layer illustrates the bicorrelation of each module eigenprotein with each trait. The cell type layer indicates enrichment of each module for cell type specific proteins as determined by Fisher's Exact Test and Benjamini-Hochberg FDR p-value adjustment. The table to the right of the diagram indicates each module's annotation. Modules were annotated based on the results of gene ontology and those with no clear ontology were not assigned an annotation. (B) Mean white:grey ratio of each protein in control samples, separated by module. Boxplots of module eigenprotein values for (C) M1 and (D) M2 by disease group. Module hub proteins are highlighted in boxes below each boxplot

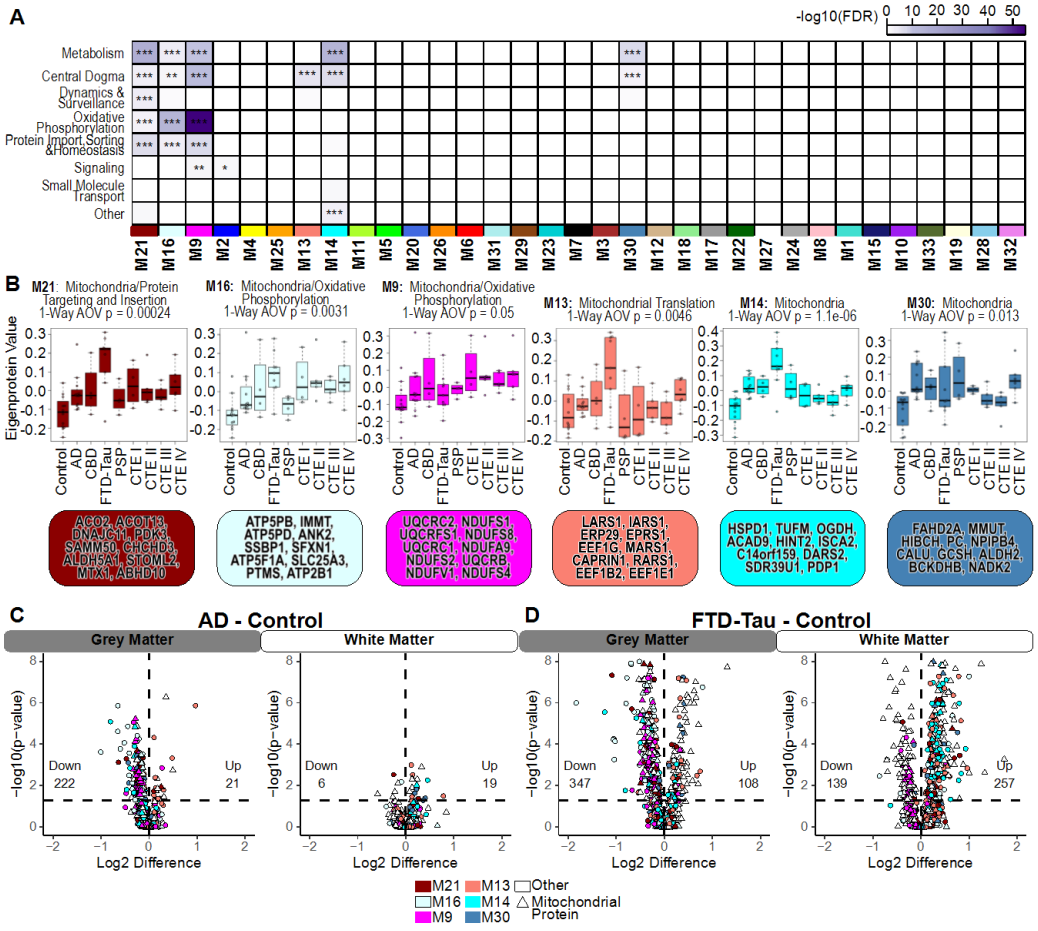

Figure 2.6. Ratio network reveals disease-associated alterations in mitochondrial proteins. (A) Heatmap of enrichment of proteins specific to mitochondrial pathways in in each ratio module as determined by Fisher's Exact Test and Benjamini-Hochberg FDR p-value adjustment. * = p-value < 0.05, ** = p-value < 0.01, *** = p-value < 0.005. (C) Boxplots of module eigenprotein values by disease group for modules enriched with mitochondrial proteins. Module hub proteins are highlighted in boxes below each boxplot. Differential expression comparing AD (C) and FTD-tau (D) tissues to control tissues within GM and WM, filtered for proteins in modules of interest (C) and mitochondrial proteins defined in Mitocarta 3.0. Colors are indicative of module membership; white indicates the protein does not belong to one of the modules of interest. Triangle shape indicates that a protein is a mitochondrial protein.

SUPPLEMENTAL FIGURES

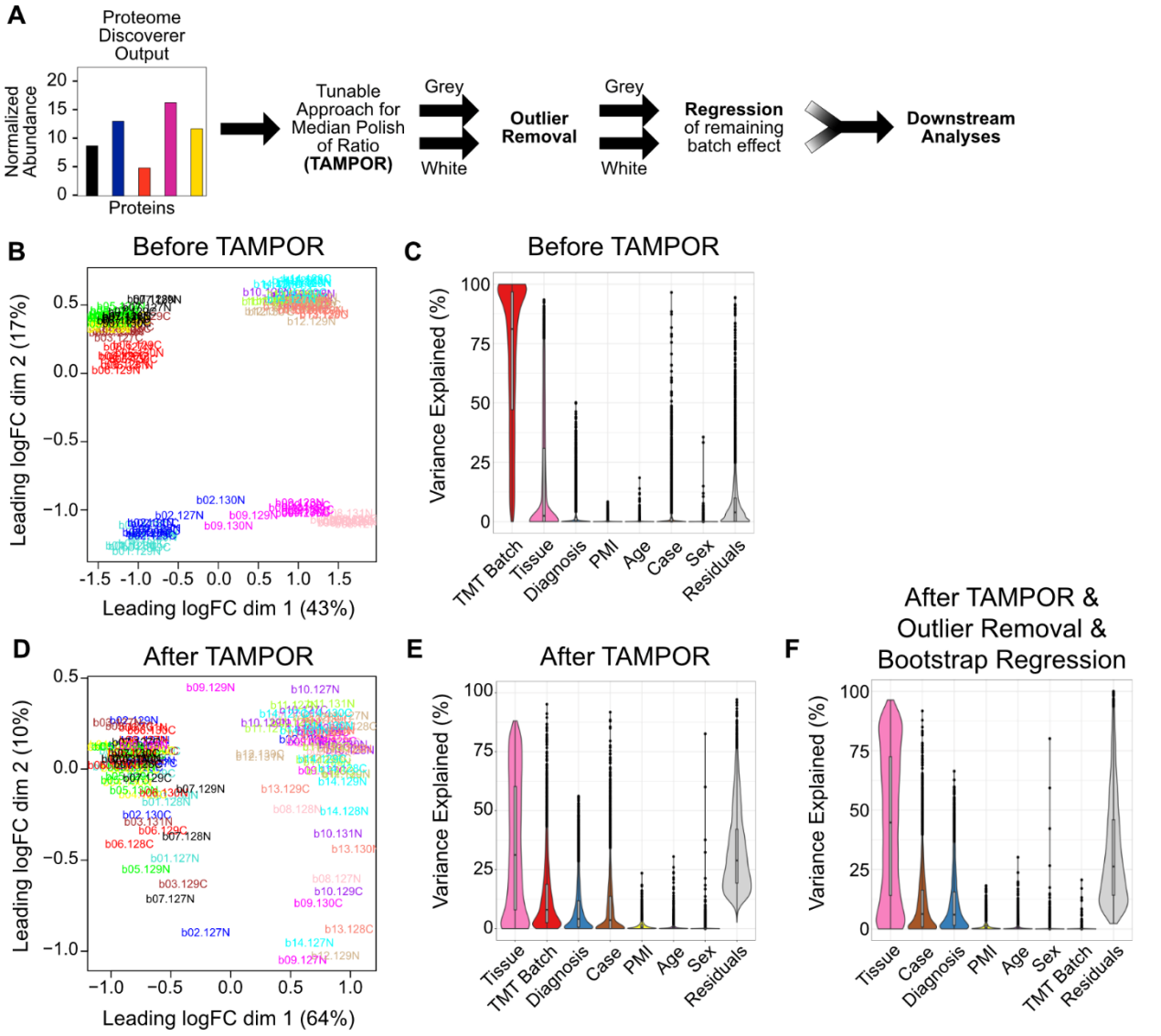

Supplementary Figure 2.1. Data processing and normalization. (A) Data processing pipeline. (B) Multidimensional scaling (MDS) plot of all samples prior to TAMPOR. Each point is a sample and each color corresponds to a TMT batch. (C) Percentage of variance explained for each protein across all covariates prior to TAMPOR. (D) MDS plot of all samples after TAMPOR. Each point is a sample and each color corresponds to a TMT batch. Percentage of variance explained for each protein across all covariates after TAMPOR (E) and after TAMPOR, outlier removal, and bootstrap regression to remove remaining any remaining batch effect (F).

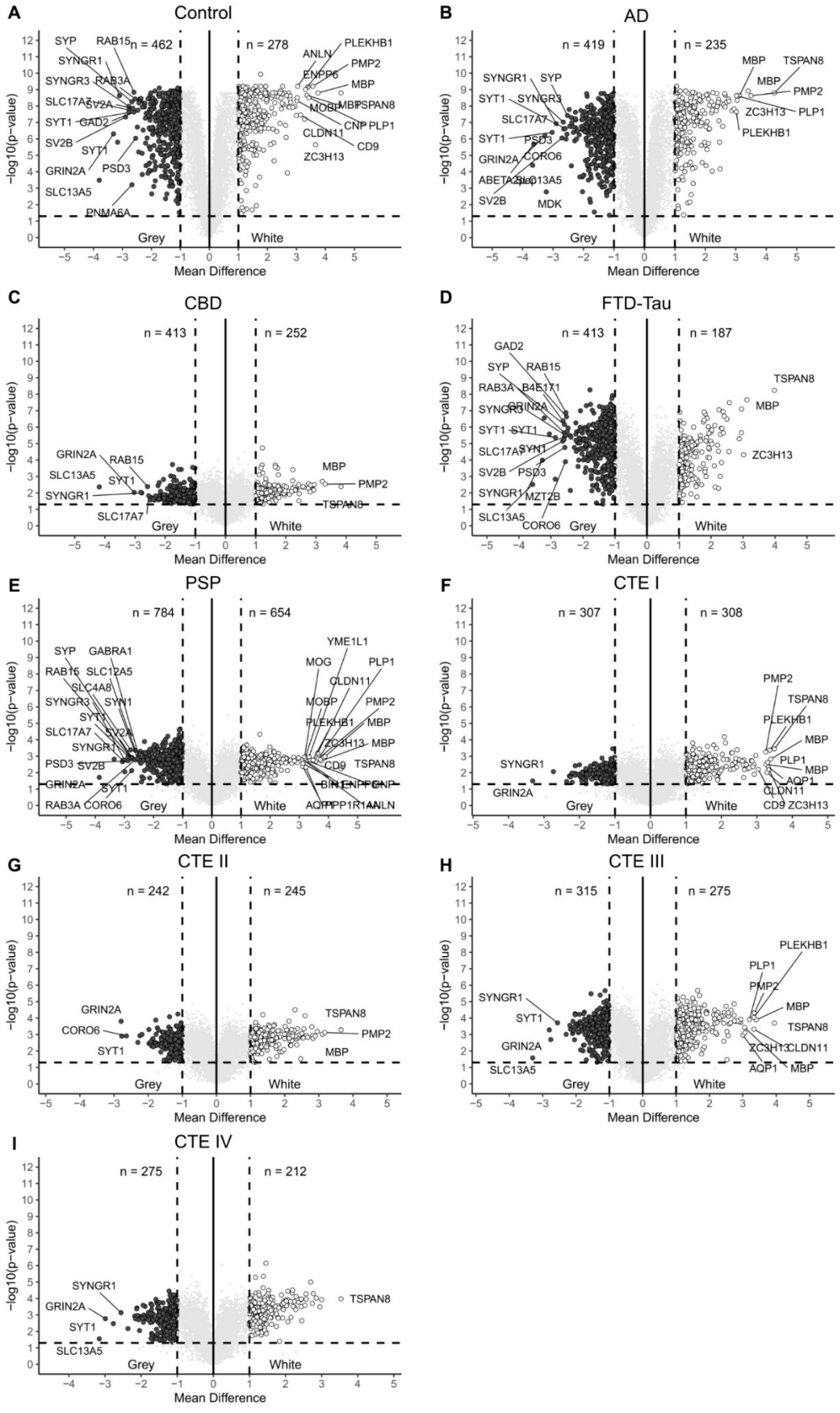
A
Control
n = 462
n = 278
SYP
RAB15
SYNGR1
SYNGR3
RAB3A
SLC17A7
SV2A
SYT1
GAD2
SV2B
SYT1
GRIN2A
PSD3
SLC13A5
PNMA6A
ANLN
PLEKHB1
PMP2
ENPP6
MBP
MOBP
TSPAN8
CNP
PLP1
CLDN11
CD9
ZC3H13
Grey
White
−log10(p−value)
Mean Difference
B
AD
n = 419
n = 235
SYNGR1
SYP
SYT1
SYNGR3
SLC17A7
SYT1
PSD3
GRIN2A
CORO6
SV2B
MDK
MBP
TSPAN8
MBP
PMP2
ZC3H13
PLP1
PLEKHB1
Grey
White
−log10(p−value)
Mean Difference
C
CBD
n = 413
n = 252
GRIN2A
RAB15
SLC13A5
SYT1
SYNGR1
SLC17A7
MBP
PMP2
TSPAN8
Grey
White
−log10(p−value)
Mean Difference
D
FTD-Tau
n = 413
n = 187
GAD2
SYP
RAB15
RAB3A
SYNGR3
SYT1
SLC17A7
SV2B
SYNGR1
SLC13A5
PSD3
MZT2B
CORO6
TSPAN8
MBP
ZC3H13
Grey
White
−log10(p−value)
Mean Difference
E
PSP
n = 784
n = 654
SYP
GABRA1
RAB15
SLC12A5
SLC4A8
SYNGR3
SYN1
SYT1
SLC17A7
SV2A
SYNGR1
PSD3
SV2B
GRIN2A
SYT1
RAB3A
CORO6
YME1L1
MOG
PLP1
CLDN11
MOBP
PMP2
PLEKHB1
MBP
ZC3H13
MBP
CD9
TSPAN8
Grey
White
−log10(p−value)
Mean Difference
F
CTE I
n = 307
n = 308
SYNGR1
GRIN2A
PMP2
TSPAN8
PLEKHB1
MBP
PLP1
MBP
AQP1
CLDN11
CD9
ZC3H13
Grey
White
−log10(p−value)
Mean Difference
G
CTE II
n = 242
n = 245
GRIN2A
CORO6
SYT1
TSPAN8
PMP2
MBP
Grey
White
−log10(p−value)
Mean Difference
H
CTE III
n = 315
n = 275
SYNGR1
SYT1
GRIN2A
SLC13A5
PLEKHB1
PLP1
PMP2
MBP
TSPAN8
ZC3H13
CLDN11
AQP1
MBP
Grey
White
−log10(p−value)
Mean Difference
I
CTE IV
n = 275
n = 212
SYNGR1
GRIN2A
SYT1
SLC13A5
TSPAN8
Grey
White
−log10(p−value)
Mean Difference

Supplementary Figure 2.2. Differential expression of GM and WM proteins. Volcano plots demonstrating differentially expressed proteins in GM (left) and WM (right) in (A) control, (B) AD, (C) CBD, (D) FTD-tau, (E) PSP, (F) CTE I, (G) CTE II, (H) CTE III, and (I) CTE IV samples. Differentially expressed proteins had an absolute mean difference greater than one and a Benjamini-Hochberg FDR adjustment p-value less than 0.05.

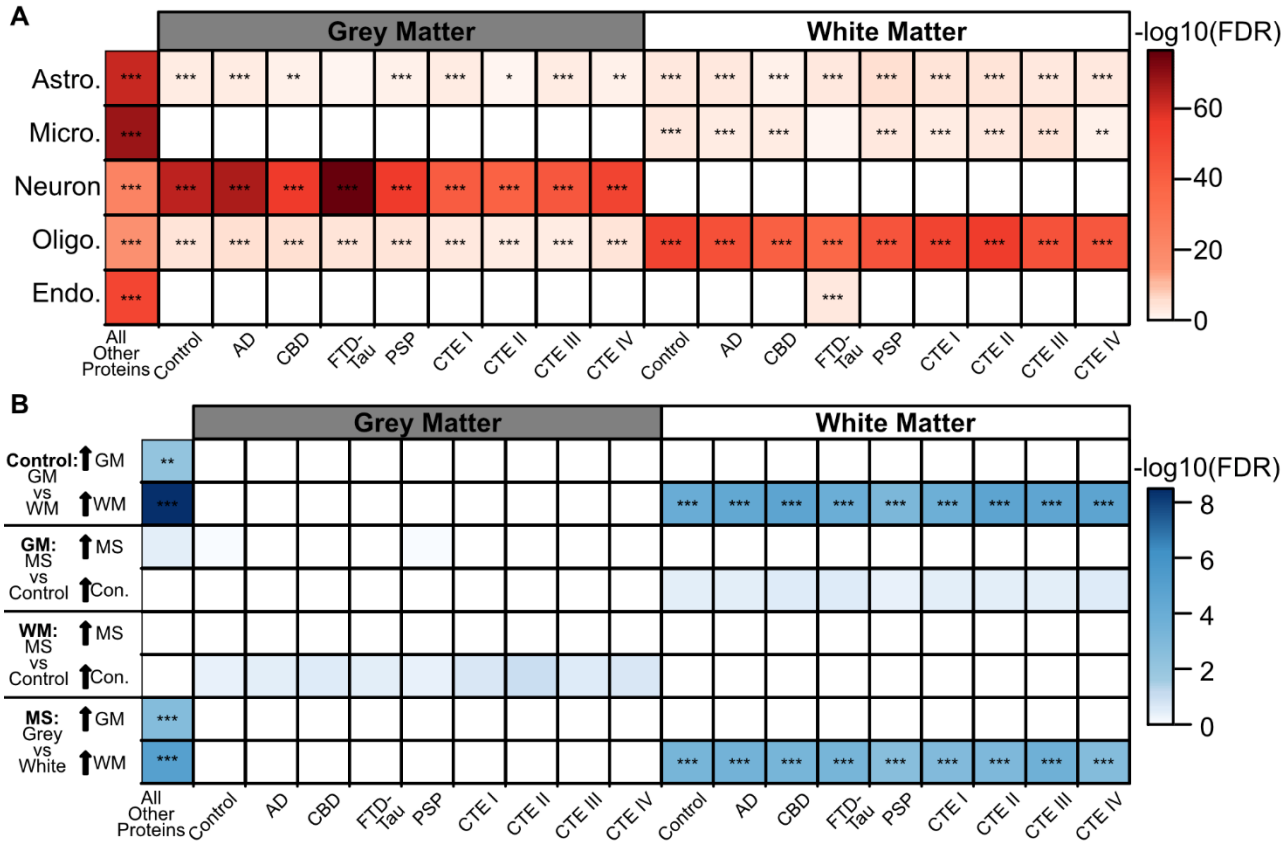

Supplemental Figure 2.3. Enrichment analyses of differentially expressed GM and WM proteins. Heatmap of enrichment of (A) cell type specific proteins and (B) microglial markers as determined by Fisher's Exact Test and Benjamini-Hochberg FDR p-value adjustment. * = p-value < 0.05, ** = p-value < 0.01, *** = p-value < 0.005.

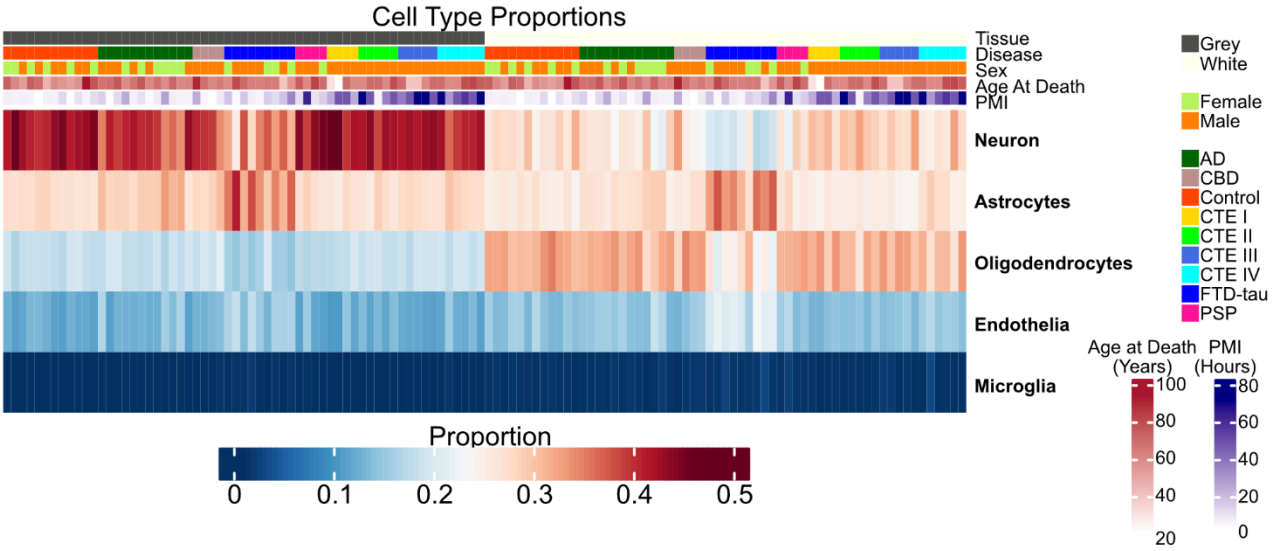

Supplemental Figure 2.4. Brain cell type proportions derived from cellular deconvolution analyses. Heatmap illustrating deconvoluted cell type proportion for each sample, including five main cell types: astrocytes, endothelia, microglia, neurons, and oligodendrocytes.

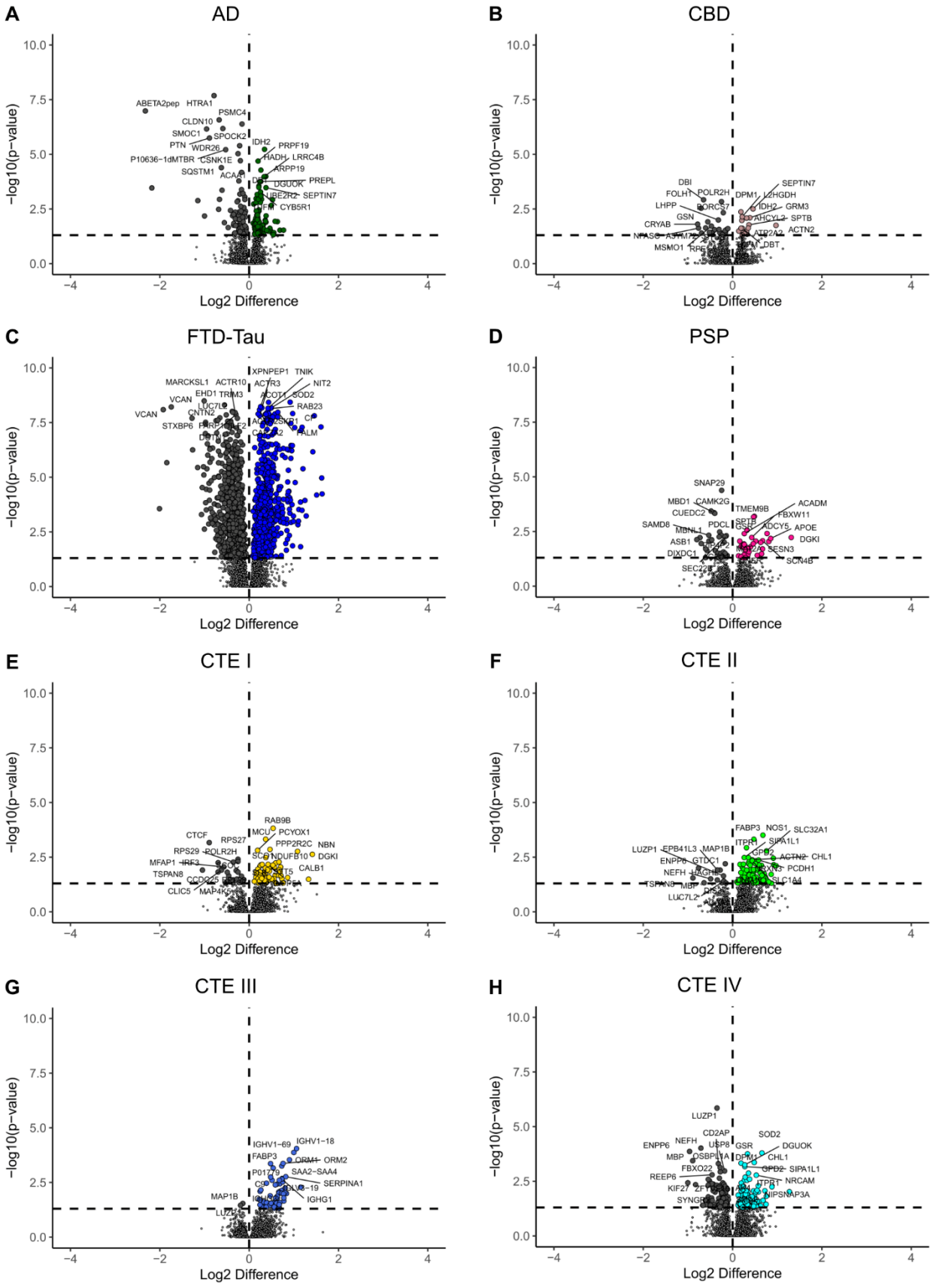
A
AD
B
CBD
C
FTD-Tau
D
PSP
E
CTE I
F
CTE II
G
CTE III
H
CTE IV
−log10(p−value)
Log2 Difference
10.0
7.5
5.0
2.5
0.0
−4
−2
0
2
4
ABETA2pep
HTRA1
PSMC4
CLDN10
SMOC1
SPOCK2
PTN
WDR26
P10636−1dMTBR
CSNK1E
SQSTM1
ACAA2
IDH2
PRPF19
HADH
LRRC4B
ARPP19
DGUOK
PREPL
UBE2R2
SEPTIN7
CYB5R1
DBI
FOLH1
POLR2H
DPM1
L2HGDH
LHPP
RORC57
IDH2
GRM3
GSN
AHCYL2
SPTB
CRYAB
ATP2A2
ACTN2
MSMO1
DBT
XPNPEP1
TNIK
MARCKSL1
ACTR10
ACTR3
NIT2
EHD1
TRM3
ACOT1
SOD2
VCAN
LUC7L
RAB23
CNTN2
STXBP6
CALM
SNAP29
MBD1
CAMK2G
ACADM
CUEDC2
TMEM9B
FBXW11
SAMD8
PDCL
SEPTB
APOE
MBNL1
ADCY5
DGKI
ASB1
DIXDC1
SESN3
SCN4B
SEC22B
RAB9B
MCU
PCYOX1
CTCF
RPS27
PPP2R2C
NBN
RPS29
POLR2H
NDUFB10
DGKI
MFAP1
IRF3
CALB1
TSPAN8
CCDC25
CLIC5
MAP4K5
FABP3
NOS1
SLC32A1
ITPR1
SIPA1L1
LUZP1
EPB41L3
MAP1B
ACTN2
CHL1
ENPP6
GTDC1
NEFH
PCDH1
TSPAN8
MBP
LUC7L2
IGHV1−69
IGHV1−18
FABP3
ORM1
ORM2
P01279
SAA2−SAA4
SERPINA1
MAP1B
IGHG1
LUZP1
CD2AP
SOD2
ENPP6
NEFH
USP8
GSR
DGUOK
MBP
OSBPL11A
CHL1
FBXO22
SPD2
SIPA1L1
REEP6
NRCAM
KIF27
ITPR1
SYNGR1
NIPSNAP3A

Supplemental Figure 2.5. Differential expression of WM:GM protein ratios in disease. Volcano plots demonstrating differentially expressed protein ratios in (A) AD, (B) CBD, (C) FTD-tau, (D) PSP, (E) CTE I, (F) CTE II, (G) CTE III, and (H) CTE IV samples, as compared to control. Within each volcano plot, colored points on the right indicate proteins with higher WM:GM ratios in the disease state. Grey points on the left indicate proteins with lower WM:GM ratios in the disease state. Differentially expressed protein ratios had a Benjamini-Hochberg FDR adjustment p-value less than 0.05.

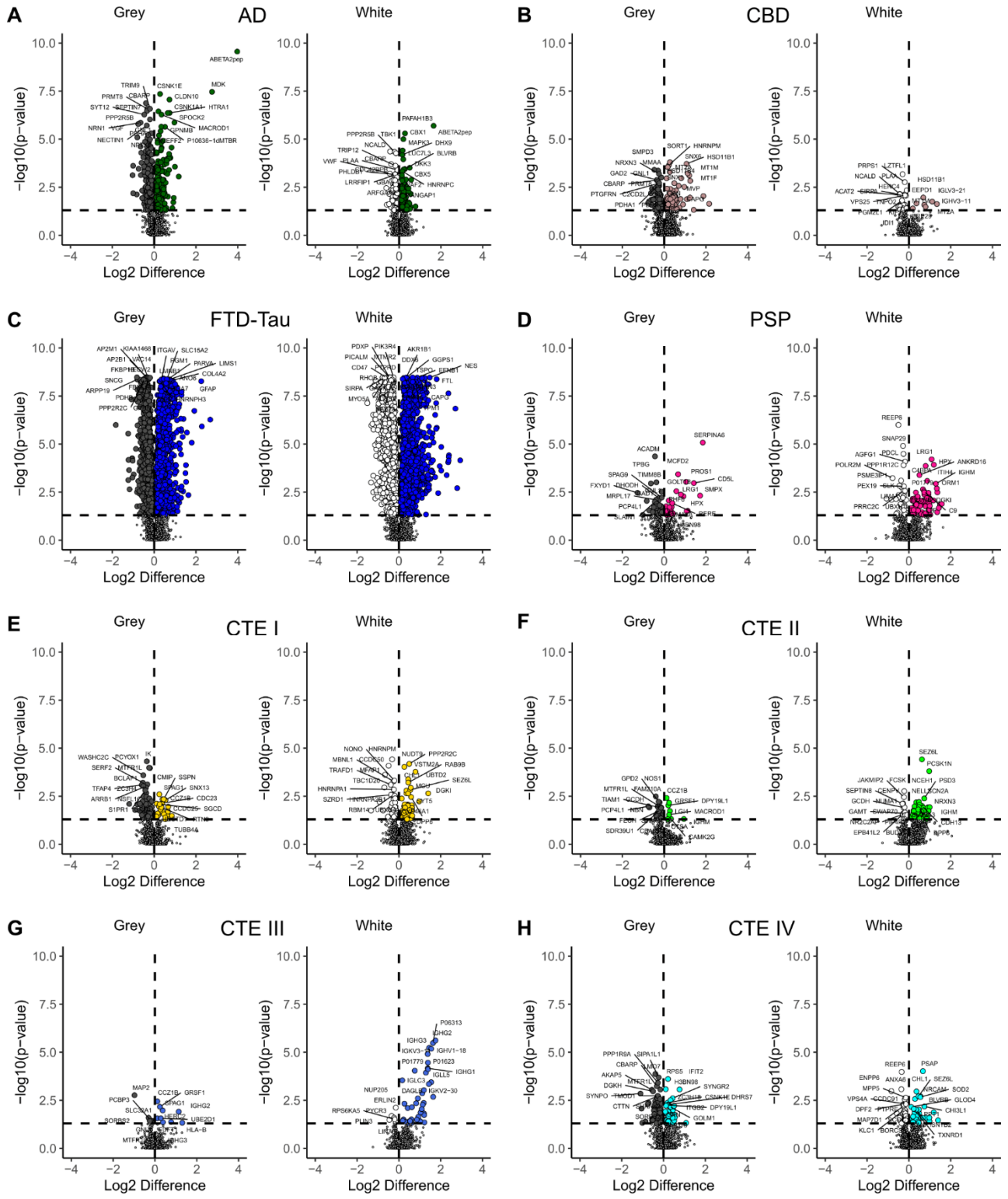
A
Grey
AD
White
B
Grey
CBD
White
C
Grey
FTD-Tau
White
D
Grey
PSP
White
E
Grey
CTE I
White
F
Grey
CTE II
White
G
Grey
CTE III
White
H
Grey
CTE IV
White
−log10(p−value)
Log2 Difference

Supplemental Figure 2.6. Differential expression of proteins in disease. Volcano plots demonstrating differentially expressed proteins in GM (left) and WM (right) in (A) AD, (B) CBD, (C) FTD-tau, (D) PSP, (E) CTE I, (F) CTE II, (G) CTE III, and (H) CTE IV samples, as compared to control. Within each volcano plot, colored points on the right indicate proteins upregulated in the disease state. Grey or white points on the left indicate proteins downregulated in the disease state. Differentially expressed proteins had a Benjamini-Hochberg FDR adjustment p-value less than 0.05.

SUPPLEMENTAL FILES

Supplemental File 2.1. Top GO terms within each K-Means cluster.

Supplemental File 2.2. Top GO terms within each consensus network module.

Supplemental File 2.3. Top GO terms within each ratio network module.

Supplemental File 2.4. Consensus network module eigenprotein boxplots and iGraphs.

Supplemental File 2.5. Ratio network module eigenprotein boxplots and iGraphs.

CHAPTER 3: GLIAL PROFILING OF HUMAN TAUOPATHY BRAIN DEMONSTRATES ENRICHMENT OF ASTROCYTIC TRANSCRIPTS IN TAU-RELATED FRONTOTEMPORAL DEGENERATION

3.1 CONTEXT, AUTHOR'S CONTRIBUTION, AND ACKNOWLEDGMENT OF REPRODUCTION

This chapter describes glial transcript expression in control and tauopathy human brain. The dissertation author contributed to design and execution of experiments, analysis of data, and writing the manuscript under the guidance of Dr. Chad Hales. James Webster contributed to conducting experiments. This chapter is reproduced from Johnson AG, Webster JA, Hales CM (2022) Glial profiling of human tauopathy brain demonstrates enrichment of astrocytic transcripts in tau-related frontotemporal degeneration. *Neurobiol Aging.*

3.2 ABSTRACT

To understand how glia may be altered in frontotemporal degeneration with tau pathology (FTD-tau), we used a NanoString glial profiling panel to measure 770 transcripts related to glial biology in human control (n = 8), Alzheimer's disease (AD) (n = 8), and FTD-tau (n = 8) dorsolateral prefrontal cortex. Compared to control, 43 genes were upregulated and 86 genes were downregulated in the FTD-tau samples. Only 3 genes were upregulated and 2 were downregulated in AD. Pathway analysis revealed many astrocyte-, microglia-, and oligodendrocyte-related pathway scores increased in FTD-tau, while neuron-related pathway scores decreased. We compared these results to a previously published proteomic dataset containing many of the same samples and found that the targeted panel approach obtained measurements for genes whose proteins were not measured in the proteomics. Our results point to the utility of multi-omic approaches and marked dysregulation of glia in FTD-tau.

3.3 INTRODUCTION

Frontotemporal degeneration (FTD) is a clinically, pathologically, and genetically heterogeneous spectrum of disorders characterized by protein accumulations and degeneration of the

frontal and temporal lobes (Onyike and Huey, 2013; Olney et al., 2017). As the second most common form of dementia in people under 65 years of age, FTD results in a dramatic deviation from the neurotypical aging process (Onyike and Diehl-Schmid, 2013). Symptoms include a variety of behavioral and personality changes, memory impairments, and language deficits (Woollacott and Rohrer, 2016; Olney et al., 2017). Almost half of all FTD cases have abnormal accumulations of tau (FTD-tau). FTD-tau can be sporadic or inherited due to mutations in the gene that encodes for the tau protein, microtubule associated protein tau (*MAPT*) (Hock and Polymenidou, 2016; Oeckl et al., 2016). In FTD-tau, tau can accumulate in neurons as well as in glia, particularly in astrocytes and oligodendrocytes (Taniguchi et al., 2004; Ghetti et al., 2015). Whether glial tau pathology arises via cell autonomous or cell non-autonomous mechanisms is debated (Li and Haney, 2020), and the role of glia in tau-mediated neurodegenerative processes is an active topic of investigation.

Previously, we used tandem mass tagged (TMT) labeling and mass spectrometry to examine the total proteome of human control and tauopathy brain, including chronic traumatic encephalopathy (CTE) and FTD-tau (Gutierrez-Quiceno et al., 2021). Through differential expression and cell subtype analysis, we identified unique enrichment of glial proteins, particularly astrocytic and microglial proteins, in the FTD-tau samples relative to control. However, whether this enrichment reflects a proliferation of glial cells or a transition in the protein expression profile of glial cells is unclear. Furthermore, if this enrichment does indeed reflect a change in the molecular profile of these glial cells, it is unknown if this profile is similar to previously published phenotypes of glial cells such as A1/A2 astrocytes (Liddelow et al., 2017) or disease associated microglia (DAM) (Keren-Shaul et al., 2017). These and other characterizations of glial molecular profiles are most often defined by RNA expression (Zamanian et al., 2012; Clarke et al., 2018; Diaz-Castro et al., 2019). Since, transcriptomic and proteomic data are often discordant (Wang et al., 2019;

Mangleburg et al., 2020), we sought to further examine glia in FTD-tau using a targeted, transcriptomic approach.

To determine how glia in FTD-tau may differ from those in Alzheimer's disease (AD) and control human dorsolateral prefrontal cortex (DLPFC), we used the NanoString nCounter glial profiling panel to examine the expression of 770 genes involved in glial biology. We then compared this targeted transcriptome with the corresponding proteome to determine concordance and to measure unique glial transcriptomic changes. Defining similar and unique proteome to transcriptome changes could provide additional insights into FTD pathophysiology.

3.4 MATERIALS AND METHODS

3.4.1 Collection of postmortem brain tissue

Postmortem brain tissue was obtained from the Emory Goizueta Alzheimer's Disease Research Center Neuropathology Brain Bank in Atlanta, Georgia. Brains were collected from deceased subjects following Institutional Review Board protocols under which consent was obtained from the subjects' family. Brain hemispheres were separated such that one hemisphere was stored in coronal sections at -80 ˚C and the other hemisphere was fixed for immunohistochemistry. For this study, we used samples of DLPFC from fresh, frozen human brain. Research subjects were selected based on neuropathological diagnosis (control, AD, and FTD-tau) and demographics. Neuropathological diagnosis was carried out by board-certified neuropathologists and was determined via standard immunohistochemical methods including hematoxylin, eosin, and silver-staining as well as more targeted labeling for amyloid beta 42, hyperphosphorylated tau, alpha-synuclein, and phosphorylated TDP43. The AD samples were all Braak stage VI and had a CERAD score of 3. The FTD-tau group was composed of six samples collected from subjects with a mutation in the *MAPT* gene, and two samples collected from subjects with a neuropathological

diagnosis of Pick's disease. Five of the donors had P301L tau mutations and one donor had an R406W tau mutation. The P301L *MAPT* mutation generates primarily 4R tau pathology (Hutton et al., 1998) while R406W a mixed 3R/4R tau pathology (Ghetti et al., 2015). Pick's disease is a 3R tauopathy (Delacourte et al., 1998). Samples were matched across disease group for age and sex (Table 3.1).

3.4.2 RNA isolation and NanoString nCounter glial profiling panel

30 to 50 milligrams of frozen DLPFC, primarily gray matter, was homogenized in one milliliter of Trizol with a bullet blender. Chloroform and centrifugation were used to obtain an aqueous phase containing RNA. The aqueous phase was mixed 1:1 in 100% ethanol and then processed with the Quick-RNA Miniprep Kit (Zymo Research, USA). RNA was eluted in nuclease free water and stored at -80 ˚C until analysis. Quality of the RNA was determined by the Emory Integrated Genomics Core. All samples had concentrations greater than 20 ng/ul and DV_{200} values greater than 20%, per manufacturer's recommendation. Samples from each disease group were randomly distributed across two nCounter Human glial profiling panels (NanoString, USA) and run on an nCounter FLEX Analysis System (NanoString, USA).

3.4.3 Analysis of glial profiling panel results and comparison with corresponding proteome

Raw data were imported into nSolver 4.0 and analyzed via the nCounter Advanced Analysis plugin (version 2.1.134) to normalize the data (Supplementary File 3.1) and conduct differential expression (Supplementary File 3.2), pathway scoring (Supplementary File 3.3), and cell type profiling analyses (Supplementary File 3.4). Covariates included disease (control, AD, and FTD-tau) and cartridge ID (to control for batch effects). All samples passed the quality control analysis conducted by the Advanced Analysis plugin (Figure 3.1A). Differential expression was calculated using disease as the predictor variable and the cartridge ID as the confounder variable. P-values

were adjusted for multiple tests using the Benjamini-Yekutieli (BY) method.

We performed comparisons between the results of the glial profiling panel and a published proteomic dataset that included 11 out of 24 of the samples used for the glial panel (Gutierrez-Quiceno et al., 2021). First, we compared the number of genes measured (above threshold) via the glial panel with the number of proteins measured in our proteomic experiments, prior to batch correction. We then compared the number of above threshold genes with the number of measured proteins after batch correction. We also compared the number of significant differentially expressed genes with the number of significant differentially expressed proteins. Finally, we correlated $\log_2$ fold change values of differentially expressed genes and proteins in FTD-tau.

3.4.4 Statistical analysis and visualization methods

R (version 4.1.1) was used for statistical analysis and data visualization. To test for a difference in mean pathway score and cell type score between groups, we used One-Way Analysis of Variance (ANOVA) and p-values were adjusted for multiple tests using the BY method. We used pairwise t-tests for post-hoc comparisons and used the BY method to adjust for multiple tests. Correlations were performed using the Pearson method. Boxplots and scatterplots were created using the ggplot2 package (Wickham, 2016) and venn diagrams were created using the VennDiagram package (Chen and Boutros, 2011). Gene ontology (GO) analyses were conducted using the gprofiler2 package using the g:SCS multiple testing correction with significance threshold of .05 (Raudvere et al., 2019).

3.5 RESULTS

3.5.1 Glia- and neuron-associated transcripts display opposite patterns of differential expression in FTD-tau relative to control.

We previously performed TMT quantitative proteomics on human DLPFC and temporal cortex on 83 samples of tauopathy including CTE, FTD-tau (inherited and sporadic), progressive supranuclear palsy (PSP), corticobasal degeneration (CBD), as well as control cases (Gutierrez-Quiceno et al., 2021). Through differential expression and weighted correlation network analysis (WGCNA), we found that FTD-tau and FTD-MAPT samples were enriched with glia-associated proteins, especially from astrocytes (Gutierrez-Quiceno et al., 2021). Whether this pattern of increased glia associated proteins was also reflected in the transcriptome was unclear. To assess the expression of glial-specific genes in FTD-tau, we used a glial profiling panel to measure 770 genes related to glial biology in human control (N = 8), AD (N=8), and FTD-tau (N=8) brain. No significant differences were found between groups in post-mortem interval (PMI), APOE genotype, and race (Table 3.1). Samples loosely clustered by disease group but not by cartridge ID (Figure 3.1A). Expression data were normalized (Figure 3.1B, Supplementary File 3.1) for subsequent differential expression and pathway analysis (Figures 3.2 – 3.6). Finally, histograms of p-value frequency with co-variates cartridge ID (Figure 3.1C) and disease group (Figure 3.1D) showed that disease group is associated with lower (more significant) p-values while cartridge ID was not, indicating that there was not a significant batch effect on expression data.

For differential expression analysis, the AD and the FTD-tau groups were compared separately to the control group (Supplementary File 3.2). Three genes were upregulated, and two genes were downregulated in AD relative to control (Figures 3.2A, 3.2C). When comparing FTD-tau to control, 43 genes were upregulated and 86 genes were downregulated (Figures 3.2B, 3.2D, and

3.2E). Interestingly, 10 of the 20 most upregulated (by log_2 fold change value) genes in FTD-tau relative to control were a part of at least one astrocyte-related pathway (Figure 3.2D). A majority of the top 20 most downregulated genes (by log_2 fold change value) in FTD-tau relative to control were associated with pathways related to neuronal signaling, synapses, and cytoskeletal dynamics (Figure 3.2E).

3.5.2 Glia-associated, particularly astrocytic, pathway scores, are increased in FTD-tau samples relative to control.

Next, we compared the pathway scores of the samples in each disease group to gain a higher-level understanding of how differential expression patterns between disease groups impacted biological processes (Supplementary File 3.3). Pathway scores are greatly influenced by differential expression, and increased scores typically represent elevated expression of the pathway genes. Out of 55 total pathways, there were significant differences between disease groups in 39 pathways (Supplemental Table 3.1). Post-hoc testing revealed that there was a significant difference between control and FTD-tau in all 39 of the significant pathways but no significant differences between control and AD nor AD and FTD-tau.

3.5.2.1 Neuronal pathways

Most pathway scores were lower in the FTD-tau group relative to control for neuronal processes. Representative pathways like neuroactive ligands and receptors (Figures 3.3A, 3.3B, and 3.3C) and neurotrophin signaling (Figures 3.3D, 3.3E, and 3.3F) displayed this pattern of gene expression. In both pathways, all but one of the FTD-tau samples clustered together (Figures 3.3A and 3.3D). The FTD-tau group had lower neuroactive ligands and receptors (Figure 3.3B) and neurotrophin signaling pathway (Figure 3.3E) scores. The decrease in the neuroactive ligand and receptor pathway scores in the FTD-tau group relative to control is driven by a significant

differential decrease in expression of glycine, glutamate, and GABA receptors and receptor subunits (*GLRA3*, *GABRA4*, *GABRG2*, *GABRB3*, *GRIA3*) which were decreased by $\log_2$ fold change values of -1.41 (BY p-value = 0.00546), -1.2 (BY p-value = 0.00647), -1.74 (BY p-value = 0.0193), -1.16 (BY p-value = 0.0338), and -0.98 (BY p-value = 0.0193), respectively (Figure 3.3C). The decrease in the neurotrophin signaling pathway scores in the FTD-tau group relative to control is driven by a significant differential decrease in expression of the kinases glycogen synthase kinase 3 (*GSK3B*) and cyclin dependent kinase 5 regulatory subunit 1 (*CDK5R1*) as well as SHC-transforming protein 3 (*SHC3*), which were decreased by $\log_2$ fold change values of -0.558 (BY p-value = 0.00689), -0.867 (BY p-value = 0.0227), and -0.925 (BY p-value = 0.0181), respectively (Figure 3.3F).

3.5.2.2 Oligodendrocyte pathways

Conversely, pathway scores were higher in the FTD-tau group relative to control for pathways associated with oligodendrocytes, microglia, and astrocytes. Representative pathways like oligodendrocyte differentiation and maturation (Figures 3.4A, 3.4B, and 3.4C) and myelogenesis (Figures 3.4D, 3.4E, and 3.4F) displayed this pattern of gene expression. In both pathways, all but two of the FTD-tau samples clustered together (Figures 3.4A and 3.4D). The FTD-tau group had higher oligodendrocyte differentiation and maturation (Figure 3.4B) and myelogenesis pathway (Figure 3.4E) scores. The increased oligodendrocyte differentiation and maturation pathway scores in the FTD-tau group were likely driven by the increased differential expression of SRY-box transcription factor 9 (*SOX9*) and gelsolin (*GSN*), which were upregulated by a $\log_2$ fold change value of 1.34 (BY p-value = 0.00647) and 1.7 (BY p-value = 0.00514), respectively (Figure 3.4C). The increased myelogenesis pathway scores in the FTD-tau group are driven by the increased

differential expression of peripheral myelin protein 22 (*PMP22*) which was upregulated by a $\log_2$ fold change value of 1 (BY p-value = 0.0108).

3.5.2.3 Microglial pathways

For microglia, representative pathways included microglial markers (Figures 3.5A, 3.5B, and 3.5C) and primed microglia (Figures 3.5D, 3.5E, and 3.5F). FTD-tau samples tended to cluster near the AD samples (Figures 3.5A and 3.5D). The FTD-tau group had higher microglial markers (Figure 3.5B) and primed microglia pathway (Figure 3.5E) scores relative to control. Both pathways shared increased differential expression of several genes including of colony stimulating factor 1 receptor (*CSF1R*) and ras homolog family member B (*RHOB*) which were increased by a $\log_2$ fold change value of 1.53 (BY p-value = 0.00679), and 1.22 (BY p-value = 0.0334), respectively. Additionally, the increased microglial markers pathway scores in the FTD-tau group were also driven by the increased differential expression of plexin domain containing 2 (*PLXDC2*), and MAF BZIP transcription factor B (*MAFB*) which were upregulated by a $\log_2$ fold change value of 1.12 (BY p-value = 0.00514) and 0.973 (BY p-value = 0.00647), respectively (Figure 3.5C). The increased primed microglia pathway scores in the FTD-tau group were also driven by increased differential expression of secreted protein acidic and rich in cysteine (*SPARC*) and granulin (*GRN*) which were upregulated by a $\log_2$ fold change value of 1.82 (BY p-value = 0.00514) and 0.849 (BY p-value = 0.00514), respectively (Figure 3.5F).

3.5.2.4 Astrocyte pathways

Finally, for astrocytes, representative pathways included astrocyte differentiation and function (Figures 3.6A, 3.6B, and 3.6C) and astrocyte markers (Figures 3.6D, 3.6E, and 3.6F). In these pathways, the FTD-tau groups did not cluster as well together but the heatmaps showed increased expression for many of the genes in these pathways (Figures 3.6A and 3.6D). The FTD-tau group

had higher astrocyte differentiation and function (Figure 3.6B) and astrocyte markers pathway (Figure 3.6E) scores relative to control. Both pathways shared increased differential expression of glial fibrillary acidic protein (*GFAP*) which was increased by a $\log_2$ fold change value of 2.78 (BY p-value = 0.00514). In fact, *GFAP* was the most upregulated gene (by $\log_2$ fold change value) in the FTD-tau group relative to control. Additionally, the increased astrocyte differentiation and function pathway scores in the FTD-tau group relative to control were driven by increased differential expression of epidermal growth factor receptor (*EGFR*) and toll-like receptor 4 (*TLR4*) which were increased by a $\log_2$ fold change value of 1.18 (BY p-value = 0.00514) and 1.46 (BY p-value = 0.00647), respectively (Figure 3.6C). The increased astrocyte markers pathway scores in the FTD-tau group relative to control were driven by increased differential expression of complement component 4 A/B (*C4A/B*) and ADCYAP receptor type 1 (*ADCYAP1R1*) which were increased by a $\log_2$ fold change value of 2.75 (BY p-value = 0.00514) and 1.18 (BY p-value = 0.00514), respectively (Figure 3.6F).

3.5.3 Cell type analysis reveals enrichment of astrocytic transcripts in FTD-tau.

We used a cell type analysis to determine whether the disease group impacted enrichment or depletion of specific cell types (Supplemental Table 3.2, Supplementary File 3.4). Quality control (Figure 3.7A) led us to focus only on astrocytes (Figure 3.7B), endothelial cells (Figure 3.7C), macrophages and microglia (Figure 3.7D), and oligodendrocytes (Figure 3.7E). After adjusting for multiple comparisons, the only significant difference in cell type score between disease groups was identified in astrocytes (one way ANOVA p = .01319). Post-hoc testing determined that the FTD-tau group was enriched in astrocytic transcripts relative to the control (adjusted p-value = 0.000527) and AD (adjusted p-value = 0.02915) groups. This significant increase in astrocyte cell

type score follows the same pattern of increase as observed in astrocytic pathways (Figure 3.6) and is likely driven by increased expression of known astrocyte markers.

3.5.4 Comparison of proteomic and glial profiling panel results

Finally, we examined the concordance between the transcriptomic and proteomic approaches (Gutierrez-Quiceno et al., 2021). There were 584 genes/proteins common (overlapping) between the above threshold genes in the glial panel and all the proteins measured (prior to batch correction) (Figure 3.8A). 103 genes were measured by the glial panel that were not measured in the proteomic experiments (unique glial panel). Gene ontology (GO) analyses of the unique glial panel genes and the overlapping genes/proteins revealed that the unique glial panel genes were more likely to encode for proteins that localize to the plasma membrane (Figure 3.8A, Supplemental Figure 3.1). This pattern of unique glial panel genes being primarily membrane-bound continued when we compared our glial panel dataset to only proteins that survived batch correction (Figure 3.8B, Supplemental Figure 3.2). However, when we compared only significant genes and proteins, this pattern disappeared and the GO terms for cellular component were more heterogeneous (Figure 3.8C, Supplemental Figure 3.3).

Finally, the $\log_2$ fold change values of genes and proteins were positively correlated (Figure 3.9A, Pearson's $r = .515$, $p < 2.2 \times 10^{-16}$). We also found that fold change values of genes/proteins with significant differential expression were more positively correlated (Figure 3.9B, Pearson's $r = .798$, $p = 3.84 \times 10^{-12}$). This was surprising given that transcriptomic and proteomic concordance is often poor (Wang et al., 2019; Mangleburg et al., 2020). There were more significant downregulated genes/proteins common to both datasets than significant upregulated genes/proteins. There were two significant genes that had opposite patterns of expression in the glial panel versus the proteomic dataset (Figure 3.9C).

3.6 DISCUSSION

In this study, we profiled glial-associated transcripts in human control, AD, and FTD-tau post-mortem brain to understand how glial cells and their molecular profiles differ between control and neurodegenerative states. We identified differentially expressed genes in the FTD-tau group relative to control, but few in the AD group. Pathway analysis revealed that neuronal processes were decreased in the FTD-tau group while astrocyte, oligodendrocyte, and microglial pathways were increased. Interestingly, the AD samples often had intermediate pathway scores between control and FTD-tau samples suggesting that FTD-tau may represent a more extreme form of tauopathy with substantially more glial involvement. Finally, comparing fold change values in the targeted glial transcriptome to brain proteome revealed a significant positive correlation.

3.6.1 Comparison of glial profiling panel with proteomic data yields novel insights.

Although we were surprised by the concordance between the glial panel and the proteomic data given that there is often a mismatch between RNA and protein measurements, we also identified genes for which we did not obtain protein-level data. There were 103 genes measured by the glial panel that were not detected in the proteome. The third and fifth most upregulated genes in the FTD-tau samples, *S100A12* and *IL18*, did not survive batch correction for the proteome. Many of the genes not measured in the proteomic study predominantly encoded for membrane proteins. RNA and protein measurements often do not correlate well due to differences in factors such as turnover rate, degradation, regulation, and extraction methods, all of which could also explain the unique glial panel genes in our comparison of the two datasets (Vogel and Marcotte, 2012; Liu et al., 2016). The results of this study point to the utility of multi-omic approaches to gather more complete measurements of a sample and to gain deeper insight on the molecular underpinnings of disease.

3.6.2 Robust differential expression of astrocytic and inflammatory genes in FTD-tau

The five most upregulated genes in FTD-tau (*GFAP*, *C4A/B, S100A12*, *CD163,* and *IL18*) were previously associated with neurodegenerative diseases. The majority of these genes specifically associated with AD, but some were studied in relation to tau and tau pathology. For example, C4, a complement protein, was identified in subjects with Pick's disease (Singhrao et al., 1996). Other components of the complement pathway were upregulated in FTD-tau, including C3 and C1q, and were previously implicated in mouse models of tau-mediated neurodegeneration (Litvinchuk et al., 2018; Wu et al., 2019). The complement pathway scores of our FTD-tau samples also trended toward significance (one-way ANOVA adjusted p-value = .055). IL18 may impact expression of tau kinases and hyperphosphorylated tau (Ojala et al., 2008) and is also a downstream effector of the NLRP3 inflammasome (van de Veerdonk et al., 2011). In our study, FTD-tau samples had higher inflammasome pathway scores than control (Supplemental Table 3.1). Indeed, inhibition of the NLRP3 inflammasome in a mouse model of FTD-tau triggered a small reduction in phosphorylated tau (Hull et al., 2020). While this approach was targeted to genes associated with glial cells, the upregulated genes in FTD-tau implicate inflammatory processes and glial cells in the pathogenesis of FTD-tau.

Like the five most upregulated genes, the five most downregulated genes in FTD-tau (RIMS1, EGR1, RAB3A, GABRG2, and NEFL) were also previously associated with neurodegenerative disease. Synaptic proteins like RIMS1, RAB3A, and GABRG2 were reduced in other neurodegenerative states, likely due to the loss of neurons (and their synapses). EGR1 is a transcription factor widely studied in the fields of cancer and AD (Gómez Ravetti et al., 2010; Hu et al., 2019; Li et al., 2019). Prior literature implicated EGR1 in the phosphorylation of tau through activation of Cdk5 (Lu et al., 2011), thus modulating EGR1 may be a useful way to target tau

pathology therapeutically. NEFL is a cytoskeletal protein associated with Charcot-Marie-Tooth neuropathy (DiVincenzo et al., 2014; Sainio et al., 2018). NEFL in serum, plasma, and CSF has been widely studied for its potential as a biomarker for neurodegenerative disease, including for FTD (Halbgebauer et al., 2021; Lim et al., 2021; Schmitz et al., 2021; Silva-Spínola et al., 2021). In sum, the downregulated genes reflect the state of neurodegeneration and dysregulated processes such as synaptic function and cytoskeletal dynamics.

3.6.3 Glial pathways are increased in FTD-tau

Pathway analysis identified multiple FTD-tau associated pathways. We observed that neuronal pathways were primarily decreased in FTD-tau and pathway scores associated with oligodendrocytes, astrocytes, and microglia were increased. Of note, the astrocyte differentiation and function pathway scores had the largest F-value after one-way ANOVA analysis. Driven by a significant upregulation of *GFAP*, *EGFR*, *TLR4*, and *GRN*, it seems that astrocyte function is markedly and uniquely dysregulated in our FTD-tau group. Astrocytes express low levels of endogenous tau, but tau can aggregate in astrocytes, along with other non-neuronal cell types (LoPresti et al., 1995; Zhang et al., 2014b; Ghetti et al., 2015; Sharma et al., 2015; Kovacs et al., 2017). One study using IPSC-derived astrocytes from subjects with *MAPT* mutations reported alterations in function such as increased vulnerability to oxidative stress as well as increased expression of 4R tau (Hallmann et al., 2017). Considering the results from this study as well as the prior literature, future work should continue to focus on understanding the role of astrocytes in FTD-tau, particularly in cases where *MAPT* mutations are present. In addition to these cell-type specific observations, many pathways that are already known to be dysregulated in FTD-tau and other neurodegenerative diseases had significantly different pathway scores in the FTD-tau samples, including autophagy, phagocytosis, cytoskeletal dynamics, insulin signaling, and Wnt signaling, among others.

While statistical analysis did not reveal any significant differences in pathway scores between FTD-tau and AD samples, the mean pathway score for the AD samples tended to be midway between the means of the control and FTD-tau pathway scores. It is possible that since the FTD-tau samples were more homogenous (6 out of 8 of the samples were from subjects with a *MAPT* mutation) and the AD samples were more heterogeneous, the variability contributed to this observed pattern in the pathway scores. It is also possible that FTD-tau may represent a more extreme form a tauopathy which could contribute to this pattern as well. This pattern is similar to what we observed in our proteomic dataset, especially regarding astrocytic proteins (Gutierrez-Quiceno et al., 2021).

3.6.4 Limitations and future studies

There were several limitations to this work that are important to consider. The sample size of 24 individual brains, 8 per disease condition, is small. Our FTD-tau group was primarily composed of samples from subjects with a mutation in *MAPT* (6 out of 8 samples) and this group was compared to AD samples from subjects who had sporadic (or non-familial) AD in our pathway analyses. The prevalence of *MAPT* mutation cases in our FTD-tau group could make the group more homogenous, thus improving the chances of identifying significant changes. Another limitation of this study is that we did not have sufficient power to differentiate between 3R and 4R tauopathy in our FTD-tau group. Future studies could include larger groups of distinct 3R and 4R tauopathies to help discern the unique impacts that 3R or 4R tau pathology have on glial gene expression. A targeted transcriptomic approach with the glial profiling panel was chosen given the intriguing FTD-tau glial proteomic findings, particularly with astrocytes. This method was also attractive due to the available analysis pipelines and the lower cost relative to other sequencing approaches. However, unbiased RNA sequencing as well as single-cell/nucleus RNA sequencing

could be considered in the future to explore additional disease-related findings with increased cell-type specificity. Future studies could also include an additional group of samples from subjects with only sporadic FTD-tau. Furthermore, this study did not include samples from subjects with FTD mediated by non-tau pathology (e.g., TDP-43, FUS, etc.). Future work should include these other sub-groups of FTD to determine whether this glial enrichment is specific to FTD-tau.

3.7 CONCLUSION

Understanding how glia contribute to neurodegenerative disease is both an understudied topic but also a growing question within the field. We asked how glia may be altered in human FTD-tau DLPFC. Differential expression and pathway analysis revealed an enrichment of glial transcripts in FTD-tau samples, but not AD. Scores for the astrocyte markers and astrocyte differentiation and function pathways were especially increased in FTD-tau samples. This increase in pathway scores was driven by a robust upregulation of astrocytic genes like *GFAP*, *C4A/B*, *ADCYAP1R1*, and others. After comparison of the glial panel results with the brain proteome, we found that the targeted glial panel allowed us to measure genes that were not detected or did not survive batch correction in the proteomic dataset. Furthermore, our glial profiling panel results and the proteomic dataset correlated well. Multi-omic approaches such as this are useful to capture more complete data. Overall, glial cells and their processes appear to be more dysregulated in FTD-tau than in AD.

3.8 ACKNOWLEDGEMENTS

We thank the Goizueta Alzheimer's Disease Research Center [P30AG066511] for their neuropathological services and sample repository. We also thank the individuals and families whose specimen donations made this work possible. This study was supported, in part, by the Emory Integrated Genomics Core, which is subsidized by the Emory University School of

Medicine and is one of the Emory Integrated Core Facilities. Additional support was provided by the Georgia Clinical & Translational Science Alliance of the National Institutes of Health under Award Number UL1TR002378. The content is solely the responsibility of the authors and does not necessarily reflect the official views of the National Institutes of Health. This study was also supported by a Glial Profiling Panel Grant from NanoString Technologies which provided reagents. Study design, analysis, interpretation and writing of the manuscript were completed solely by the authors. This work was supported by the National Institutes of Health [grant numbers P30AG066511 (Allan Levey), UL1TR002378]; NanoString Technologies [Glial Profiling Panel Grant at Emory University]; the BrightFocus Foundation (CMH); and discretionary funds (CMH).

3.9 DATA STATEMENT

Raw data files are available upon request. The code for all R-based analyses can be found here: https://github.com/ashlyngjohnson/JohnsonEtAl_GlialProfilingManuscript.

TABLES

Table 3.1 Summary demographic information.

Characteristic	Control, N = 8[1]	AD, N = 8[1]	FTD, N = 8[1]	p-value[2]
Age	65 (10)	67 (6)	66 (8)	0.9
PMI	7.3 (3.7)	7.7 (3.2)	14.1 (9.9)	0.081
APOE				0.5
E2/3	1 (12%)	2 (25%)	1 (12%)	
E3/3	5 (62%)	2 (25%)	3 (38%)	
E3/4	1 (12%)	3 (38%)	1 (12%)	
E4/4	0 (0%)	1 (12%)	0 (0%)	
unknown	1 (12%)	0 (0%)	3 (38%)	
Sex				>0.9
Female	4 (50%)	4 (50%)	4 (50%)	
Male	4 (50%)	4 (50%)	4 (50%)	
Race				0.3
Black	2 (25%)	0 (0%)	0 (0%)	
White	6 (75%)	8 (100%)	8 (100%)	

[1]Mean (SD); n (%)

[2]One-way ANOVA; Fisher's exact test

FIGURES

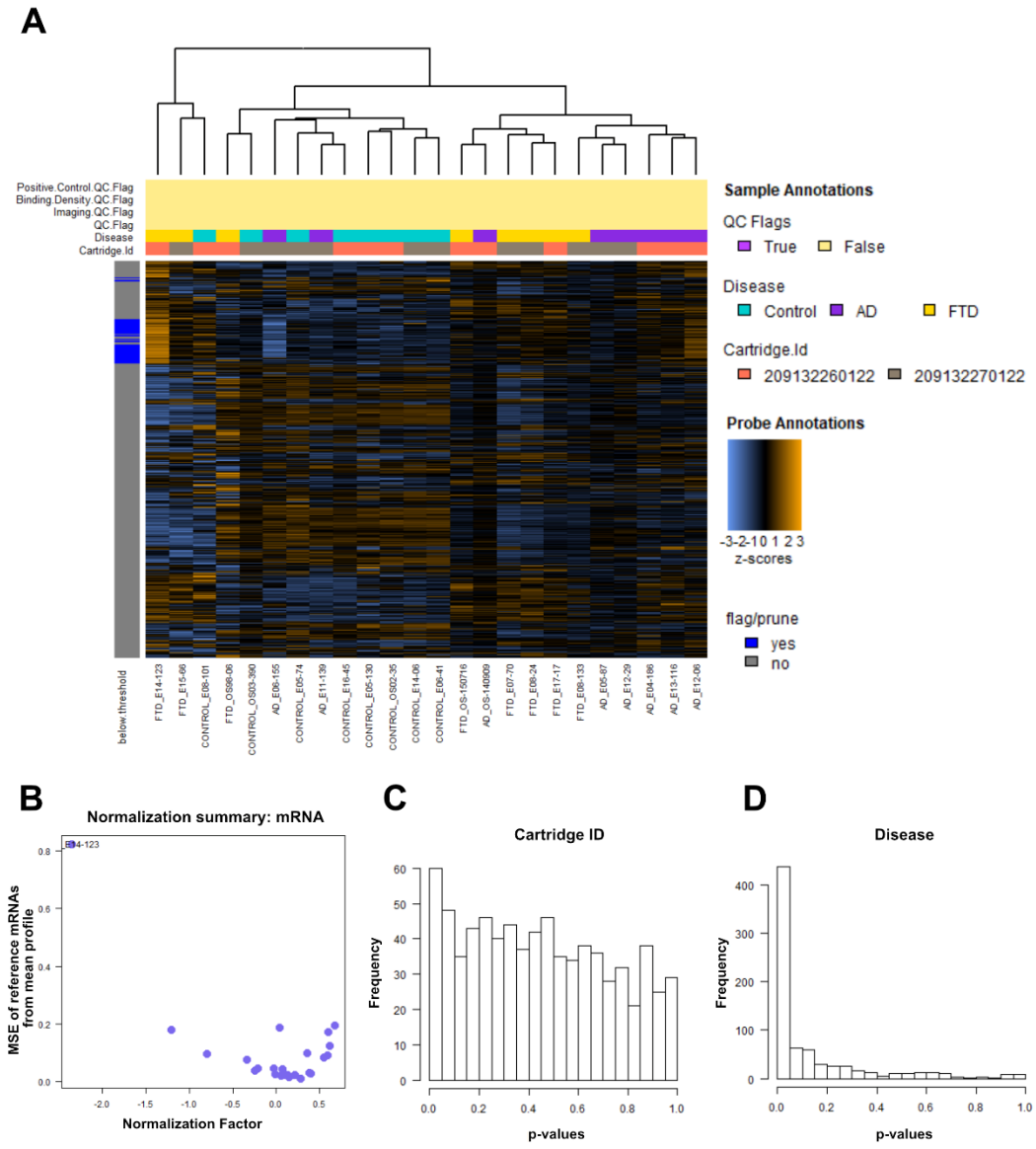

Figure 3.1. Overview of quality control results for the glial profiling panel. A) Overview heatmap of all normalized data displaying z-scored expression data. Each row represents an individual probe and each column is a sample. Across the top are rows for quality control flags, disease group, and cartridge ID. Blue marks on the left side of the heat map indicate whether the probe was pruned due to not reaching threshold for analysis. B) Normalization factors for each sample. C) Frequency of p-values based on cartridge ID. D) Frequency of p-values based on disease.

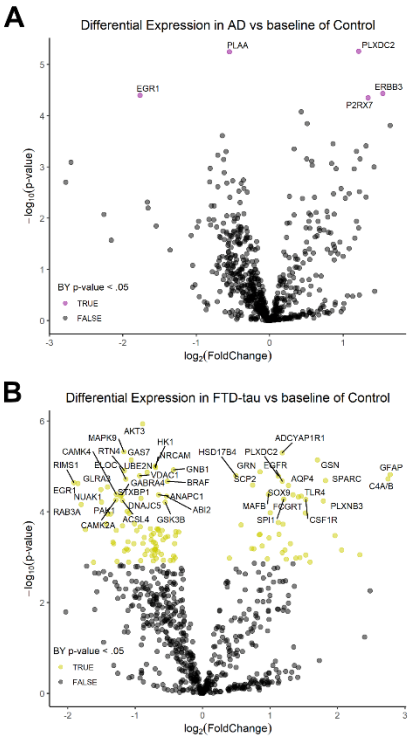

C

Differentially Expressed Genes in AD vs Control

Gene Symbol	Log_2 Fold Change	BY p-value	Nanostring Annotated Gene Sets
ERBB3	1.54	0.043	MAPK & PI3K, Neurogenesis
P2RX7	1.34	0.043	Calcium Signaling, Inflammasome, Neuroactive Ligands and Receptors
PLXDC2	1.21	0.014	Microglial Markers
PLAA	-0.55	0.014	Neurogenesis, Proteotoxic Stress
EGR1	-1.77	0.043	Cytokines, Interferon Signaling, Microglia Neurodegenerative Phenotype (MGnD), Microglial Markers

D

20 Most Upregulated Genes in FTD-tau vs Control

Gene Symbol	Log_2 Fold Change	BY p-value	Nanostring Annotated Gene Sets
GFAP	2.8	0.0051	Astrocyte DifferentiationFunction, Astrocyte Markers, Cytoskeletal Dynamics, JAK-STAT
C4A/B	2.8	0.0051	Astrocyte Markers, Complement System, Cytoskeletal Dynamics
S100A12	2.3	0.0391	Cytokines
CD163	2.1	0.0334	n/a
IL18	2.0	0.0216	Astrocyte Markers, Cytokines
SPARC	1.8	0.0051	Homeostatic Microglia, Primed Microglia
PLXNB3	1.8	0.0068	Neurogenesis
GSN	1.7	0.0051	Cytoskeletal Dynamics, Oligodendrocyte DifferentiationMaturation, Phagocytosis
C3	1.6	0.0486	Complement System, Neuroactive Ligands and Receptors, Primed Microglia
CSF1R	1.5	0.0068	Cytokines, Homeostatic Microglia, Microglia Neurodegenerative Phenotype (MGnD), Microglial Markers, Primed Microglia
NWD1	1.5	0.0392	n/a
IGFBP5	1.5	0.0108	Insulin Signaling
TLR4	1.5	0.0065	Apoptosis, Astrocyte DifferentiationFunction, NF-kappaB Signaling, NO Metabolism and Signaling
C1QA	1.4	0.0432	Astrocyte DifferentiationFunction, Complement System, Homeostatic Microglia, Microglial Markers
FCGRT	1.4	0.0065	Astrocyte Markers
SERPING1	1.4	0.0437	A1 Astrocyte, Complement System
SOX9	1.3	0.0065	Astrocyte Markers, Neurogenesis, Oligodendrocyte DifferentiationMaturation
RFX4	1.3	0.0271	Astrocyte Markers
AQP4	1.3	0.0053	Astrocyte Markers
PLEKHB1	1.2	0.0447	n/a

E

20 Most Downregulated Genes in FTD-tau vs Control

Gene Symbol	Log_2 Fold Change	BY p-value	Nanostring Annotated Gene Sets
RIMS1	-1.9	0.0052	Cannabinoid Signaling, Cholinergic Synapse, Dopaminergic Synapse, GABAergic Synapse, Glutamatergic Synapse
EGR1	-1.8	0.0052	Cytokines, Interferon Signaling, Microglia Neurodegenerative Phenotype (MGnD), Microglial Markers
RAB3A	-1.8	0.0076	GABAergic Synapse, Glutamatergic Synapse
GABRG2	-1.7	0.0193	Cannabinoid Signaling, GABAergic Synapse, Neuroactive Ligands and Receptors
NEFL	-1.6	0.0486	Cytoskeletal Dynamics, Neurogenesis, Neuronal Markers
NIJAK1	-1.5	0.0060	Primed Microglia
PAK1	-1.5	0.0069	Cell Migration, Cytoskeletal Dynamics, MAPK & PI3K, Neurogenesis, Phagocytosis, T-cell signaling
GNG2	-1.4	0.0167	Cannabinoid Signaling, Cholinergic Synapse, Dopaminergic Synapse, GABAergic Synapse, Glutamatergic Synapse, Primed Microglia, Serotonergic Synapse
GLRA3	-1.4	0.0055	Neuroactive Ligands and Receptors
INPP5F	-1.4	0.0108	Cytoskeletal Dynamics, Neurogenesis
PTK2B	-1.4	0.0108	Calcium Signaling, Cytoskeletal Dynamics, NO Metabolism and Signaling
ADAM22	-1.3	0.0268	Cytoskeletal Dynamics, Myelogenesis
RTN1	-1.3	0.0271	Neurogenesis
CAMK2A	-1.3	0.0068	Calcium Signaling
CAMK4	-1.3	0.0065	Calcium Signaling
ATP8A2	-1.3	0.0193	Microglial Markers, Neurogenesis, Primed Microglia
ATP1B1	-1.3	0.0476	Ion Transport
STXBP1	-1.2	0.0065	Neurogenesis
GABRA4	-1.2	0.0065	Cannabinoid Signaling, GABAergic Synapse, Neuroactive Ligands and Receptors
ACSL4	-1.2	0.0068	Lipid Metabolism, Neurogenesis

Figure 3.2. Transcriptomic profiling reveals differentially expressed genes in post-mortem AD and FTD-tau human DLPFC relative to control brain. Volcano plots demonstrate differentially expressed genes in AD (A) and FTD-tau (B) relative to control. Purple (A) or yellow (B) points indicate significant differential expression (Benjamini–Yekutieli p-value < .05). Tables demonstrate the log_2 fold change, Benjamini–Yekutieli p-value, and NanoString annotated gene sets of all differentially expressed genes in AD brain (C), the 20 most upregulated genes (D), and the 20 most downregulated genes (E) in FTD-tau brain by fold change value.

Neuroactive Ligands and Receptors

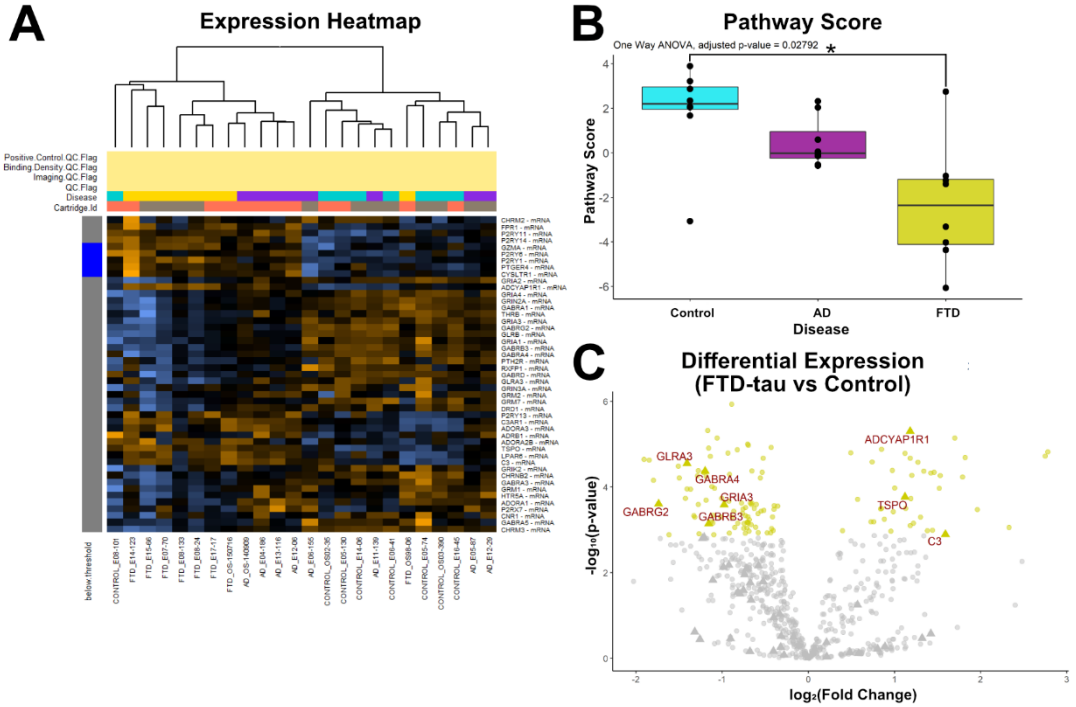

Neurotrophin Signaling

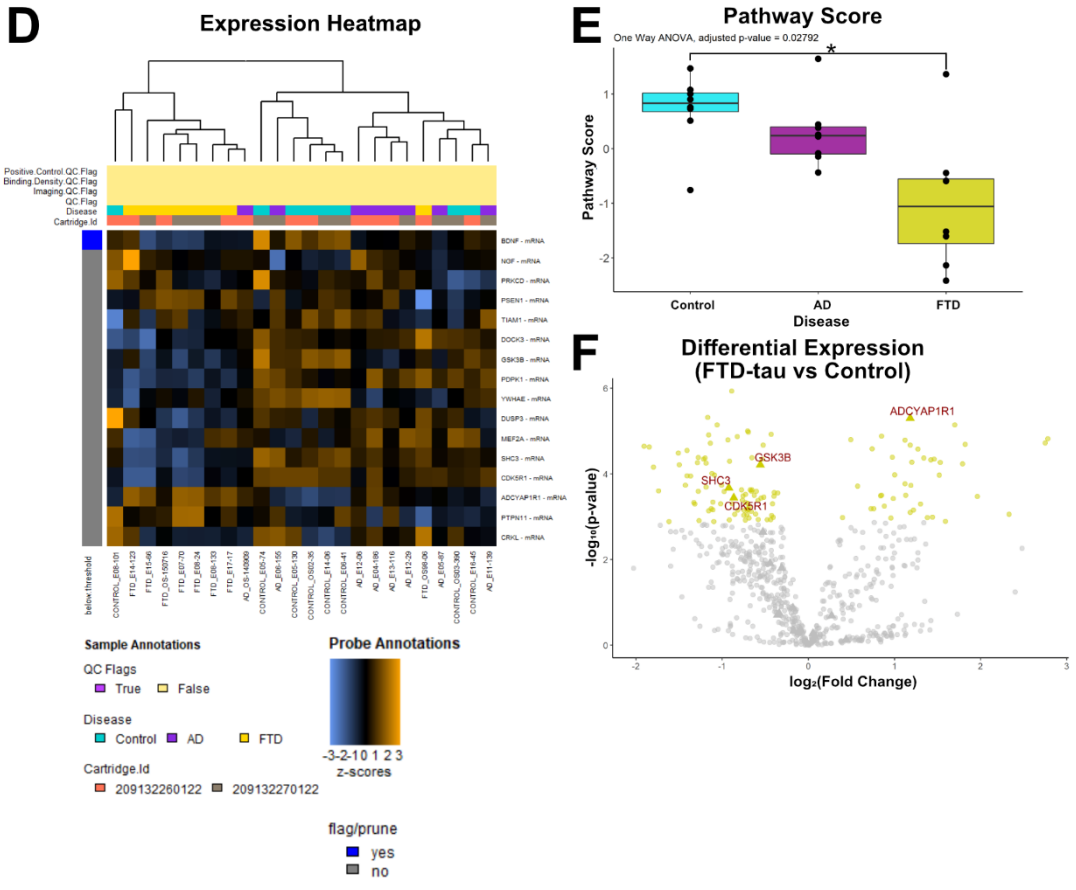

Figure 3.3. Transcripts associated with neuronal pathways are decreased in FTD-tau relative to control. Representative pathways include neuroactive ligands and receptors (A-C) and neurotrophin signaling (D-F). Heatmaps of each pathway (A, D) reveal that samples cluster generally by disease. Boxplots of the pathway score for each sample (B, E) demonstrate decreased pathway scores for the FTD-tau group (neuroactive ligands and receptors: one-way ANOVA adjusted p-value = .028, post-hoc control vs FTD adjusted p-value = 0.019574; neurotrophin signaling: one-way ANOVA adjusted p-value = .028, post-hoc control vs FTD adjusted p-value = 0.019574). Significance bar and * indicate a post-hoc p-value < .05. Volcano plots of differentially expressed genes in FTD-tau brain relative to control illustrate the differential expression of genes in the neuroactive ligands and receptors (C) and neurotrophin signaling pathways (F). Yellow points indicate significant differentially expressed genes (Benjamini–Yekutieli p-value < .05) in FTD-tau relative to control. Triangle-shaped points indicate that the gene is part of the pathway and significant genes that are part of the pathway are also labelled in red text.

Oligodendrocyte Differentiation and Maturation

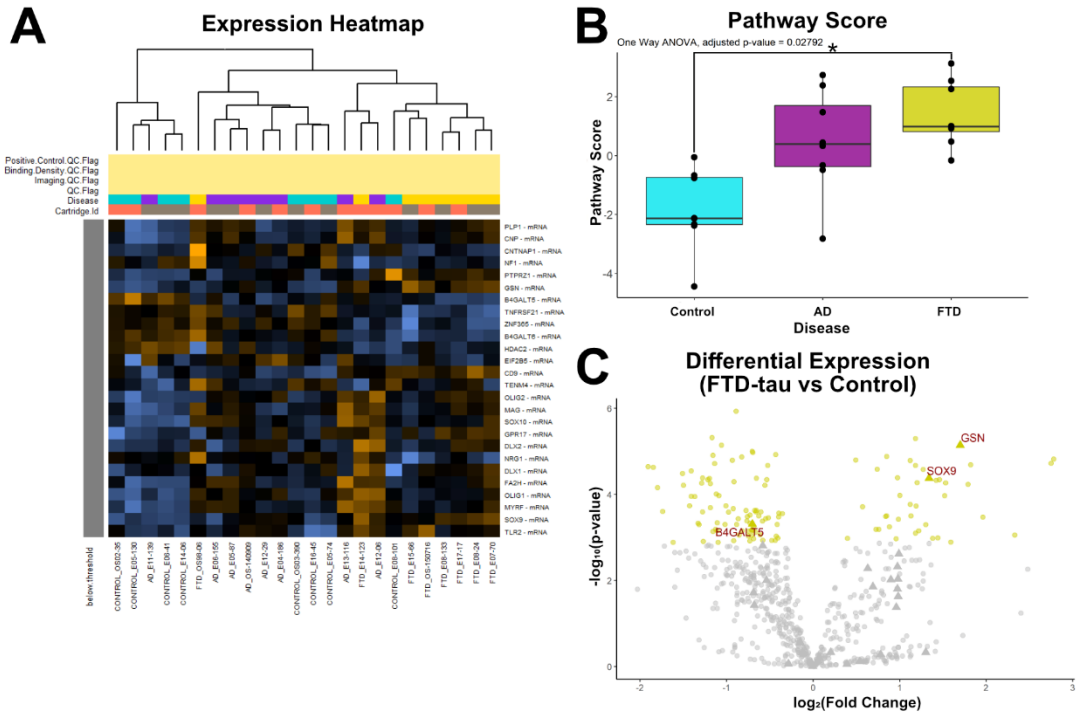

Myelogenesis

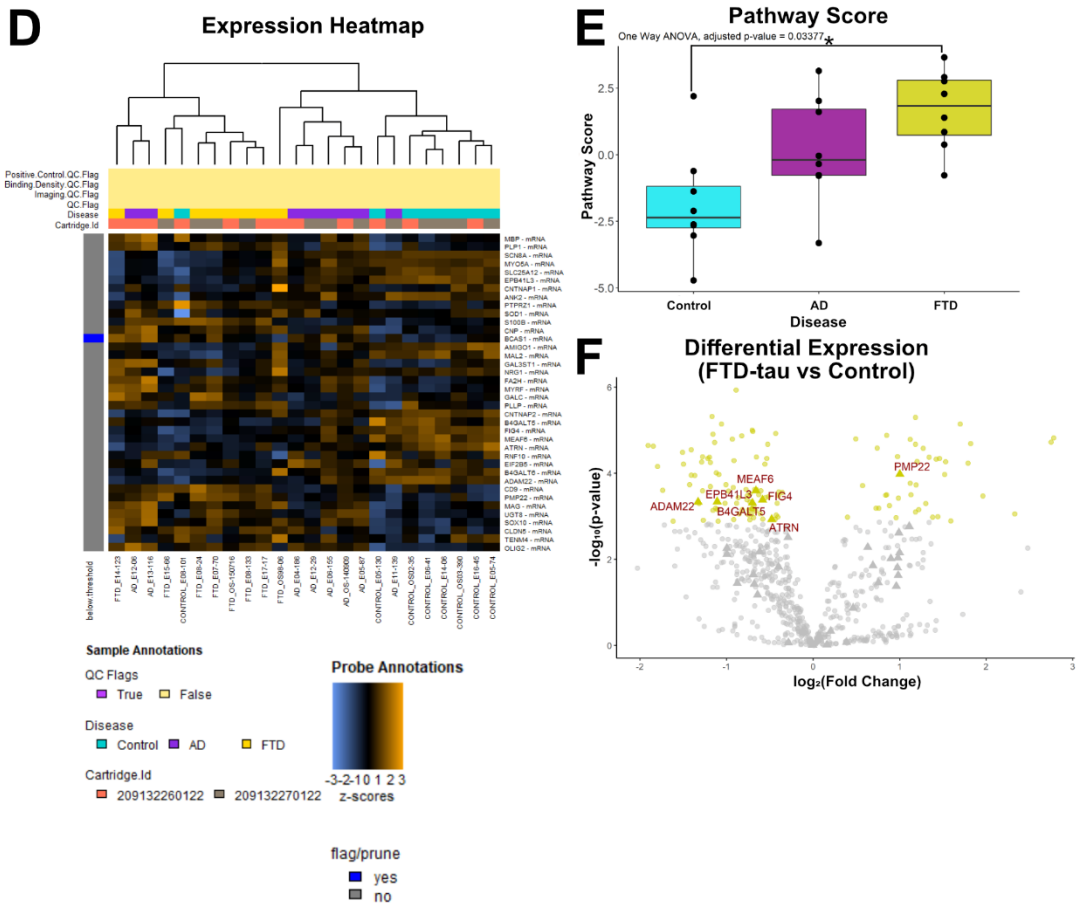

Figure 3.4. Transcripts associated with oligodendroglial pathways are increased in FTD-tau relative to control. Representative pathways include oligodendrocyte differentiation and maturation (A-C) and myelogenesis (D-F). Heatmaps of each pathway (A, D) reveal that samples cluster generally by disease. Boxplots of the pathway score for each sample (B, E) demonstrate increased pathway scores for the FTD-tau group (oligodendrocyte differentiation and maturation: one-way ANOVA adjusted p-value = .028, post-hoc control vs FTD adjusted p-value = 0.019574; myelogenesis: one-way ANOVA adjusted p-value = .034, post-hoc control vs FTD adjusted p-value = 0.023068). Significance bar and * indicate a post-hoc p-value < .05. Volcano plots of differentially expressed genes in FTD-tau brain relative to control illustrate the differential expression of genes in the oligodendrocyte differentiation and maturation (C) and myelogenesis pathways (F). Yellow points indicate significant differentially expressed genes (Benjamini–Yekutieli p-value < .05) in FTD-tau relative to control. Triangle-shaped points indicate that the gene is part of the pathway and significant genes that are part of the pathway are also labelled in red text.

Microglial Markers

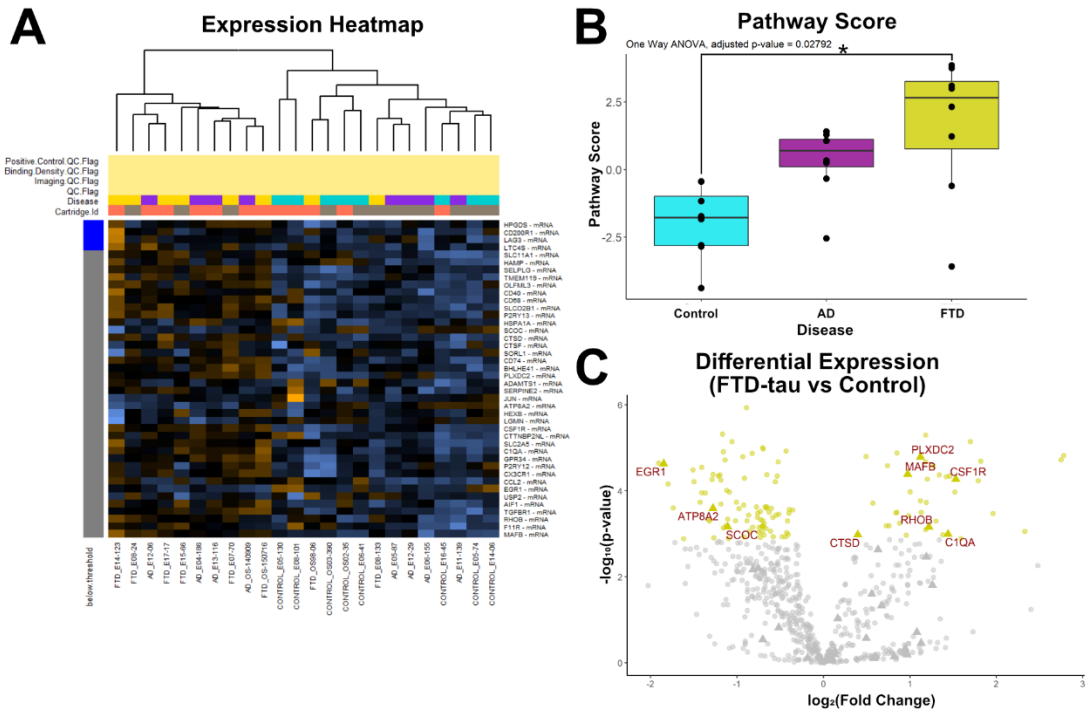

Primed Microglia

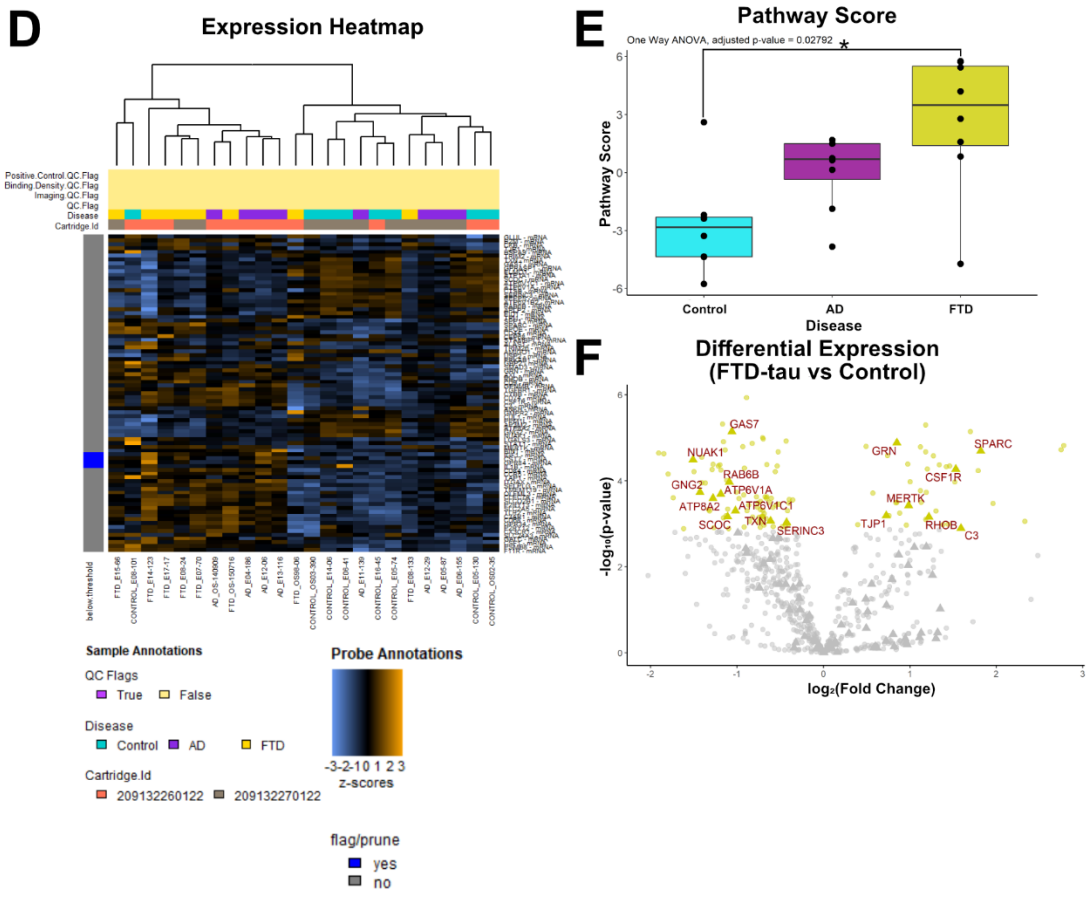

Figure 3.5. Transcripts associated with microglial pathways are increased in FTD-tau relative to control.

Representative pathways include microglial markers (A-C) and primed microglia (D-F). Heatmaps of each pathway (A, D). Boxplots of the pathway score for each sample (B, E) demonstrate increased pathway scores for the FTD-tau group (microglial markers: one-way ANOVA adjusted p-value = .028, post-hoc control vs FTD adjusted p-value = 0.019574; primed microglia: one-way ANOVA adjusted p-value = .028, post-hoc control vs FTD adjusted p-value = 0.019574). Significance bar and * indicate a post-hoc p-value < .05. Volcano plots of differentially expressed genes in FTD-tau brain relative to control illustrate the differential expression of genes in the microglial markers (C) and primed microglia (F). Yellow points indicate significant differentially expressed genes (Benjamini–Yekutieli p-value < .05) in FTD-tau relative to control. Triangle-shaped points indicate that the gene is part of the pathway and significant genes that are part of the pathway are also labelled in red text.

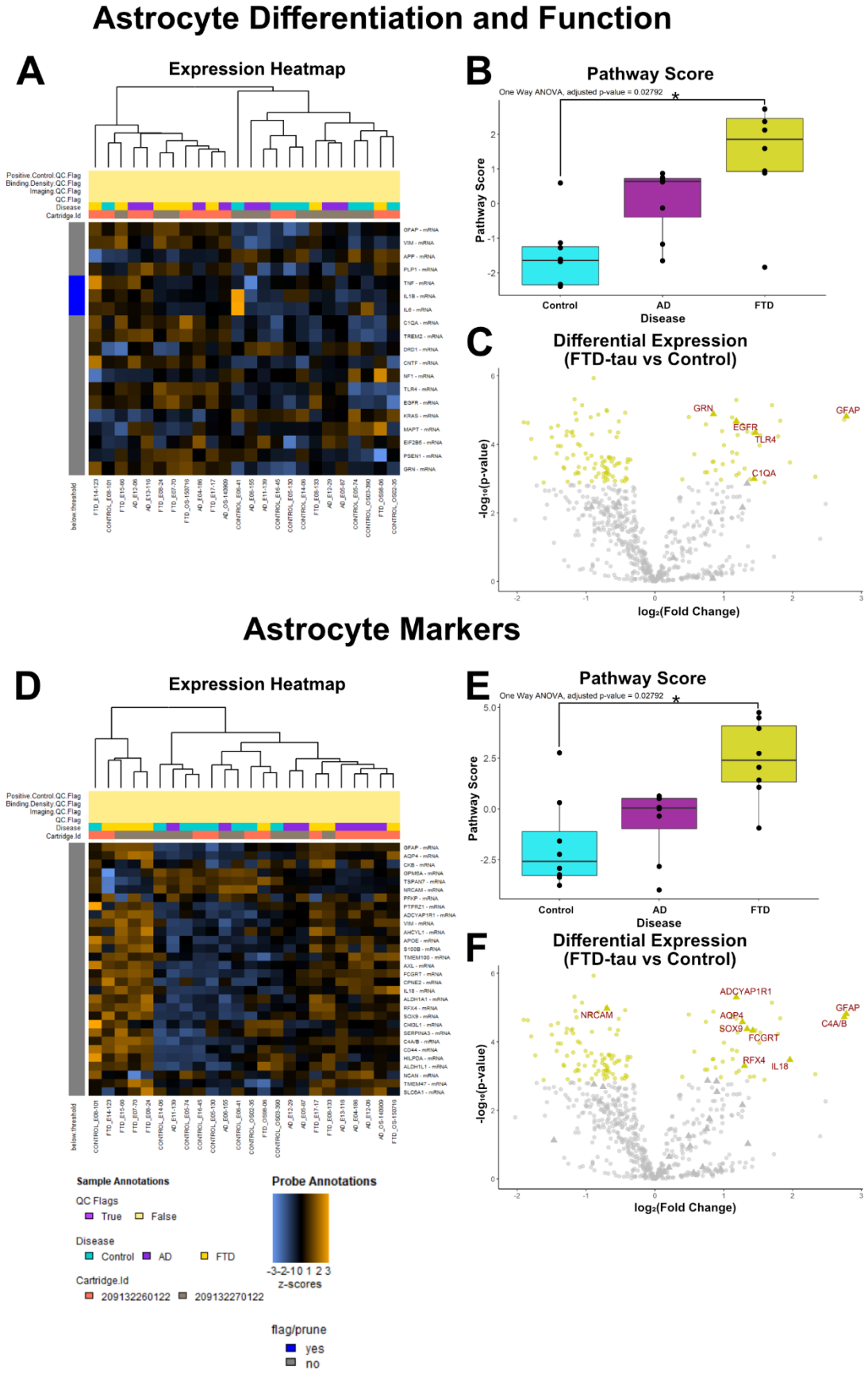
Astrocyte Differentiation and Function
A
Expression Heatmap
B
Pathway Score
One Way ANOVA, adjusted p-value = 0.02792
Pathway Score
Control
AD
FTD
Disease
C
Differential Expression
(FTD-tau vs Control)
-log10(p-value)
log2(Fold Change)
GRN
EGFR
TLR4
C1QA
GFAP
Astrocyte Markers
D
Expression Heatmap
E
Pathway Score
One Way ANOVA, adjusted p-value = 0.02792
F
Differential Expression
(FTD-tau vs Control)
ADCYAP1R1
NRCAM
AQP4
SOX9
FCGRT
RFX4
IL18
GFAP
C4A/B
Sample Annotations
QC Flags
True
False
Disease
Control
AD
FTD
Cartridge.Id
209132260122
209132270122
Probe Annotations
-3-2-10 1 2 3
z-scores
flag/prune
yes
no

Figure 3.6. Transcripts associated with astrocytic pathways are increased in FTD-tau relative to control.

Representative pathways include astrocyte differentiation and function (A-C) and astrocyte markers (D-F). Heatmaps of each pathway (A, D). Boxplots of the pathway score for each sample (B, E) demonstrate increased pathway scores for the FTD-tau group (astrocyte differentiation and function: one-way ANOVA adjusted p-value = .028, post-hoc control vs FTD adjusted p-value = 0.019574; astrocyte markers: one-way ANOVA adjusted p-value = .028, post-hoc control vs FTD adjusted p-value = 0.019574). Volcano plots of differentially expressed genes in FTD-tau brain relative to control illustrate the differential expression of genes in the astrocyte differentiation and function (C) and astrocyte markers (F). Yellow points indicate significant differentially expressed genes (Benjamini–Yekutieli p-value < .05) in FTD-tau relative to control. Triangle-shaped points indicate that the gene is part of the pathway and significant genes that are part of the pathway are also labelled in red text.

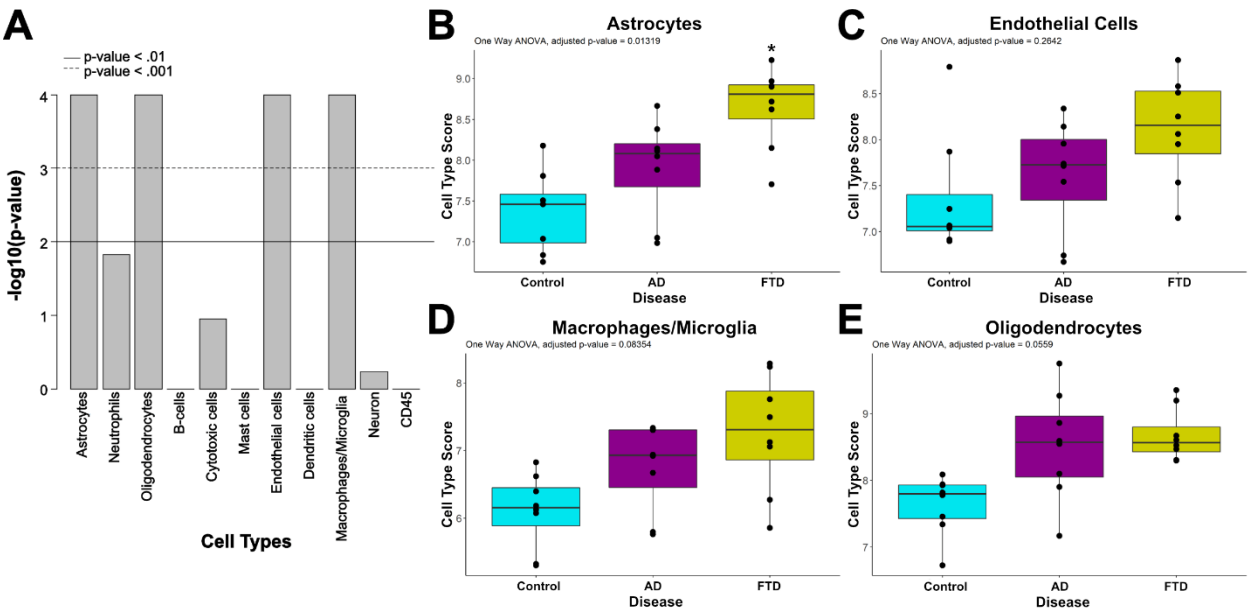

Figure 3.7. Cell type analysis indicates that astrocytes are enriched in FTD-tau samples relative to AD and control samples. The $\log_{10}$ transformed results (p-values) of a test for cell type marker co-expression (A). Boxplots of cell type scores (astrocytes (B), endothelial cells (C), macrophages and microglia (D) and oligodendrocytes (E)) for each sample. Only cellular populations whose markers were significantly correlated (A) are shown. Astrocytes are enriched in the FTD-tau group (One-way ANOVA adjusted p-value = .013 relative to control (adjusted p-value = 0.000527) and AD (adjusted p-value = 0.02915) brain. * indicates post-hoc p-value < .05.

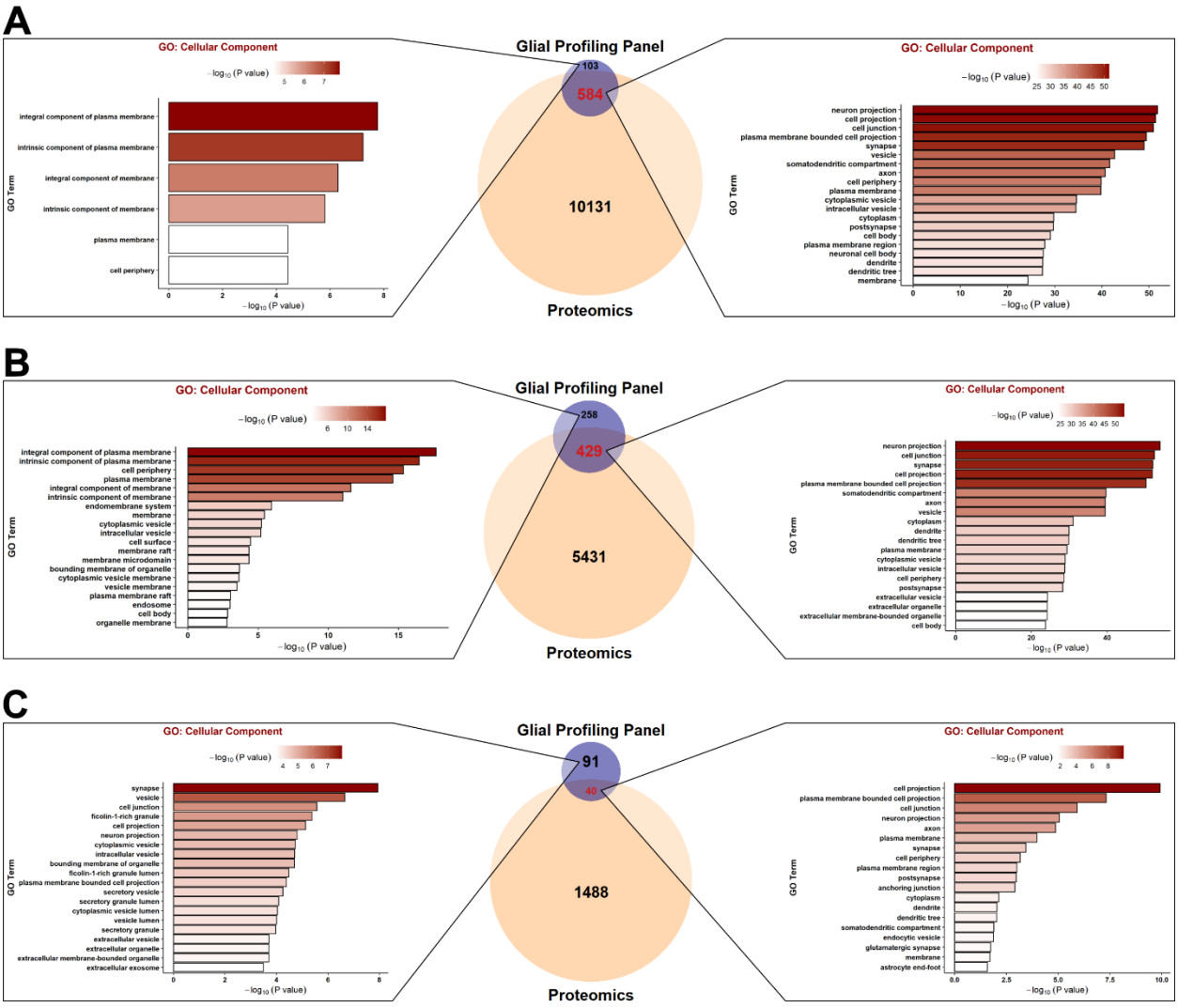

Figure 3.8. Genes unique to the glial profiling panel are associated with membrane-related cellular component GO terms. Up to the 20 most significant cellular component GO terms are displayed on the left for genes unique to the glial profiling panel and on the right for genes that were measured in both datasets. Comparisons include above threshold genes in the glial profiling panel with all measured proteins (prior to batch correction) (A) and only proteins that survived batch correction (B). Finally, only significant differentially expressed genes in the glial profiling panel and proteins were compared (C), where the tendency for the unique glial profiling panel genes to be localized to the membrane disappeared.

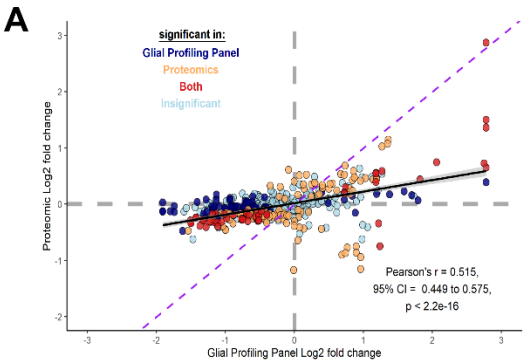

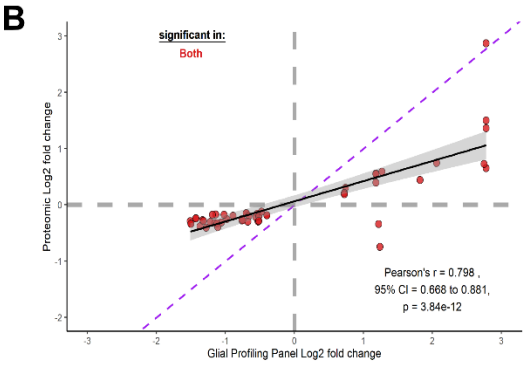

C

Expression Pattern	Gene Symbols
Up in Both Datasets	ADCYAP1R1, AQP4, C4A, CD163, EGFR, GFAP, SCP2, SPARC, TJP1
Down in Both Datasets	ABI2, ADAM22, AKT3, ATP2A2, ATP6V1A, ATP6V1C1, ATP6V1D, ATRN, BRAF, CACNA2D1, CAMK4, CLTC, ELOC, EPB41L3, GAS7, GNG2, GRIA3, GSK3B, MAP2K4, NRCAM, NUAK1, PAK1, PDHA1, PTK2B, RASGRF1, RTN1, RTN4, STXBP1, TANC2
Up in Glial Profiling Panel and Down in Proteomics	PLEKHB1, RHOB
Down in Glial Profiling Panel and Up in Proteomics	

Figure 3.9. Significant differentially expressed transcripts and proteins in FTD-tau relative to control brain are positively correlated. Scatterplot of $\log_2$ fold change values for differentially expressed transcripts (x-axis) and proteins (y-axis) as measured by the glial panel and quantitative proteomic analysis (A). Points vary in color based on whether the transcript/protein was significant in the two datasets. The purple dashed line indicates a perfect correlation while the black line indicates the line of best fit for the data. The $\log_2$ fold change values of the glial panel and proteomic datasets are positively correlated (Pearson's r = .515, $p < 2.2 \times 10^{-16}$). Log_2 fold change values of only transcripts/proteins that are significant in both datasets are more positively correlated (Pearson's r = .798, $p = 3.84 \times 10^{-12}$) (B). Table highlighting the expression pattern of significant transcripts/proteins that are common between both datasets (C).

SUPPLEMENTAL TABLES

Supplemental Table 3.1: Mean pathway scores from glial profiling panel.

	Mean (SD)			ANOVA Results		
Pathway	**Control**	**AD**	**FTD**	**F-value**	**P-value**	**Adj P-value**
A1 Astrocyte	-0.44 (1.57)	-0.72 (0.93)	1.17 (1.17)	5.325	0.01347	0.07914
A2 Astrocyte	-0.37 (1.88)	-0.68 (0.93)	1.05 (1.52)	3.072	0.06758	0.33477
Angiogenesis	0.79 (1.22)	0.26 (0.67)	-1.05 (1.30)	5.970	0.00886	0.05457
Antigen Processing and Presentation	1.27 (1.52)	0.28 (1.14)	-1.56 (1.96)	6.634	0.00585	**0.03994**
Apoptosis	-1.02 (0.69)	0.12 (0.73)	0.90 (1.42)	7.427	0.00364	**0.03282**
Astrocyte DifferentiationFunction	-1.53 (0.99)	0.08 (0.98)	1.44 (1.51)	12.502	0.00027	**0.02792**
Astrocyte Markers	-1.76 (2.24)	-0.68 (1.75)	2.44 (1.94)	9.607	0.00109	**0.02792**
Autophagy	0.79 (0.63)	-0.05 (0.53)	-0.74 (0.94)	9.048	0.00147	**0.02792**
Blood Brain Barrier	-0.94 (1.48)	-0.21 (1.05)	1.16 (1.37)	5.286	0.01382	0.07935
Calcium Signaling	1.29 (2.16)	0.78 (0.78)	-2.07 (2.55)	6.707	0.00559	**0.03925**
Cannabinoid Signaling	1.44 (1.75)	0.50 (0.80)	-1.94 (2.00)	9.471	0.00117	**0.02792**
Cell Cycle	1.06 (1.17)	0.01 (0.71)	-1.07 (1.10)	8.794	0.00168	**0.02792**
Cell Migration	-1.29 (1.70)	-0.12 (1.05)	1.41 (1.85)	5.918	0.00915	0.05506
Chemokines	0.13 (1.43)	-0.42 (0.79)	0.30 (0.89)	0.976	0.39325	1.00000
Cholinergic Synapse	1.20 (1.31)	0.31 (0.60)	-1.51 (1.77)	8.832	0.00165	**0.02792**
Circadian Signaling	0.40 (0.56)	0.08 (0.47)	-0.48 (0.62)	5.112	0.01553	0.08531
Complement System	-1.36 (1.34)	-0.17 (1.12)	1.53 (2.32)	5.995	0.00872	0.05457
Cytokines	-1.62 (1.19)	0.13 (0.97)	1.49 (2.02)	9.087	0.00144	**0.02792**
Cytoskeletal Dynamics	2.36 (2.63)	0.58 (1.56)	-2.94 (3.36)	8.428	0.00206	**0.02792**

Dopaminergic Synapse	1.28 (1.90)	0.62 (0.84)	-1.90 (2.31)	7.045	0.00456	**0.03600**
GABAergic Synapse	1.79 (1.93)	0.38 (1.04)	-2.17 (2.50)	8.713	0.00176	**0.02792**
Gap Junctions	0.78 (0.51)	-0.00 (0.57)	-0.78 (0.84)	11.360	0.00045	**0.02792**
Glucose Metabolism	1.04 (0.67)	-0.12 (0.69)	-0.92 (1.51)	7.261	0.00401	**0.03377**
Glutamatergic Synapse	1.54 (2.26)	0.50 (0.89)	-2.03 (2.43)	6.852	0.00512	**0.03921**
Homeostatic Microglia	-1.11 (0.84)	0.37 (0.67)	0.74 (2.07)	4.230	0.02860	0.14746
Hypoxia	-0.41 (0.95)	-0.05 (0.52)	0.46 (1.45)	1.424	0.26300	1.00000
Inflammasome	-0.72 (0.55)	0.28 (0.51)	0.44 (0.79)	7.907	0.00276	**0.02792**
Insulin Signaling	0.72 (0.47)	0.01 (0.55)	-0.72 (0.92)	9.109	0.00142	**0.02792**
Interferon Signaling	-0.50 (1.99)	-0.53 (0.57)	1.03 (1.28)	3.228	0.05994	0.30288
Ion Transport	1.61 (2.10)	0.35 (0.94)	-1.95 (2.70)	6.215	0.00759	**0.04914**
JAK-STAT	-0.82 (0.96)	-0.13 (0.71)	0.95 (0.57)	11.039	0.00053	**0.02792**
Lipid Metabolism	-1.18 (1.18)	0.06 (0.95)	1.12 (0.89)	10.223	0.00079	**0.02792**
MAPK & PI3K	1.49 (1.89)	0.36 (1.18)	-1.85 (1.91)	8.034	0.00256	**0.02792**
Microglia Neurodegenerative Phenotype (MGnD)	-2.20 (1.44)	0.76 (1.37)	1.45 (3.06)	6.765	0.00540	**0.03925**
Microglial Markers	-1.95 (1.35)	0.32 (1.30)	1.64 (2.57)	7.805	0.00292	**0.02792**
Myelogenesis	-1.86 (2.03)	0.19 (2.02)	1.68 (1.48)	7.290	0.00394	**0.03377**
Neuroactive Ligands and Receptors	1.88 (2.12)	0.46 (1.12)	-2.34 (2.71)	8.426	0.00206	**0.02792**
Neurogenesis	2.94 (3.58)	0.67 (1.98)	-3.61 (4.11)	7.902	0.00276	**0.02792**
Neuronal Markers	0.79 (1.22)	0.46 (0.53)	-1.24 (1.94)	5.162	0.01502	0.08431
Neurotrophin Signaling	0.71 (0.66)	0.28 (0.62)	-0.99 (1.20)	8.306	0.00220	**0.02792**
NF-kappaB Signaling	-0.80 (0.97)	-0.27 (0.99)	1.07 (1.60)	4.981	0.01696	0.09117

NO Metabolism and Signaling	-1.25 (0.90)	-0.10 (0.82)	1.34 (1.35)	12.189	0.00031	**0.02792**
Oligodendrocyte Differentiation-tionMaturation	-1.86 (1.37)	0.47 (1.78)	1.39 (1.13)	10.670	0.00063	**0.02792**
Oligodendrocyte Markers	-1.22 (1.19)	0.72 (1.82)	0.50 (0.91)	4.848	0.01857	0.09775
Oxidative & Nitrosative Stress	0.29 (0.55)	0.04 (0.42)	-0.33 (1.03)	1.506	0.24483	1.00000
Phagocytosis	1.64 (1.60)	0.19 (1.03)	-1.83 (2.37)	7.885	0.00279	**0.02792**
Primed Microglia	-2.76 (2.50)	0.06 (1.95)	2.70 (3.55)	7.904	0.00276	**0.02792**
Proteotoxic Stress	1.09 (1.08)	-0.11 (0.86)	-0.97 (1.41)	6.583	0.00603	**0.04012**
Purinergic Signaling	-1.16 (0.86)	0.06 (1.14)	1.10 (1.37)	7.804	0.00292	**0.02792**
Serotonergic Synapse	1.10 (1.53)	0.45 (0.69)	-1.55 (2.00)	6.726	0.00553	**0.03925**
Stage 1 DAM	-0.76 (0.87)	0.30 (0.63)	0.47 (1.89)	2.263	0.12881	0.62584
Stage 2 DAM	-1.17 (0.84)	0.19 (1.02)	0.98 (1.49)	7.103	0.00440	**0.03588**
T-cell signaling	-0.99 (0.78)	-0.06 (0.78)	1.05 (1.42)	7.768	0.00298	**0.02792**
TGF-Beta Signaling	-0.74 (0.86)	-0.06 (0.64)	0.80 (0.77)	8.281	0.00223	**0.02792**
Wnt Signaling	0.78 (0.95)	0.09 (0.51)	-0.88 (0.92)	8.354	0.00214	**0.02792**

Mean pathway scores were compared via one-way ANOVA and adjusted for multiple comparisons using the Benjamini-Yekutieli method. Significant pathway names are **bold**.

Supplemental Table 3.2: Cell type scores from glial profiling panel.

	Mean (SD)			ANOVA Results		
Cell Type	**Control**	**AD**	**FTD**	**F-value**	**P-value**	**Adj P-value**
Astrocytes	7.38 (0.49)	7.91 (0.60)	8.65 (0.49)	11.636	0.00040	**0.01319**
Neutrophils	6.12 (0.64)	6.79 (0.43)	7.33 (0.93)	6.025	0.00855	0.07579
Oligodendrocytes	7.63 (0.44)	8.52 (0.81)	8.68 (0.39)	7.560	0.00337	0.05590
B-cells	6.08 (0.86)	5.41 (0.46)	5.64 (0.45)	2.359	0.11910	0.43959
Cytotoxic cells	4.92 (0.51)	5.23 (0.87)	5.83 (0.71)	3.389	0.05303	0.25164
Mast cells	4.95 (0.81)	5.15 (0.73)	5.74 (0.84)	2.153	0.14102	0.46846
Endothelial Cells	7.36 (0.66)	7.60 (0.61)	8.11 (0.57)	3.150	0.06363	0.26420
DC	5.69 (0.32)	6.10 (0.87)	6.52 (0.49)	3.771	0.03987	0.22076
Macrophages_Microglia	6.11 (0.55)	6.75 (0.64)	7.26 (0.87)	5.429	0.01257	0.08354
Neuron	6.48 (0.44)	6.77 (0.39)	6.79 (0.44)	1.351	0.28049	0.84706
CD45	5.63 (0.43)	6.32 (0.47)	6.70 (0.89)	5.923	0.00913	0.07579

Mean cell type scores were compared via one-way ANOVA and adjusted for multiple comparisons using the Benjamini-Yekutieli method. Significant cell types are **bold**.

SUPPLEMENTAL FIGURES

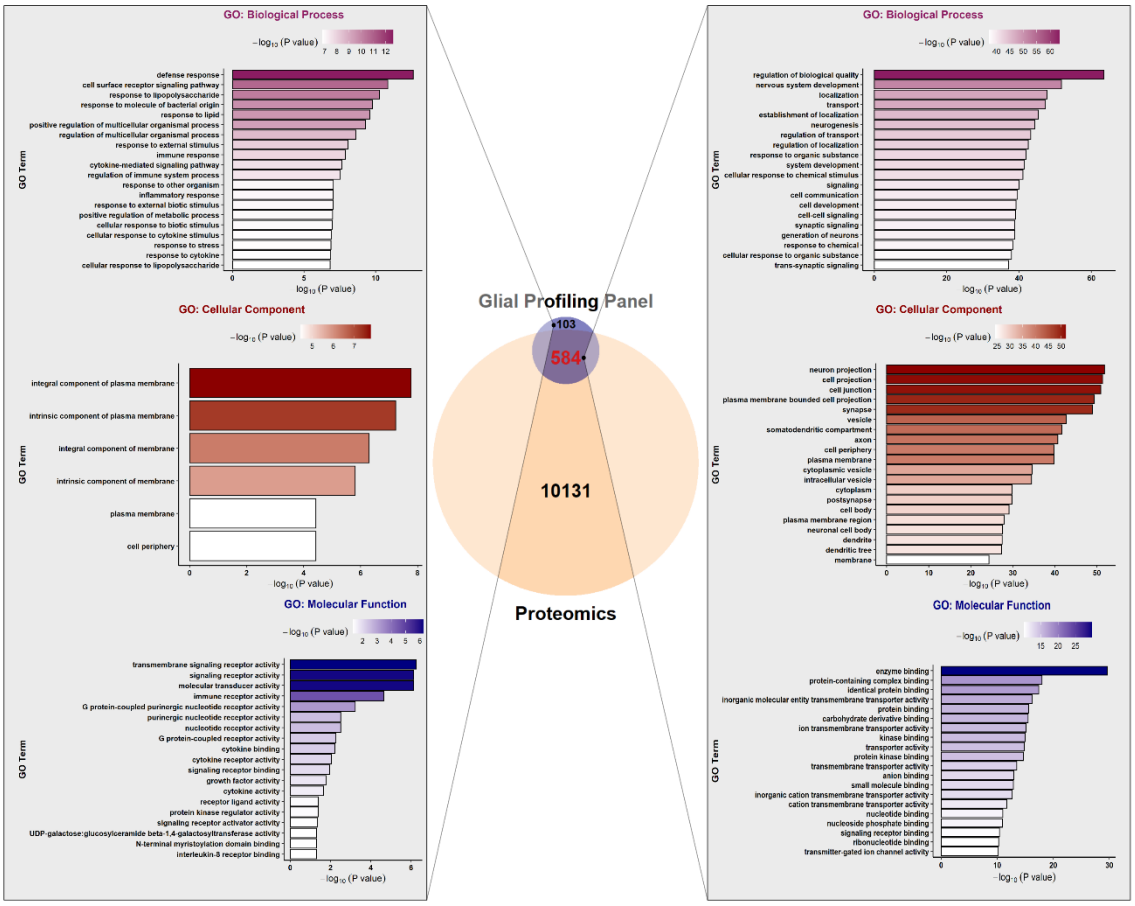

Supplemental Figure 3.1. Comparison of transcripts and proteins measured via the Glial Profiling Panel and quantitative proteomics respectively, prior to batch correction. GO ontology analyses are displayed on the right for transcripts/proteins that were measured in both the glial profiling panel and proteomic datasets. On the left are GO analyses for transcripts that were only measured in the glial profiling panel.

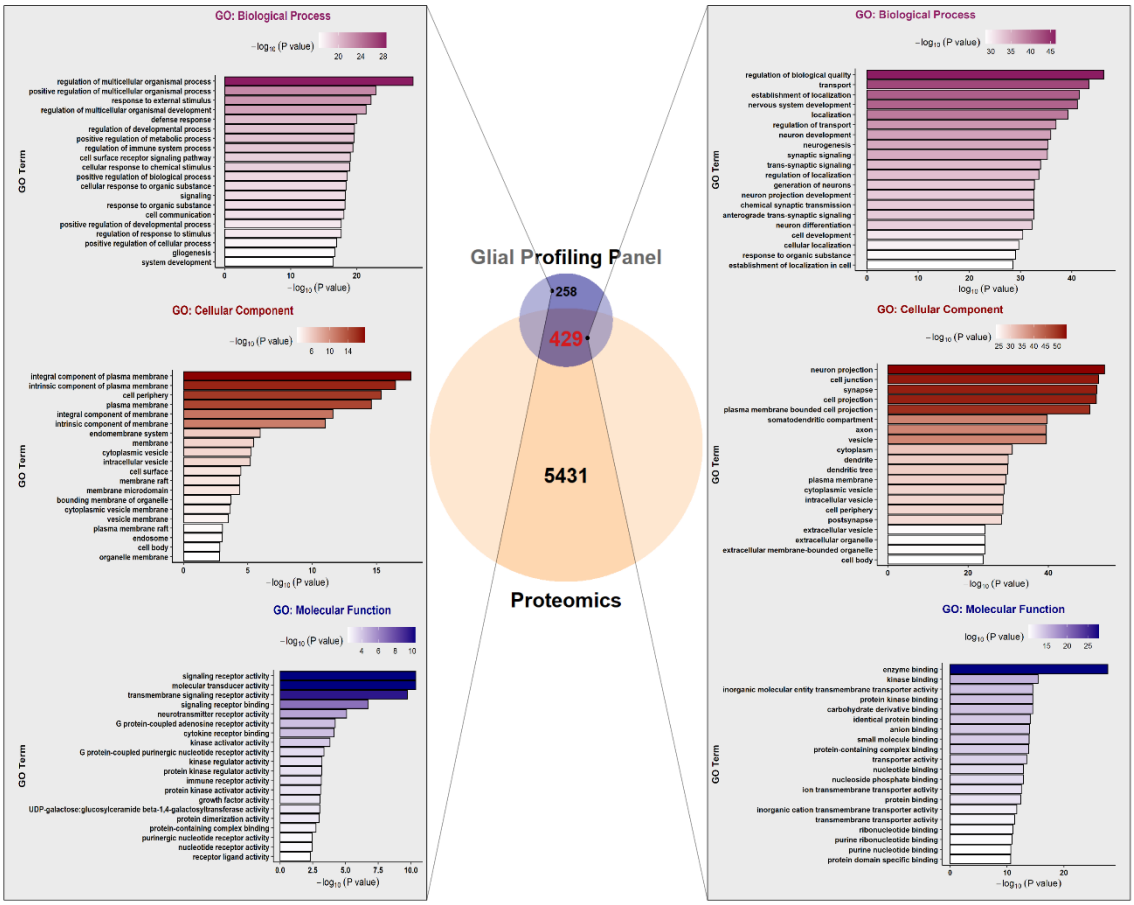

Supplemental Figure 3.2. Comparison of transcripts and proteins measured via Glial Profiling Panel and quantitative proteomics respectively, after batch correction. GO ontology analyses are displayed on the right for transcripts/proteins that were measured in both the glial profiling panel and proteomic datasets. On the left are GO analyses for transcripts that were only measured in the glial profiling panel.

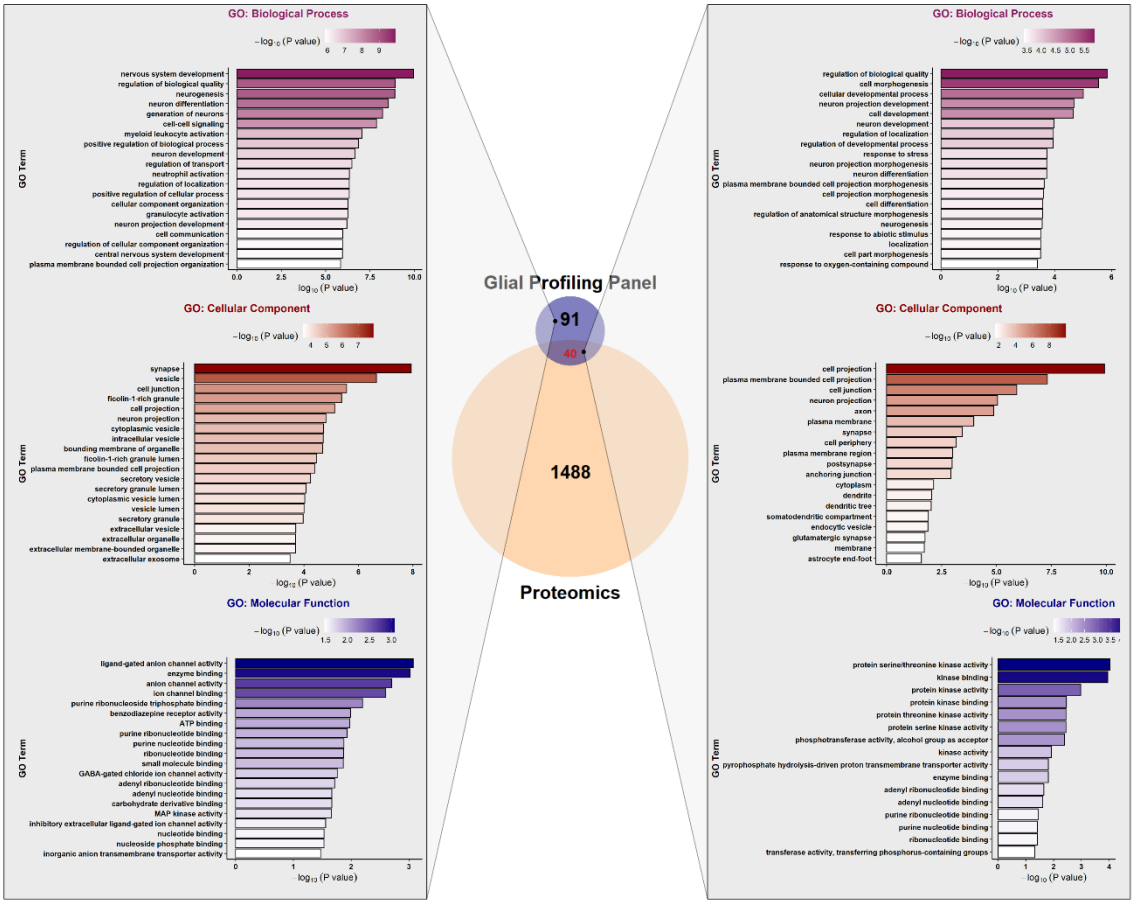

Supplemental Figure 3.3. Comparison of significant differentially expressed transcripts and proteins measured via the Glial Profiling Panel and quantitative proteomics in FTD-tau relative to control brain. GO ontology analyses are displayed on the right for transcripts/proteins that were measured in both the glial panel and proteomic datasets. On the left are GO analyses for transcripts that were only measured in the glial profiling panel.

SUPPLEMENTAL FILES

Supplementary files may be located at https://doi.org/10.1016/j.neurobiolaging.2021.12.005.

Supplementary File 3.1. Glial profiling panel data. Excel file composed of four sheets. 1) "raw" - Raw count data. Each column is a sample annotated with the disease group. Each row is an individual probe. 2) "normalized" – Normalized count data. Each column is a sample annotated with the disease group. 3) "annotations" – Important annotations for each probe as provided by NanoString. 4) "covariates" – Cartridge ID and disease group classifications for each sample.

Supplementary File 3.2. Differential expression data from glial profiling panel. Excel file composed of two sheets. 1) "FTD" - FTD-tau vs control. 2) "AD" - AD vs control. Columns contain statistical data. Each row is an individual probe.

Supplementary File 3.3. Raw pathway scores for each sample. Excel file. Each column is a pathway. Each row is a sample. Disease group is annotated within the sample name.

Supplementary File 3.4. Raw cell type scores for each sample. Excel file. Each column is a cell type. Each row is a sample. Disease group is annotated within the sample name.

CHAPTER 4: DISCUSSION AND FUTURE DIRECTIONS

4.1 SUMMARY OF RESULTS

The aim of this dissertation was to define how tauopathy impacts the human brain on a molecular level. To this aim, I investigated proteomic (Chapter 2) and transcriptomic (Chapter 3) changes in samples of human dorsolateral prefrontal cortex (DLPFC) from control and tauopathy subjects. I leveraged systems biology approaches to generate insights into the impact of tau pathology on cell type-specific and pathway level transcript and protein expression. Collectively, the results of this dissertation highlighted disease-associated changes in microglia, endothelia, astrocytes, and mitochondria in human tauopathy across transcripts and proteins. Notably, the insights generated from this study were not readily evident from simple differential expression analyses.

To address a deficit in understanding of how tauopathy impacts white matter and to expand on findings from previous work (Gutierrez-Quiceno et al., 2021), I examined proteomic changes in grey (GM) and white (WM) matter DLPFC through differential expression and weighted gene correlation network analyses (WGCNA). Differential expression identified an enrichment of microglial proteins in WM while cellular deconvolution analysis identified an enrichment of astrocytes in FTD-tau. Consensus WGCNA identified shared and unique microglial and endothelial disease-associated changes in GM and WM. Ratio WGCNA identified higher white:grey ratios of mitochondrial proteins in all disease groups, relative to control. Collectively, the findings from this study demonstrate the importance of considering both GM and WM to better understand the pathophysiology of neurodegenerative disease.

To further investigate marked astrocytic enrichment in human FTD-tau identified from prior work in the lab (Gutierrez-Quiceno et al., 2021) and Chapter 2 of this dissertation, I used a targeted transcriptomic approach to profile glial transcripts in control, AD, and FTD-tau DLPFC (Chapter 3). Over 129 transcripts were differentially expressed in FTD-tau samples relative to

control while only 5 were significant in AD. Pathway scores analysis demonstrated marked dysregulation of glia-related pathway scores in FTD-tau. AD samples usually demonstrated intermediate pathway scores compared to both control and AD, suggesting that FTD-tau may represent a more extreme form of tauopathy. Finally, comparison of the fold change values in the targeted transcriptomic dataset with the brain proteome demonstrated a significant positive correlation, but also revealed that the glial panel measured over 100 transcripts not detected in the proteome - many of which encoded for membrane proteins. Together, these findings demonstrate that glia, especially astrocytes, are greatly dysregulated in FTD-tau, even more so than AD.

4.2 SYSTEMS BIOLOGY APPROACHES REVEAL THE MOLECULAR PATHWAYS THROUGH THE FOREST OF THOUSANDS OF MOLECULAR TREES

Systems biology approaches aim to derive big picture insights from granular data (Wanjek, 2022). As transcriptomic and proteomic datasets have grown larger and larger, systems biology approaches have grown increasingly popular as a way to make sense of highly dimensional data (Karahalil, 2016; Hampel et al., 2021). Throughout this dissertation, I used systems biology approaches including considering multiple omic datasets, cellular deconvolution, cell type and pathway analyses, and multiple WGCNA networks. These methods across the two datasets presented in this dissertation led to the following overarching conclusions:

4.2.1 Astrocytic transcripts and proteins are increased in FTD-tau

Our lab previously demonstrated a unique enrichment of astrocytic proteins in FTD-tau human brain that exceeded that of AD and CTE (Gutierrez-Quiceno et al., 2021). In Chapter 2, we identified a similar enrichment of astrocytic proteins in FTD-tau in GM and WM that was particularly evident in the cellular deconvolution results (Supplemental Figure 2.4). Chapter 3 featured a targeted investigation of astrocytic transcripts in AD and FTD-tau and, once again, identified

astrocytic enrichment in FTD-tau through both cell type and pathway analysis (Figure 3.6 and 3.7). The replication of this finding across three separate studies and multiple levels of expression suggests that astrocytes can be a target for both biomarker and therapeutic studies in FTD-tau. Given that levels of these astrocytic transcripts/proteins in AD were often in the middle of control and FTD-tau values, perhaps FTD-tau represents an extreme state of neuroinflammation. To follow up on this marked enrichment of astrocytic proteins, specifically astrocytic endfoot proteins (Figure 1.2), we have isolated and quantified the proteins within gliovascular units of wildtype and mice expressing mutant human tau to better understand how mutant tau impacts the astrocytic endfeet. This study is ongoing in the lab, but nearing completion.

4.2.2 Microglial changes in tauopathy

Chapters 2 and 3 both demonstrated microglial changes in tauopathy. In GM, microglia markers are increased in FTD-tau at the transcript and protein level (Figure 3.5, 2.2). Interestingly, in WM, CBD and PSP demonstrated increases in microglial proteins, but not FTD-tau (Figure 2.2). Microglial changes in tauopathy appear to varied and not as consistent as the astrocytic enrichment in FTD-tau. Given the enrichment of microglia in WM (Figure 2.1, 2.2), future studies aiming to understand neuroinflammation should consider WM changes in addition to GM changes.

4.2.3 White:Grey protein ratios reveal disease-associated signature of neurodegeneration

In Chapter 2, we used white:grey protein ratios to generate a WGCNA network to group proteins together based on how their expression changed in both GM and WM across disease states. An advantage of this ratio approach over the consensus network is that the protein ratio as input for WGCNA allows the algorithm to consider not only the correlation between proteins but also how those proteins differ between distinct issues when creating protein modules, providing an extra dimension of information that is typically absent from other WGCNA studies. In doing

so, we identify a disease-associated increase in mitochondria in WM and decrease in GM. This reciprocal change in mitochondrial protein expression could serve as a biomarker for neurodegenerative disorders as positron emission tomography (PET) tracers for mitochondria already exist (van den Ameele et al., 2021; Detmer et al., 2022).

4.3 LIMITATIONS AND FUTURE DIRECTIONS

Both studies in this dissertation suffer from similar limitations that are important to consider. Sample size is low, particularly for the glial profiling study. Except for most of the CTE samples in Chapter 2, all the samples were from Emory's Goizueta Alzheimer's Disease Research Center. Validation in cohorts from other regions would increase confidence in the widespread applicability of our findings or demonstrate potential regional effects that would also be interesting to investigate. The ARTFL-LEFFTDS Longitudinal Frontotemporal Lobar Degeneration (ALLFTD) study (Rohrer and Boxer, 2021) and the National Centralized Repository for Alzheimer's Disease and Related Dementias could serve as access points for additional biospecimens while strategic collaborations with other major brain banks could allow for more direct comparison of regional variation between cases.

The FTD-tau group in both studies contains mostly (but not only) cases with *MAPT* mutations. The presence of these mutations in the FTD-tau group could lead to increased homogeneity within the group, leading to comparison of groups with unequal variance, driving significant findings in the more homogeneous group. Future studies could compare these genetic FTD-tau cases to genetic forms of AD, eliminating any concern about comparing sporadic and genetic forms of different disorders.

We were not powered or designed to make any comparisons between 3R and 4R tauopathy cases. Future proteomic studies with access to an abundance of tauopathy cases (for sufficient

statistical power) and careful neuropathological characterization could directly compare molecular changes due to 3R, 4R, or mixed tau pathology. Comparison of transcriptomes from SH-SY5Y cells expressing either 4R or 3R demonstrated differences in Wnt signaling and transcripts related to development and neurite outgrowth (Chen et al., 2010), thus examination of the impact of 3R and 4R tau pathology on the human brain should be fruitful.

Finally, our studies were limited to bulk tissue which lacks resolution on cell-type specific contributions to disease. While we made substantial use of *in silico* methods to parse apart the contribution of brain cell types to tauopathy including cellular deconvolution (Cai et al., 2022) and enrichment analyses (Dammer, 2023), future studies would benefit from methods that are optimized to parse apart cell-type contributions. Single-cell sequencing is a transcriptomic approach capable of obtaining individual cell transcriptomes in human post-mortem tissue and this method has already been applied to studies of human AD and other neurodegenerative diseases (Mathys et al., 2019; Pozojevic and Spielmann, 2023). Single-cell proteomics in post-mortem human brain is more challenging, but in active technical development (Bennett et al., 2023). Spatial proteomics can also provide insight into the contributions of particular cell-type specific proteins to neuropathological changes, but would require some *a priori* knowledge of proteins of interest (Vijayaragavan et al., 2022). Given this need for *a priori* knowledge, spatial proteomics would be a suitable way to follow up on the results of this dissertation, particularly the mitochondrial findings in Chapter 2.

The results of this dissertation also point to avenues of future research outside of addressing limitations. Creation of a WGCNA network from protein ratios derived from protein measurements from two different tissues demonstrates feasibility for this approach to understanding protein changes across tissues or even sample types in states of control and disease. Instead of

examining grey and white matter, one could examine a brain region and the regions to which it projects. Outside of region-to-region comparisons, this approach may be applied to any two samples in which you expect that changes in one may affect the other such as brain and cerebrospinal fluid (CSF), and CSF and blood. Imaging studies have employed ratio-based techniques to identify neuropathological changes in neurodegeneration (Moccia et al., 2017; Son et al., 2019; Putcha et al., 2023), further pointing to the feasibility and utility of this approach in future transcriptomic and proteomic studies.

The identification of WM-specific changes in tauopathy begs the question of whether these proteomic changes in disease are secondary to tau-mediated changes in GM or related to pathological tau in WM cell types. Since human tissues are limited to a single time point, mouse models of tauopathy may provide insight into the origin of WM changes in tauopathy. Viral or genetic expression of wildtype or mutant human tau in oligodendrocytes in mice would provide a more concentrated model of WM tauopathy and allow separation of the impact of tau pathology on WM from the impact of tau pathology in GM on WM. One such study found that expression of human P301L tau in mouse oligodendrocytes induced tau inclusions and axonal degeneration (Higuchi et al., 2005). Future studies could alter specific tau mutations, tau isoform, or level of expression/overexpression to further understand the impact of tau on WM.

The identification of increased glial-specific transcripts in FTD-tau that exceeds that of AD in Chapter 3 also opens avenues for further questions regarding whether this neuroinflammatory phenotype is related to tau or just a reflection of an extreme disease state. Comparison of FTD-tau to other FTD subtypes like FTD with TDP-43 or FUS pathology, sporadic or genetic, could provide insight into the specificity of this finding to tau-mediated neurodegeneration. One proteomic study of human middle frontal gyrus from subjects with FTD with tau pathology and FTD with TDP-43

pathology demonstrated an increase in astrocytic and endothelial proteins in FTD-tau that was not evident in FTD-TDP (Bridel et al., 2023). Studies that include FTD samples from across the neuropathological and genetic spectrum of FTLD with sufficient power to detect differences between the groups would provide insight into the molecular differences between FTD subtypes and generate better targets for biomarker and therapeutic development.

4.4 TRANSLATIONAL POTENTIAL

Studies such as those in this dissertation are important for characterizing the molecular changes underlying neurodegenerative disorders with the principle that this increased understanding may lead to therapeutic interventions. These system biology approaches also identify processes and pathways that are altered in disease which can then be monitored to assess efficacy of new therapies. Results from this dissertation suggest that markers of neuroinflammation and glia may be useful when differentiating FTD-tau from AD in the clinic. Indeed, astrocytic protein YKL-40 (Zhang et al., 2016) was increased in CSF from FTD subjects relative to AD subjects (Teunissen et al., 2016). An important next step that would increase the therapeutic potential for this work is to correlate the brain transcriptome and proteome with CSF and other biofluid measurements and clinical traits. Correlation of the WM proteome with biofluids may also yield novel biomarkers and therapeutic targets, as WM molecular changes have been largely ignored in favor of GM.

4.5 CONCLUSION

The aim of this dissertation was to define how tauopathy impacts the human brain on a molecular level. Proteomic profiling of GM and WM in control and tauopathy conditions identified tissue-specific changes in microglia and endothelia as well as mitochondria proteins in tauopathy. The GM and WM specific effects demonstrated the importance of studying both tissues to gain a more complete picture of the impact of tau pathology on the human brain. Profiling of glial

transcripts in AD and FTD-tau identified an enrichment of glial, and particularly astrocytic, transcripts in FTD-tau. Findings suggest that astrocytes, perhaps beyond their role as just inflammatory cells, could serve as important mediators in disease progression. Important contributions have been made to improving our understanding of disease pathogenesis for tauopathies. The hope is that these findings will ultimately lead to novel diagnostics or treatments that will reduce the suffering for patients and families dealing with tauopathies.

REFERENCES

Abraha A, Ghoshal N, Gamblin TC, Cryns V, Berry RW, Kuret J, Binder LI (2000) C-terminal inhibition of tau assembly in vitro and in Alzheimer's disease. J Cell Sci 113 Pt 21:3737–3745 Available at: http://dx.doi.org/10.1242/jcs.113.21.3737.

Adav SS, Park JE, Sze SK (2019) Quantitative profiling brain proteomes revealed mitochondrial dysfunction in Alzheimer's disease. Mol Brain 12:8 Available at: http://dx.doi.org/10.1186/s13041-019-0430-y.

Agrawal S, Fox JH (2019) Novel proteomic changes in brain mitochondria provide insights into mitochondrial dysfunction in mouse models of Huntington's disease. Mitochondrion 47:318–329 Available at: http://dx.doi.org/10.1016/j.mito.2019.03.004.

Aisen PS, Cummings J, Jack CR Jr, Morris JC, Sperling R, Frölich L, Jones RW, Dowsett SA, Matthews BR, Raskin J, Scheltens P, Dubois B (2017) On the path to 2025: understanding the Alzheimer's disease continuum. Alzheimers Res Ther 9 Available at: http://dx.doi.org/10.1186/s13195-017-0283-5.

Alexander-Kaufman K, Dedova I, Harper C, Matsumoto I (2007) Proteome analysis of the dorsolateral prefrontal region from healthy individuals. Neurochem Int 51:433–439 Available at: http://dx.doi.org/10.1016/j.neuint.2007.04.016.

Alosco ML et al. (2023) Decreased myelin proteins in brain donors exposed to football-related repetitive head impacts. Brain Commun 5:fcad019 Available at: http://dx.doi.org/10.1093/braincomms/fcad019.

Alquezar C, Arya S, Kao AW (2020) Tau Post-translational Modifications: Dynamic Transformers of Tau Function, Degradation, and Aggregation. Front Neurol 11:595532 Available at: http://dx.doi.org/10.3389/fneur.2020.595532.

Alzheimer A (1907) Uber eine eigenartige Erkrankung der Hirnrinde. Allg Z Psychiatrie Psych Ger Med 64:146–148 Available at: https://cir.nii.ac.jp/crid/1572261550432407936 [Accessed October 4, 2023].

Alzheimer A (1911) über eigenartige Krankheitsfälle des späteren Alters. Z Gesamte Neurol Psychiatr 4:356–385 Available at: http://dx.doi.org/10.1007/bf02866241.

Alzheimer's Association (2023) 2023 Alzheimer's disease facts and figures. Alzheimers Dement 19:1598–1695 Available at: http://dx.doi.org/10.1002/alz.13016.

Andrews SJ, Renton AE, Fulton-Howard B, Podlesny-Drabiniok A, Marcora E, Goate AM (2023) The complex genetic architecture of Alzheimer's disease: novel insights and future directions. EBioMedicine 90:104511 Available at: http://dx.doi.org/10.1016/j.ebiom.2023.104511.

Atherton K et al. (2022) Association of APOE genotypes and chronic traumatic encephalopathy. JAMA Neurol 79:787–796 Available at: http://dx.doi.org/10.1001/jamaneurol.2022.1634.

Barber IS et al. (2017) Mutation analysis of sporadic early-onset Alzheimer's disease using the NeuroX array. Neurobiol Aging 49:215.e1-215.e8 Available at: http://dx.doi.org/10.1016/j.neurobiolaging.2016.09.008.

Bennett HM, Stephenson W, Rose CM, Darmanis S (2023) Single-cell proteomics enabled by next-generation sequencing or mass spectrometry. Nat Methods 20:363–374 Available at: http://dx.doi.org/10.1038/s41592-023-01791-5.

Bi B, Choi H-P, Hyeon SJ, Sun S, Su N, Liu Y, Lee J, Kowall NW, McKee AC, Yang J-H, Ryu H (2019) Quantitative proteomic analysis reveals impaired axonal guidance signaling in human postmortem brain tissues of chronic traumatic encephalopathy. Exp Neurobiol 28:362–375 Available at: http://dx.doi.org/10.5607/en.2019.28.3.362.

Bieniek KF, Cairns NJ, Crary JF, Dickson DW, Folkerth RD, Keene CD, Litvan I, Perl DP, Stein TD, Vonsattel J-P, Stewart W, Dams-O'Connor K, Gordon WA, Tripodis Y, Alvarez VE, Mez J, Alosco ML, McKee AC, TBI/CTE Research Group (2021) The second NINDS/NIBIB consensus meeting to define neuropathological criteria for the diagnosis of chronic traumatic encephalopathy. J Neuropathol Exp Neurol 80:210–219 Available at: http://dx.doi.org/10.1093/jnen/nlab001.

Binder LI, Frankfurter A, Rebhun LI (1985) The distribution of tau in the mammalian central nervous system. J Cell Biol 101:1371–1378 Available at: http://dx.doi.org/10.1083/jcb.101.4.1371.

Bishof I, Dammer EB, Duong DM, Kundinger SR, Gearing M, Lah JJ, Levey AI, Seyfried NT (2018) RNA-binding proteins with basic-acidic dipeptide (BAD) domains self-assemble and aggregate in Alzheimer's disease. J Biol Chem 293:11047–11066 Available at: http://dx.doi.org/10.1074/jbc.ra118.001747.

Boyarko B, Hook V (2021) Human tau isoforms and proteolysis for production of toxic tau fragments in neurodegeneration. Front Neurosci 15:702788 Available at: http://dx.doi.org/10.3389/fnins.2021.702788.

Braak H, Alafuzoff I, Arzberger T, Kretzschmar H, Del Tredici K (2006) Staging of Alzheimer disease-associated neurofibrillary pathology using paraffin sections and immunocytochemistry. Acta Neuropathol 112:389–404 Available at: http://dx.doi.org/10.1007/s00401-006-0127-z.

Braak H, Braak E (1991) Neuropathological stageing of Alzheimer-related changes. Acta Neuropathol 82:239–259 Available at: http://dx.doi.org/10.1007/bf00308809.

Brandt R, Léger J, Lee G (1995) Interaction of tau with the neural plasma membrane mediated by tau's amino-terminal projection domain. J Cell Biol 131:1327–1340 Available at: http://dx.doi.org/10.1083/jcb.131.5.1327.

Brandt R, Trushina NI, Bakota L (2020) Much more than a cytoskeletal protein: Physiological and pathological functions of the non-microtubule binding region of tau. Front Neurol 11:590059 Available at: http://dx.doi.org/10.3389/fneur.2020.590059.

Bridel C, van Gils JHM, Miedema SSM, Hoozemans JJM, Pijnenburg YAL, Smit AB, Rozemuller AJM, Abeln S, Teunissen CE (2023) Clusters of co-abundant proteins in the brain cortex associated with fronto-temporal lobar degeneration. Alzheimers Res Ther 15:59 Available at: http://dx.doi.org/10.1186/s13195-023-01200-1.

Brion JP, Couck AM, Passareiro E, Flament-Durand J (1985) Neurofibrillary tangles of Alzheimer's disease: an immunohistochemical study. J Submicrosc Cytol 17:89–96 Available at: https://www.ncbi.nlm.nih.gov/pubmed/3973960.

Brunello CA, Merezhko M, Uronen R-L, Huttunen HJ (2020) Mechanisms of secretion and spreading of pathological tau protein. Cell Mol Life Sci 77:1721–1744 Available at: http://dx.doi.org/10.1007/s00018-019-03349-1.

Budd Haeberlein S et al. (2022) Two randomized phase 3 studies of aducanumab in early Alzheimer's disease. J Prev Alzheimers Dis 9:197–210 Available at: http://dx.doi.org/10.14283/jpad.2022.30.

Bugiani O, Murrell JR, Giaccone G, Hasegawa M, Ghigo G, Tabaton M, Morbin M, Primavera A, Carella F, Solaro C, Grisoli M, Savoiardo M, Spillantini MG, Tagliavini F, Goedert M, Ghetti B (1999) Frontotemporal dementia and corticobasal degeneration in a family with a P301S mutation in tau. J Neuropathol Exp Neurol 58:667–677 Available at: http://dx.doi.org/10.1097/00005072-199906000-00011.

Cai M, Yue M, Chen T, Liu J, Forno E, Lu X, Billiar T, Celedón J, McKennan C, Chen W, Wang J (2022) Robust and accurate estimation of cellular fraction from tissue omics data via ensemble deconvolution. Bioinformatics 38:3004–3010 Available at: http://dx.doi.org/10.1093/bioinformatics/btac279.

Cairns NJ et al. (2007) Neuropathologic diagnostic and nosologic criteria for frontotemporal lobar degeneration: consensus of the Consortium for Frontotemporal Lobar Degeneration. Acta Neuropathol 114:5–22 Available at: http://dx.doi.org/10.1007/s00401-007-0237-2.

Chai K, Zhang X, Tang H, Gu H, Ye W, Wang G, Chen S, Wan F, Liang J, Shen D (2022) The Application of Consensus Weighted Gene Co-expression Network Analysis to Comparative Transcriptome Meta-Datasets of Multiple Sclerosis in Gray and White Matter. Front Neurol 13:807349 Available at: http://dx.doi.org/10.3389/fneur.2022.807349.

Chancellor KB, Chancellor SE, Duke-Cohan JE, Huber BR, Stein TD, Alvarez VE, Okaty BW, Dymecki SM, McKee AC (2021) Altered oligodendroglia and astroglia in chronic traumatic encephalopathy. Acta Neuropathol 142:295–321 Available at: http://dx.doi.org/10.1007/s00401-021-02322-2.

Chaudhry A, Houlden H, Rizig M (2020) Novel fluid biomarkers to differentiate frontotemporal dementia and dementia with Lewy bodies from Alzheimer's disease: A systematic review. J Neurol Sci 415:116886 Available at: http://dx.doi.org/10.1016/j.jns.2020.116886.

Chen H, Boutros PC (2011) VennDiagram: a package for the generation of highly-customizable

Venn and Euler diagrams in R. BMC Bioinformatics 12:35 Available at: http://dx.doi.org/10.1186/1471-2105-12-35.

Chen S, Townsend K, Goldberg TE, Davies P, Conejero-Goldberg C (2010) MAPT isoforms: differential transcriptional profiles related to 3R and 4R splice variants. J Alzheimers Dis 22:1313–1329 Available at: http://dx.doi.org/10.3233/JAD-2010-101155.

Chen Z-R, Huang J-B, Yang S-L, Hong F-F (2022) Role of cholinergic signaling in Alzheimer's disease. Molecules 27:1816 Available at: http://dx.doi.org/10.3390/molecules27061816.

Cherry JD et al. (2018a) Variation in TMEM106B in chronic traumatic encephalopathy. Acta Neuropathol Commun 6:115 Available at: http://dx.doi.org/10.1186/s40478-018-0619-9.

Cherry JD, Zeineddin A, Dammer EB, Webster JA, Duong D, Seyfried NT, Levey AI, Alvarez VE, Huber BR, Stein TD, Kiernan PT, McKee AC, Lah JJ, Hales CM (2018b) Characterization of detergent insoluble proteome in chronic traumatic encephalopathy. J Neuropathol Exp Neurol 77:40–49 Available at: http://dx.doi.org/10.1093/jnen/nlx100.

Chung D-EC, Roemer S, Petrucelli L, Dickson DW (2021) Cellular and pathological heterogeneity of primary tauopathies. Mol Neurodegener 16:57 Available at: http://dx.doi.org/10.1186/s13024-021-00476-x.

Clarke LE, Liddelow SA, Chakraborty C, Münch AE, Heiman M, Barres BA (2018) Normal aging induces A1-like astrocyte reactivity. Proc Natl Acad Sci U S A 115:E1896–E1905 Available at: http://dx.doi.org/10.1073/pnas.1800165115.

Congdon EE, Ji C, Tetlow AM, Jiang Y, Sigurdsson EM (2023) Tau-targeting therapies for Alzheimer disease: current status and future directions. Nat Rev Neurol:1–22 Available at: https://www.nature.com/articles/s41582-023-00883-2 [Accessed October 24, 2023].

Constantinides VC, Paraskevas GP, Paraskevas PG, Stefanis L, Kapaki E (2019) Corticobasal degeneration and corticobasal syndrome: A review. Clin Park Relat Disord 1:66–71 Available at: http://dx.doi.org/10.1016/j.prdoa.2019.08.005.

Cordivari C, Misra VP, Catania S, Lees AJ (2001) Treatment of dystonic clenched fist with botulinum toxin. Mov Disord 16:907–913 Available at: http://dx.doi.org/10.1002/mds.1186.

Coughlin DG, Hiniker A, Peterson C, Kim Y, Arezoumandan S, Giannini L, Pizzo D, Weintraub D, Siderowf A, Litvan I, Rissman RA, Galasko D, Hansen L, Trojanowski JQ, Lee E, Grossman M, Irwin D (2022) Digital Histological Study of Neocortical Grey and White Matter Tau Burden Across Tauopathies. J Neuropathol Exp Neurol Available at: http://dx.doi.org/10.1093/jnen/nlac094.

Coughlin DG, Litvan I (2020) Progressive supranuclear palsy: Advances in diagnosis and management. Parkinsonism Relat Disord 73:105–116 Available at: http://dx.doi.org/10.1016/j.parkreldis.2020.04.014.

Critchley M (1957) Medical aspects of boxing, particularly from a neurological standpoint. BMJ

1:357–362 Available at: http://dx.doi.org/10.1136/bmj.1.5015.357.

Cummings J, Rabinovici GD, Atri A, Aisen P, Apostolova LG, Hendrix S, Sabbagh M, Selkoe D, Weiner M, Salloway S (2022) Aducanumab: Appropriate Use Recommendations update. J Prev Alzheimers Dis 9:221–230 Available at: http://dx.doi.org/10.14283/jpad.2022.34.

Dammer E (2022a) GOparallel: Uses monthly updated .GMT formatted ontology gene lists for Fisher exact enrichment into differential or co-expression or other user-supplied gene lists. Compatible with the Seyfried systems biology pipeline. Github. Available at: https://github.com/edammer/GOparallel [Accessed May 24, 2023].

Dammer E (2022b) parANOVA: Fast parallel ANOVA+Tukey statistics with fallback option and volcano plot function. Github. Available at: https://github.com/edammer/parANOVA [Accessed May 24, 2023].

Dammer E (2023) CellTypeFET: Calculate and Plot Significance of Gene List Overlap. Github. Available at: https://github.com/edammer/CellTypeFET [Accessed May 24, 2023].

Dammer EB, Ping L, Duong DM, Modeste ES, Seyfried NT, Lah JJ, Levey AI, Johnson ECB (2022) Multi-platform proteomic analysis of Alzheimer's disease cerebrospinal fluid and plasma reveals network biomarkers associated with proteostasis and the matrisome. Alzheimers Res Ther 14:174 Available at: http://dx.doi.org/10.1186/s13195-022-01113-5.

Dammer EB, Seyfried NT, Johnson ECB (2023) Batch correction and harmonization of -omics datasets with a tunable median polish of ratio. Front Syst Biol 3 Available at: http://dx.doi.org/10.3389/fsysb.2023.1092341.

Delacourte A, Sergeant N, Wattez A, Gauvreau D, Robitaille Y (1998) Vulnerable neuronal subsets in Alzheimer's and Pick's disease are distinguished by their tau isoform distribution and phosphorylation. Ann Neurol 43:193–204 Available at: http://dx.doi.org/10.1002/ana.410430209.

Detmer FJ, Alpert NM, Moon S-H, Dhaynaut M, Guerrero JL, Guehl NJ, Xing F, Brugarolas P, Shoup TM, Normandin MD, Pelletier-Galarneau M, El Fakhri G, Petibon Y (2022) PET imaging of mitochondrial function in acute doxorubicin-induced cardiotoxicity: a proof-of-principle study. Sci Rep 12:6122 Available at: http://dx.doi.org/10.1038/s41598-022-10004-6.

Diaz-Castro B, Gangwani MR, Yu X, Coppola G, Khakh BS (2019) Astrocyte molecular signatures in Huntington's disease. Sci Transl Med 11 Available at: http://dx.doi.org/10.1126/scitranslmed.aaw8546.

Dickson DW, Bergeron C, Chin SS, Duyckaerts C, Horoupian D, Ikeda K, Jellinger K, Lantos PL, Lippa CF, Mirra SS, Tabaton M, Vonsattel JP, Wakabayashi K, Litvan I, Office of Rare Diseases of the National Institutes of Health (2002) Office of Rare Diseases neuropathologic criteria for corticobasal degeneration. J Neuropathol Exp Neurol 61:935–946 Available at: http://dx.doi.org/10.1093/jnen/61.11.935.

DiVincenzo C, Elzinga CD, Medeiros AC, Karbassi I, Jones JR, Evans MC, Braastad CD, Bishop

CM, Jaremko M, Wang Z, Liaquat K, Hoffman CA, York MD, Batish SD, Lupski JR, Higgins JJ (2014) The allelic spectrum of Charcot-Marie-Tooth disease in over 17,000 individuals with neuropathy. Mol Genet Genomic Med 2:522–529 Available at: http://dx.doi.org/10.1002/mgg3.106.

Doher N, Davoudi V, Magaki S, Townley RA, Haeri M, Vinters HV (2023) Illustrated neuropathologic diagnosis of Alzheimer's disease. Neurol Int 15:857–867 Available at: http://dx.doi.org/10.3390/neurolint15030054.

Fields RD (2010) Neuroscience. Change in the brain's white matter. Science 330:768–769 Available at: http://dx.doi.org/10.1126/science.1199139.

Fischer Priv.-Doz. Dr. O (1907) Miliare Nekrosen mit drusigen Wucherungen der Neurofibrillen, eine regelmässige Veränderung der Hirnrinde bei seniler Demenz. Eur Neurol 22:361–372 Available at: https://karger.com/mng/article-pdf/22/4/361/3106822/000211873.pdf.

Forrest SL, Lee S, Nassir N, Martinez-Valbuena I, Sackmann V, Li J, Ahmed A, Tartaglia MC, Ittner LM, Lang AE, Uddin M, Kovacs GG (2023) Cell-specific MAPT gene expression is preserved in neuronal and glial tau cytopathologies in progressive supranuclear palsy. Acta Neuropathol Available at: http://dx.doi.org/10.1007/s00401-023-02604-x.

Frost B, Jacks RL, Diamond MI (2009) Propagation of tau misfolding from the outside to the inside of a cell. J Biol Chem 284:12845–12852 Available at: http://dx.doi.org/10.1074/jbc.M808759200.

Fu Z-Q, Yang Y, Song J, Jiang Q, Lin Z-C, Wang Q, Zhu L-Q, Wang J-Z, Tian Q (2010) LiCl attenuates thapsigargin-induced tau hyperphosphorylation by inhibiting GSK-3β in vivo and in vitro. J Alzheimers Dis 21:1107–1117 Available at: http://dx.doi.org/10.3233/jad-2010-100687.

Gauthier-Kemper A, Suárez Alonso M, Sündermann F, Niewidok B, Fernandez M-P, Bakota L, Heinisch JJ, Brandt R (2018) Annexins A2 and A6 interact with the extreme N terminus of tau and thereby contribute to tau's axonal localization. J Biol Chem 293:8065–8076 Available at: http://dx.doi.org/10.1074/jbc.ra117.000490.

Ghetti B, Oblak AL, Boeve BF, Johnson KA, Dickerson BC, Goedert M (2015) Invited review: Frontotemporal dementia caused by microtubule-associated protein tau gene (MAPT) mutations: a chameleon for neuropathology and neuroimaging. Neuropathol Appl Neurobiol 41:24–46 Available at: http://dx.doi.org/10.1111/nan.12213.

Gibb WRG, Luthert PJ, Marsden CD (1989) CORTICOBASAL DEGENERATION. Brain 112:1171–1192 Available at: http://dx.doi.org/10.1093/brain/112.5.1171.

Giebel CM, Knopman D, Mioshi E, Khondoker M (2021) Distinguishing frontotemporal dementia from Alzheimer disease through everyday function profiles: Trajectories of change. J Geriatr Psychiatry Neurol 34:66–75 Available at: http://dx.doi.org/10.1177/0891988720901791.

Goedert M (2009) Oskar Fischer and the study of dementia. Brain 132:1102–1111 Available at:

http://dx.doi.org/10.1093/brain/awn256.

Goedert M, Spillantini MG, Potier MC, Ulrich J, Crowther RA (1989) Cloning and sequencing of the cDNA encoding an isoform of microtubule-associated protein tau containing four tandem repeats: differential expression of tau protein mRNAs in human brain. EMBO J 8:393–399 Available at: http://dx.doi.org/10.1002/j.1460-2075.1989.tb03390.x.

Gómez Ravetti M, Rosso OA, Berretta R, Moscato P (2010) Uncovering molecular biomarkers that correlate cognitive decline with the changes of hippocampus' gene expression profiles in Alzheimer's disease. PLoS One 5:e10153 Available at: http://dx.doi.org/10.1371/journal.pone.0010153.

Gorno-Tempini ML et al. (2011) Classification of primary progressive aphasia and its variants. Neurology 76:1006–1014 Available at: http://dx.doi.org/10.1212/WNL.0b013e31821103e6.

Greaves CV, Rohrer JD (2019) An update on genetic frontotemporal dementia. J Neurol 266:2075–2086 Available at: http://dx.doi.org/10.1007/s00415-019-09363-4.

Greene D, Richardson S, Turro E (2017) ontologyX: a suite of R packages for working with ontological data. Bioinformatics 33:1104–1106 Available at: http://dx.doi.org/10.1093/bioinformatics/btw763.

Grundke-Iqbal I, Iqbal K, Tung YC, Quinlan M, Wisniewski HM, Binder LI (1986) Abnormal phosphorylation of the microtubule-associated protein tau (tau) in Alzheimer cytoskeletal pathology. Proc Natl Acad Sci U S A 83:4913–4917 Available at: http://dx.doi.org/10.1073/pnas.83.13.4913.

Gutierrez-Quiceno L, Dammer EB, Johnson AG, Webster JA, Shah R, Duong D, Yin L, Seyfried NT, Alvarez VE, Stein TD, McKee AC, Hales CM (2021) A proteomic network approach resolves stage-specific molecular phenotypes in chronic traumatic encephalopathy. Mol Neurodegener 16:1–14 Available at: https://molecularneurodegeneration.biomedcentral.com/articles/10.1186/s13024-021-00462-3 [Accessed June 28, 2021].

Hahn O, Foltz AG, Atkins M, Kedir B, Moran-Losada P, Guldner IH, Munson C, Kern F, Pálovics R, Lu N, Zhang H, Kaur A, Hull J, Huguenard JR, Grönke S, Lehallier B, Partridge L, Keller A, Wyss-Coray T (2023) Atlas of the aging mouse brain reveals white matter as vulnerable foci. Cell 0 Available at: http://www.cell.com/article/S009286742300805X/abstract [Accessed August 16, 2023].

Halbgebauer S, Steinacker P, Verde F, Weishaupt J, Oeckl P, von Arnim C, Dorst J, Feneberg E, Mayer B, Rosenbohm A, Silani V, Ludolph AC, Otto M (2021) Comparison of CSF and serum neurofilament light and heavy chain as differential diagnostic biomarkers for ALS. J Neurol Neurosurg Psychiatry Available at: http://dx.doi.org/10.1136/jnnp-2021-327129.

Hales CM, Dammer EB, Deng Q, Duong DM, Gearing M, Troncoso JC, Thambisetty M, Lah JJ, Shulman JM, Levey AI, Seyfried NT (2016) Changes in the detergent-insoluble brain

proteome linked to amyloid and tau in Alzheimer's Disease progression. Proteomics 16:3042–3053 Available at: http://dx.doi.org/10.1002/pmic.201600057.

Hallmann A-L, Araúzo-Bravo MJ, Mavrommatis L, Ehrlich M, Röpke A, Brockhaus J, Missler M, Sterneckert J, Schöler HR, Kuhlmann T, Zaehres H, Hargus G (2017) Astrocyte pathology in a human neural stem cell model of frontotemporal dementia caused by mutant TAU protein. Sci Rep 7:42991 Available at: http://dx.doi.org/10.1038/srep42991.

Hampel H et al. (2021) Omics sciences for systems biology in Alzheimer's disease: State-of-the-art of the evidence. Ageing Res Rev 69:101346 Available at: http://dx.doi.org/10.1016/j.arr.2021.101346.

Hardy J (2006) Alzheimer's disease: the amyloid cascade hypothesis: an update and reappraisal. J Alzheimers Dis 9:151–153 Available at: http://dx.doi.org/10.3233/jad-2006-9s317.

Hardy JA, Higgins GA (1992) Alzheimer's disease: the amyloid cascade hypothesis. Science 256:184–185 Available at: http://dx.doi.org/10.1126/science.1566067.

Hartnell IJ, Woodhouse D, Jasper W, Mason L, Marwaha P, Graffeuil M, Lau LC, Norman JL, Chatelet DS, Buee L, Nicoll JAR, Blum D, Dorothee G, Boche D (2023) Glial reactivity and T cell infiltration in frontotemporal lobar degeneration with tau pathology. Brain Available at: http://dx.doi.org/10.1093/brain/awad309.

Hase Y, Ding R, Harrison G, Hawthorne E, King A, Gettings S, Platten C, Stevenson W, Craggs LJL, Kalaria RN (2019) White matter capillaries in vascular and neurodegenerative dementias. Acta Neuropathol Commun 7:16 Available at: http://dx.doi.org/10.1186/s40478-019-0666-x.

He HJ, Wang XS, Pan R, Wang DL, Liu MN, He RQ (2009) The proline-rich domain of tau plays a role in interactions with actin. BMC Cell Biol 10:81 Available at: http://dx.doi.org/10.1186/1471-2121-10-81.

Hernández F, Merchán-Rubira J, Vallés-Saiz L, Rodríguez-Matellán A, Avila J (2020) Differences between human and Murine tau at the N-terminal end. Front Aging Neurosci 12:11 Available at: http://dx.doi.org/10.3389/fnagi.2020.00011.

Hickman DT, López-Deber MP, Ndao DM, Silva AB, Nand D, Pihlgren M, Giriens V, Madani R, St-Pierre A, Karastaneva H, Nagel-Steger L, Willbold D, Riesner D, Nicolau C, Baldus M, Pfeifer A, Muhs A (2011) Sequence-independent control of peptide conformation in liposomal vaccines for targeting protein misfolding diseases. J Biol Chem 286:13966–13976 Available at: http://dx.doi.org/10.1074/jbc.M110.186338.

Higuchi M, Zhang B, Forman MS, Yoshiyama Y, Trojanowski JQ, Lee VM-Y (2005) Axonal degeneration induced by targeted expression of mutant human tau in oligodendrocytes of transgenic mice that model glial tauopathies. J Neurosci 25:9434–9443 Available at: http://dx.doi.org/10.1523/JNEUROSCI.2691-05.2005.

Hirokawa N, Shiomura Y, Okabe S (1988) Tau proteins: the molecular structure and mode of binding on microtubules. J Cell Biol 107:1449–1459 Available at:

http://dx.doi.org/10.1083/jcb.107.4.1449.

Hock E-M, Polymenidou M (2016) Prion-like propagation as a pathogenic principle in frontotemporal dementia. J Neurochem 138 Suppl 1:163–183 Available at: http://dx.doi.org/10.1111/jnc.13668.

Hoffman GE, Schadt EE (2016) variancePartition: interpreting drivers of variation in complex gene expression studies. BMC Bioinformatics 17:483 Available at: http://dx.doi.org/10.1186/s12859-016-1323-z.

Holleran L, Kim JH, Gangolli M, Stein T, Alvarez V, McKee A, Brody DL (2017) Axonal disruption in white matter underlying cortical sulcus tau pathology in chronic traumatic encephalopathy. Acta Neuropathol 133:367–380 Available at: http://dx.doi.org/10.1007/s00401-017-1686-x.

Houlden H et al. (2001) Corticobasal degeneration and progressive supranuclear palsy share a common tau haplotype. Neurology 56:1702–1706 Available at: http://dx.doi.org/10.1212/wnl.56.12.1702.

Hu Y-T, Chen X-L, Huang S-H, Zhu Q-B, Yu S-Y, Shen Y, Sluiter A, Verhaagen J, Zhao J, Swaab D, Bao A-M (2019) Early growth response-1 regulates acetylcholinesterase and its relation with the course of Alzheimer's disease. Brain Pathol 29:502–512 Available at: http://dx.doi.org/10.1111/bpa.12688.

Hull C, Dekeryte R, Buchanan H, Kamli-Salino S, Robertson A, Delibegovic M, Platt B (2020) NLRP3 inflammasome inhibition with MCC950 improves insulin sensitivity and inflammation in a mouse model of frontotemporal dementia. Neuropharmacology 180:108305 Available at: http://dx.doi.org/10.1016/j.neuropharm.2020.108305.

Hutton M et al. (1998) Association of missense and 5'-splice-site mutations in tau with the inherited dementia FTDP-17. Nature 393:702–705 Available at: http://dx.doi.org/10.1038/31508.

Hyman BT, Phelps CH, Beach TG, Bigio EH, Cairns NJ, Carrillo MC, Dickson DW, Duyckaerts C, Frosch MP, Masliah E, Mirra SS, Nelson PT, Schneider JA, Thal DR, Thies B, Trojanowski JQ, Vinters HV, Montine TJ (2012) National Institute on Aging–Alzheimer's Association guidelines for the neuropathologic assessment of Alzheimer's disease. Alzheimers Dement 8:1–13 Available at: http://dx.doi.org/10.1016/j.jalz.2011.10.007.

Imbimbo BP, Balducci C, Ippati S, Watling M (2023) Initial failures of anti-tau antibodies in Alzheimer's disease are reminiscent of the amyloid-β story. Neural Regen Res 18:117–118 Available at: http://dx.doi.org/10.4103/1673-5374.340409.

Irwin DJ, Brettschneider J, McMillan CT, Cooper F, Olm C, Arnold SE, Van Deerlin VM, Seeley WW, Miller BL, Lee EB, Lee VM-Y, Grossman M, Trojanowski JQ (2016) Deep clinical and neuropathological phenotyping of Pick disease. Ann Neurol 79:272–287 Available at: http://dx.doi.org/10.1002/ana.24559.

Jack CR Jr, Knopman DS, Jagust WJ, Petersen RC, Weiner MW, Aisen PS, Shaw LM, Vemuri P,

Wiste HJ, Weigand SD, Lesnick TG, Pankratz VS, Donohue MC, Trojanowski JQ (2013) Tracking pathophysiological processes in Alzheimer's disease: an updated hypothetical model of dynamic biomarkers. Lancet Neurol 12:207–216 Available at: http://dx.doi.org/10.1016/S1474-4422(12)70291-0.

Jansen WJ et al. (2022) Prevalence estimates of amyloid abnormality across the Alzheimer disease clinical spectrum. JAMA Neurol 79:228–243 Available at: http://dx.doi.org/10.1001/jamaneurol.2021.5216.

Jeganathan S, von Bergen M, Mandelkow E-M, Mandelkow E (2008) The natively unfolded character of tau and its aggregation to Alzheimer-like paired helical filaments. Biochemistry 47:10526–10539 Available at: http://dx.doi.org/10.1021/bi800783d.

Johnson AG, Webster JA, Hales CM (2021) Glial profiling of human tauopathy brain demonstrates enrichment of astrocytic transcripts in tau-related frontotemporal degeneration. Neurobiol Aging Available at: https://linkinghub.elsevier.com/retrieve/pii/S0197458021003602.

Johnson ECB et al. (2020) Large-scale proteomic analysis of Alzheimer's disease brain and cerebrospinal fluid reveals early changes in energy metabolism associated with microglia and astrocyte activation. Nat Med Available at: http://dx.doi.org/10.1038/s41591-020-0815-6.

Johnson ECB et al. (2022) Large-scale deep multi-layer analysis of Alzheimer's disease brain reveals strong proteomic disease-related changes not observed at the RNA level. Nat Neurosci 25:213–225 Available at: http://dx.doi.org/10.1038/s41593-021-00999-y.

Johnson ECB, Dammer EB, Duong DM, Yin L, Thambisetty M, Troncoso JC, Lah JJ, Levey AI, Seyfried NT (2018) Deep proteomic network analysis of Alzheimer's disease brain reveals alterations in RNA binding proteins and RNA splicing associated with disease. Mol Neurodegener 13:52 Available at: http://dx.doi.org/10.1186/s13024-018-0282-4.

Kadavath H, Hofele RV, Biernat J, Kumar S, Tepper K, Urlaub H, Mandelkow E, Zweckstetter M (2015) Tau stabilizes microtubules by binding at the interface between tubulin heterodimers. Proc Natl Acad Sci U S A 112:7501–7506 Available at: http://dx.doi.org/10.1073/pnas.1504081112.

Karahalil B (2016) Overview of systems biology and omics technologies. Curr Med Chem 23:4221–4230 Available at: https://www.ncbi.nlm.nih.gov/pubmed/27686657.

Kassambra A, Mundt F (2020) factoextra: Extract and Visualize the Results of Multivariate Data Analyses. Available at: https://CRAN.R-project.org/package=factoextra.

Keren-Shaul H, Spinrad A, Weiner A, Matcovitch-Natan O, Dvir-Szternfeld R, Ulland TK, David E, Baruch K, Lara-Astaiso D, Toth B, Itzkovitz S, Colonna M, Schwartz M, Amit I (2017) A Unique Microglia Type Associated with Restricting Development of Alzheimer's Disease. Cell 169:1276-1290.e17 Available at: http://dx.doi.org/10.1016/j.cell.2017.05.018.

Kidd M (1963) Paired helical filaments in electron microscopy of Alzheimer's disease. Nature

197:192–193 Available at: http://dx.doi.org/10.1038/197192b0.

Knopman DS, Roberts RO (2011) Estimating the number of persons with frontotemporal lobar degeneration in the US population. J Mol Neurosci 45:330–335 Available at: http://dx.doi.org/10.1007/s12031-011-9538-y.

Kompoliti K, Goetz CG, Boeve BF, Maraganore DM, Ahlskog JE, Marsden CD, Bhatia KP, Greene PE, Przedborski S, Seal EC, Burns RS, Hauser RA, Gauger LL, Factor SA, Molho ES, Riley DE (1998) Clinical presentation and pharmacological therapy in corticobasal degeneration. Arch Neurol 55:957–961 Available at: http://dx.doi.org/10.1001/archneur.55.7.957.

Kontsekova E, Zilka N, Kovacech B, Novak P, Novak M (2014) First-in-man tau vaccine targeting structural determinants essential for pathological tau-tau interaction reduces tau oligomerisation and neurofibrillary degeneration in an Alzheimer's disease model. Alzheimers Res Ther 6:44 Available at: http://dx.doi.org/10.1186/alzrt278.

Kosik KS, Joachim CL, Selkoe DJ (1986) Microtubule-associated protein tau (tau) is a major antigenic component of paired helical filaments in Alzheimer disease. Proc Natl Acad Sci U S A 83:4044–4048 Available at: http://dx.doi.org/10.1073/pnas.83.11.4044.

Kouri N, Carlomagno Y, Baker M, Liesinger AM, Caselli RJ, Wszolek ZK, Petrucelli L, Boeve BF, Parisi JE, Josephs KA, Uitti RJ, Ross OA, Graff-Radford NR, DeTure MA, Dickson DW, Rademakers R (2014) Novel mutation in MAPT exon 13 (p.N410H) causes corticobasal degeneration. Acta Neuropathol 127:271–282 Available at: http://dx.doi.org/10.1007/s00401-013-1193-7.

Kovacs GG (2015) Invited review: Neuropathology of tauopathies: principles and practice. Neuropathol Appl Neurobiol 41:3–23 Available at: http://dx.doi.org/10.1111/nan.12208.

Kovacs GG et al. (2020) Distribution patterns of tau pathology in progressive supranuclear palsy. Acta Neuropathol 140:99–119 Available at: http://dx.doi.org/10.1007/s00401-020-02158-2.

Kovacs GG, Lee VM, Trojanowski JQ (2017) Protein astrogliopathies in human neurodegenerative diseases and aging. Brain Pathol 27:675–690 Available at: http://dx.doi.org/10.1111/bpa.12536.

Li Q, Haney MS (2020) The role of glia in protein aggregation. Neurobiol Dis 143:105015 Available at: http://dx.doi.org/10.1016/j.nbd.2020.105015.

Li T-T, Liu M-R, Pei D-S (2019) Friend or foe, the role of EGR-1 in cancer. Med Oncol 37:7 Available at: http://dx.doi.org/10.1007/s12032-019-1333-6.

Liao L, Cheng D, Wang J, Duong DM, Losik TG, Gearing M, Rees HD, Lah JJ, Levey AI, Peng J (2004) Proteomic Characterization of Postmortem Amyloid Plaques Isolated by Laser Capture Microdissection*. J Biol Chem 279:37061–37068 Available at: https://www.sciencedirect.com/science/article/pii/S0021925820859596.

Liddelow SA et al. (2017) Neurotoxic reactive astrocytes are induced by activated microglia. Nature 541:481–487 Available at: http://dx.doi.org/10.1038/nature21029.

Lim B, Grøntvedt GR, Bathala P, Kale SS, Campbell CT, Stengelin M, Sando SB, Prassas I, Diamandis EP, Bråthen G (2021) CSF neurofilament light may predict progression from amnestic mild cognitive impairment to Alzheimer's disease dementia. Neurobiol Aging 107:78–85 Available at: http://dx.doi.org/10.1016/j.neurobiolaging.2021.07.013.

Lindsley CW (2017) Chronic traumatic encephalopathy (CTE): A brief historical overview and recent focus on NFL players. ACS Chem Neurosci 8:1629–1631 Available at: http://dx.doi.org/10.1021/acschemneuro.7b00291.

Litvinchuk A, Wan Y-W, Swartzlander DB, Chen F, Cole A, Propson NE, Wang Q, Zhang B, Liu Z, Zheng H (2018) Complement C3aR inactivation attenuates tau pathology and reverses an immune network deregulated in tauopathy models and Alzheimer's disease. Neuron 100:1337-1353.e5 Available at: http://dx.doi.org/10.1016/j.neuron.2018.10.031.

Liu Y, Beyer A, Aebersold R (2016) On the Dependency of Cellular Protein Levels on mRNA Abundance. Cell 165:535–550 Available at: http://dx.doi.org/10.1016/j.cell.2016.03.014.

LoPresti P, Szuchet S, Papasozomenos SC, Zinkowski RP, Binder LI (1995) Functional implications for the microtubule-associated protein tau: localization in oligodendrocytes. Proc Natl Acad Sci U S A 92:10369–10373 Available at: http://dx.doi.org/10.1073/pnas.92.22.10369.

Lu Y, Li T, Qureshi HY, Han D, Paudel HK (2011) Early growth response 1 (Egr-1) regulates phosphorylation of microtubule-associated protein tau in mammalian brain. J Biol Chem 286:20569–20581 Available at: http://dx.doi.org/10.1074/jbc.M111.220962.

Macedo AC, Tissot C, Therriault J, Servaes S, Wang Y-T, Fernandez-Arias J, Rahmouni N, Lussier FZ, Vermeiren M, Bezgin G, Vitali P, Ng KP, Zimmer ER, Guiot M-C, Pascoal TA, Gauthier S, Rosa-Neto P (2023) The use of tau PET to stage Alzheimer disease according to the Braak staging framework. J Nucl Med 64:1171–1178 Available at: http://dx.doi.org/10.2967/jnumed.122.265200.

Mangleburg CG, Wu T, Yalamanchili HK, Guo C, Hsieh Y-C, Duong DM, Dammer EB, De Jager PL, Seyfried NT, Liu Z, Shulman JM (2020) Integrated analysis of the aging brain transcriptome and proteome in tauopathy. Mol Neurodegener 15:56 Available at: http://dx.doi.org/10.1186/s13024-020-00405-4.

Martland HS (1928) PUNCH DRUNK. J Am Med Assoc 91:1103 Available at: http://dx.doi.org/10.1001/jama.1928.02700150029009.

Marucci G, Buccioni M, Ben DD, Lambertucci C, Volpini R, Amenta F (2021) Efficacy of acetylcholinesterase inhibitors in Alzheimer's disease. Neuropharmacology 190:108352 Available at: http://dx.doi.org/10.1016/j.neuropharm.2020.108352.

Mathys H, Davila-Velderrain J, Peng Z, Gao F, Mohammadi S, Young JZ, Menon M, He L, Abdurrob F, Jiang X, Martorell AJ, Ransohoff RM, Hafler BP, Bennett DA, Kellis M, Tsai

L-H (2019) Single-cell transcriptomic analysis of Alzheimer's disease. Nature 570:332–337 Available at: http://dx.doi.org/10.1038/s41586-019-1195-2.

McKee AC et al. (2013) The spectrum of disease in chronic traumatic encephalopathy. Brain 136:43–64 Available at: http://dx.doi.org/10.1093/brain/aws307.

Merezhko M, Uronen R-L, Huttunen HJ (2020) The cell biology of tau secretion. Front Mol Neurosci 13:569818 Available at: http://dx.doi.org/10.3389/fnmol.2020.569818.

Mez J et al. (2017) Clinicopathological evaluation of chronic traumatic encephalopathy in players of American football. JAMA 318:360–370 Available at: http://dx.doi.org/10.1001/jama.2017.8334.

Miedema SSM, Mol MO, Koopmans FTW, Hondius DC, van Nierop P, Menden K, de Veij Mestdagh CF, van Rooij J, Ganz AB, Paliukhovich I, Melhem S, Li KW, Holstege H, Rizzu P, van Kesteren RE, van Swieten JC, Heutink P, Smit AB (2022) Distinct cell type-specific protein signatures in GRN and MAPT genetic subtypes of frontotemporal dementia. Acta Neuropathol Commun 10:100 Available at: http://dx.doi.org/10.1186/s40478-022-01387-8.

Mills JD, Kavanagh T, Kim WS, Chen BJ, Kawahara Y, Halliday GM, Janitz M (2013) Unique transcriptome patterns of the white and grey matter corroborate structural and functional heterogeneity in the human frontal lobe. PLoS One 8:e78480 Available at: http://dx.doi.org/10.1371/journal.pone.0078480.

Millspaugh JA (1937) Dementia pugilistica. U S Nav Med 35:297–303.

Minaya MA, Mahali S, Iyer AK, Eteleeb AM, Martinez R, Huang G, Budde J, Temple S, Nana AL, Seeley WW, Spina S, Grinberg LT, Harari O, Karch CM (2023) Conserved gene signatures shared among MAPT mutations reveal defects in calcium signaling. Front Mol Biosci 10:1051494 Available at: http://dx.doi.org/10.3389/fmolb.2023.1051494.

Mirra SS, Heyman A, McKeel D, Sumi SM, Crain BJ, Brownlee LM, Vogel FS, Hughes JP, van Belle G, Berg L (1991) The Consortium to Establish a Registry for Alzheimer's Disease (CERAD). Part II. Standardization of the neuropathologic assessment of Alzheimer's disease. Neurology 41:479–486 Available at: http://dx.doi.org/10.1212/wnl.41.4.479.

Mittelbronn M, Dietz K, Schluesener HJ, Meyermann R (2001) Local distribution of microglia in the normal adult human central nervous system differs by up to one order of magnitude. Acta Neuropathol 101:249–255 Available at: http://dx.doi.org/10.1007/s004010000284.

Mizee MR, Miedema SSM, van der Poel M, Adelia, Schuurman KG, van Strien ME, Melief J, Smolders J, Hendrickx DA, Heutinck KM, Hamann J, Huitinga I (2017) Isolation of primary microglia from the human post-mortem brain: effects of ante- and post-mortem variables. Acta Neuropathol Commun 5 Available at: http://dx.doi.org/10.1186/s40478-017-0418-8.

Moccia M, Quarantelli M, Lanzillo R, Cocozza S, Carotenuto A, Carotenuto B, Alfano B, Prinster A, Triassi M, Nardone A, Palladino R, Brunetti A, Brescia Morra V (2017) Grey:white

matter ratio at diagnosis and the risk of 10-year multiple sclerosis progression. Eur J Neurol 24:195–204 Available at: http://dx.doi.org/10.1111/ene.13183.

Montenigro PH, Baugh CM, Daneshvar DH, Mez J, Budson AE, Au R, Katz DI, Cantu RC, Stern RA (2014) Clinical subtypes of chronic traumatic encephalopathy: literature review and proposed research diagnostic criteria for traumatic encephalopathy syndrome. Alzheimers Res Ther 6:68 Available at: http://dx.doi.org/10.1186/s13195-014-0068-z.

Montenigro PH, Bernick C, Cantu RC (2015) Clinical features of repetitive traumatic brain injury and chronic traumatic encephalopathy. Brain Pathol 25:304–317 Available at: http://dx.doi.org/10.1111/bpa.12250.

Montine TJ, Phelps CH, Beach TG, Bigio EH, Cairns NJ, Dickson DW, Duyckaerts C, Frosch MP, Masliah E, Mirra SS, Nelson PT, Schneider JA, Thal DR, Trojanowski JQ, Vinters HV, Hyman BT, National Institute on Aging, Alzheimer's Association (2012) National Institute on Aging-Alzheimer's Association guidelines for the neuropathologic assessment of Alzheimer's disease: a practical approach. Acta Neuropathol 123:1–11 Available at: http://dx.doi.org/10.1007/s00401-011-0910-3.

Mummery CJ et al. (2023) Tau-targeting antisense oligonucleotide MAPTRx in mild Alzheimer's disease: a phase 1b, randomized, placebo-controlled trial. Nat Med 29:1437–1447 Available at: http://dx.doi.org/10.1038/s41591-023-02326-3.

Musa G, Slachevsky A, Muñoz-Neira C, Méndez-Orellana C, Villagra R, González-Billault C, Ibáñez A, Hornberger M, Lillo P (2020) Alzheimer's disease or behavioral variant frontotemporal dementia? Review of key points toward an accurate clinical and neuropsychological diagnosis. J Alzheimers Dis 73:833–848 Available at: http://dx.doi.org/10.3233/JAD-190924.

Neve RL, Harris P, Kosik KS, Kurnit DM, Donlon TA (1986) Identification of cDNA clones for the human microtubule-associated protein tau and chromosomal localization of the genes for tau and microtubule-associated protein 2. Brain Res Mol Brain Res 1:271–280 Available at: http://dx.doi.org/10.1016/0169-328x(86)90033-1.

Noori A, Mezlini AM, Hyman BT, Serrano-Pozo A, Das S (2021) Systematic review and meta-analysis of human transcriptomics reveals neuroinflammation, deficient energy metabolism, and proteostasis failure across neurodegeneration. Neurobiol Dis 149:105225 Available at: http://dx.doi.org/10.1016/j.nbd.2020.105225.

Novak P et al. (2017) Safety and immunogenicity of the tau vaccine AADvac1 in patients with Alzheimer's disease: a randomised, double-blind, placebo-controlled, phase 1 trial. Lancet Neurol 16:123–134 Available at: http://dx.doi.org/10.1016/S1474-4422(16)30331-3.

Oeckl P, Steinacker P, Feneberg E, Otto M (2016) Neurochemical biomarkers in the diagnosis of frontotemporal lobar degeneration: an update. J Neurochem 138 Suppl 1:184–192 Available at: http://dx.doi.org/10.1111/jnc.13669.

Ojala JO, Sutinen EM, Salminen A, Pirttilä T (2008) Interleukin-18 increases expression of kinases

involved in tau phosphorylation in SH-SY5Y neuroblastoma cells. J Neuroimmunol 205:86–93 Available at: http://dx.doi.org/10.1016/j.jneuroim.2008.09.012.

Olney NT, Spina S, Miller BL (2017) Frontotemporal Dementia. Neurol Clin 35:339–374 Available at: http://dx.doi.org/10.1016/j.ncl.2017.01.008.

Omalu BI, DeKosky ST, Hamilton RL, Minster RL, Kamboh MI, Shakir AM, Wecht CH (2006) Chronic traumatic encephalopathy in a national football league player: part II. Neurosurgery 59:1086–1092; discussion 1092-3 Available at: http://dx.doi.org/10.1227/01.NEU.0000245601.69451.27.

Omalu BI, DeKosky ST, Minster RL, Kamboh MI, Hamilton RL, Wecht CH (2005) Chronic traumatic encephalopathy in a National Football League player. Neurosurgery 57:128–134; discussion 128-34 Available at: http://dx.doi.org/10.1227/01.neu.0000163407.92769.ed.

Omalu BI, Hamilton RL, Kamboh MI, DeKosky ST, Bailes J (2010) Chronic traumatic encephalopathy (CTE) in a National Football League Player: Case report and emerging medicolegal practice questions. J Forensic Nurs 6:40–46 Available at: http://dx.doi.org/10.1111/j.1939-3938.2009.01064.x.

Onyike CU, Diehl-Schmid J (2013) The epidemiology of frontotemporal dementia. Int Rev Psychiatry 25:130–137 Available at: http://dx.doi.org/10.3109/09540261.2013.776523.

Onyike CU, Huey ED (2013) Frontotemporal dementia and psychiatry. Int Rev Psychiatry 25:127–129 Available at: http://dx.doi.org/10.3109/09540261.2013.785169.

Pansieri J, Hadley G, Lockhart A, Pisa M, DeLuca GC (2023) Regional contribution of vascular dysfunction in white matter dementia: clinical and neuropathological insights. Front Neurol 14:1199491 Available at: http://dx.doi.org/10.3389/fneur.2023.1199491.

Pick A (1892) Uber die Beziehungen der senilen Hirnatrophie zur Aphasie. Prag Med Wochenschr 17:165–167 Available at: https://ci.nii.ac.jp/naid/10021235320/ [Accessed July 1, 2020].

Pierre K, Dyson K, Dagra A, Williams E, Porche K, Lucke-Wold B (2021) Chronic traumatic encephalopathy: Update on current clinical diagnosis and management. Biomedicines 9:415 Available at: http://dx.doi.org/10.3390/biomedicines9040415.

Pittman AM (2005) Linkage disequilibrium fine mapping and haplotype association analysis of the tau gene in progressive supranuclear palsy and corticobasal degeneration. J Med Genet 42:837–846 Available at: http://dx.doi.org/10.1136/jmg.2005.031377.

Polsinelli AJ, Apostolova LG (2022) Atypical Alzheimer disease variants. Continuum (Minneap Minn) 28:676–701 Available at: http://dx.doi.org/10.1212/CON.0000000000001082.

Poorkaj P, Bird TD, Wijsman E, Nemens E, Garruto RM, Anderson L, Andreadis A, Wiederholt WC, Raskind M, Schellenberg GD (1998) Tau is a candidate gene for chromosome 17 frontotemporal dementia. Ann Neurol 43:815–825 Available at: http://dx.doi.org/10.1002/ana.410430617.

Pozojevic J, Spielmann M (2023) Single-cell sequencing in neurodegenerative disorders. Mol Diagn Ther 27:553–561 Available at: http://dx.doi.org/10.1007/s40291-023-00668-9.

Putcha D, Katsumi Y, Brickhouse M, Flaherty R, Salat DH, Touroutoglou A, Dickerson BC (2023) Gray to white matter signal ratio as a novel biomarker of neurodegeneration in Alzheimer's disease. NeuroImage Clin 37:103303 Available at: http://dx.doi.org/10.1016/j.nicl.2022.103303.

R Core Team (2023) R: A Language and Environment for Statistical Computing. Vienna, Austria: R Foundation for Statistical Computing. Available at: https://www.R-project.org/.

Rabinovici GD (2019) Late-onset Alzheimer disease. Continuum (Minneap Minn) 25:14–33 Available at: http://dx.doi.org/10.1212/con.0000000000000700.

Rai NK, Singh V, Li L, Willard B, Tripathi A, Dutta R (2021) Comparative Proteomic Profiling Identifies Reciprocal Expression of Mitochondrial Proteins Between White and Gray Matter Lesions From Multiple Sclerosis Brains. Front Neurol 12:779003 Available at: http://dx.doi.org/10.3389/fneur.2021.779003.

Rajan KB, Weuve J, Barnes LL, McAninch EA, Wilson RS, Evans DA (2021) Population estimate of people with clinical Alzheimer's disease and mild cognitive impairment in the United States (2020-2060). Alzheimers Dement 17:1966–1975 Available at: http://dx.doi.org/10.1002/alz.12362.

Rangaraju S, Dammer EB, Raza SA, Rathakrishnan P, Xiao H, Gao T, Duong DM, Pennington MW, Lah JJ, Seyfried NT, Levey AI (2018) Identification and therapeutic modulation of a pro-inflammatory subset of disease-associated-microglia in Alzheimer's disease. Mol Neurodegener 13 Available at: http://dx.doi.org/10.1186/s13024-018-0254-8.

Rascovsky K et al. (2011) Sensitivity of revised diagnostic criteria for the behavioural variant of frontotemporal dementia. Brain 134:2456–2477 Available at: http://dx.doi.org/10.1093/brain/awr179.

Rath S et al. (2021) MitoCarta3.0: an updated mitochondrial proteome now with sub-organelle localization and pathway annotations. Nucleic Acids Res 49:D1541–D1547 Available at: http://dx.doi.org/10.1093/nar/gkaa1011.

Raudvere U, Kolberg L, Kuzmin I, Arak T, Adler P, Peterson H, Vilo J (2019) g:Profiler: a web server for functional enrichment analysis and conversions of gene lists (2019 update). Nucleic Acids Res 47:W191–W198 Available at: http://dx.doi.org/10.1093/nar/gkz369.

Rayaprolu S, Higginbotham L, Bagchi P, Watson CM, Zhang T, Levey AI, Rangaraju S, Seyfried NT (2021) Systems-based proteomics to resolve the biology of Alzheimer's disease beyond amyloid and tau. Neuropsychopharmacology 46:98–115 Available at: http://dx.doi.org/10.1038/s41386-020-00840-3.

Reardon S (2023) FDA approves Alzheimer's drug lecanemab amid safety concerns. Nature 613:227–228 Available at: http://dx.doi.org/10.1038/d41586-023-00030-3.

Rebeiz JJ, Kolodny EH, Richardson EP Jr (1967) Corticodentatonigral degeneration with neuronal achromasia: a progressive disorder of late adult life. Trans Am Neurol Assoc 92:23–26 Available at: https://www.ncbi.nlm.nih.gov/pubmed/5634049.

Rehiman SH, Lim SM, Neoh CF, Majeed ABA, Chin A-V, Tan MP, Kamaruzzaman SB, Ramasamy K (2020) Proteomics as a reliable approach for discovery of blood-based Alzheimer's disease biomarkers: A systematic review and meta-analysis. Ageing Res Rev 60:101066 Available at: http://dx.doi.org/10.1016/j.arr.2020.101066.

Reitz C, Rogaeva E, Beecham GW (2020) Late-onset vs nonmendelian early-onset Alzheimer disease: A distinction without a difference? Neurol Genet 6:e512 Available at: http://dx.doi.org/10.1212/NXG.0000000000000512.

Roberts M et al. (2020) Pre-clinical characterisation of E2814, a high-affinity antibody targeting the microtubule-binding repeat domain of tau for passive immunotherapy in Alzheimer's disease. Acta Neuropathol Commun 8:13 Available at: http://dx.doi.org/10.1186/s40478-020-0884-2.

Robinson JL, Yan N, Caswell C, Xie SX, Suh E, Van Deerlin VM, Gibbons G, Irwin DJ, Grossman M, Lee EB, Lee VM-Y, Miller B, Trojanowski JQ (2020) Primary tau pathology, not copathology, correlates with clinical symptoms in PSP and CBD. J Neuropathol Exp Neurol 79:296–304 Available at: http://dx.doi.org/10.1093/jnen/nlz141.

Rohrer JD, Boxer AL (2021) The frontotemporal dementia Prevention Initiative: Linking together genetic frontotemporal dementia cohort studies. Adv Exp Med Biol 1281:113–121 Available at: http://dx.doi.org/10.1007/978-3-030-51140-1_8.

Rohrer JD, Guerreiro R, Vandrovcova J, Uphill J, Reiman D, Beck J, Isaacs AM, Authier A, Ferrari R, Fox NC, Mackenzie IRA, Warren JD, de Silva R, Holton J, Revesz T, Hardy J, Mead S, Rossor MN (2009) The heritability and genetics of frontotemporal lobar degeneration. Neurology 73:1451–1456 Available at: http://dx.doi.org/10.1212/WNL.0b013e3181bf997a.

Rossi G, Marelli C, Farina L, Laurà M, Maria Basile A, Ciano C, Tagliavini F, Pareyson D (2008) The G389R mutation in the MAPT gene presenting as sporadic corticobasal syndrome. Mov Disord 23:892–895 Available at: http://dx.doi.org/10.1002/mds.21970.

Safaiyan S, Besson-Girard S, Kaya T, Cantuti-Castelvetri L, Liu L, Ji H, Schifferer M, Gouna G, Usifo F, Kannaiyan N, Fitzner D, Xiang X, Rossner MJ, Brendel M, Gokce O, Simons M (2021) White matter aging drives microglial diversity. Neuron 109:1100-1117.e10 Available at: http://dx.doi.org/10.1016/j.neuron.2021.01.027.

Sainio MT, Ylikallio E, Mäenpää L, Lahtela J, Mattila P, Auranen M, Palmio J, Tyynismaa H (2018) Absence of NEFL in patient-specific neurons in early-onset Charcot-Marie-Tooth neuropathy. Neurol Genet 4:e244 Available at: http://dx.doi.org/10.1212/NXG.0000000000000244.

Saranza GM, Whitwell JL, Kovacs GG, Lang AE (2019) Corticobasal degeneration. In:

International Review of Neurobiology, pp 87–136 International review of neurobiology. Elsevier. Available at: http://dx.doi.org/10.1016/bs.irn.2019.10.014.

Satoh J-I, Kino Y (2015) Expression profiles of RNA-Seq-based grey matter-specific genes versus white matter-specific genes in grey matter lesions of multiple sclerosis. Clin Exp Neuroimmunol 6:289–298 Available at: http://dx.doi.org/10.1111/cen3.12218.

Sawyer RP, Stone HK, Salim H, Lu X, Weirauch MT, Kottyan L (2022) Frontotemporal degeneration genetic risk loci and transcription regulation as a possible mechanistic link to disease risk. Medicine (Baltimore) 101:e31078 Available at: http://dx.doi.org/10.1097/MD.0000000000031078.

Schmitz M, Canaslan S, Villar-Piqué A, Gmitterová K, Varges D, Lingor P, Llorens F, Hermann P, Maass F, Zerr I (2021) Validation of plasma neurofilament light chain as a marker for α-synucleinopathies. Mov Disord Available at: http://dx.doi.org/10.1002/mds.28724.

Scoles DR, Minikel EV, Pulst SM (2019) Antisense oligonucleotides. Neurol Genet 5:e323 Available at: http://dx.doi.org/10.1212/nxg.0000000000000323.

Seo J-S et al. (2017) Transcriptome analyses of chronic traumatic encephalopathy show alterations in protein phosphatase expression associated with tauopathy. Exp Mol Med 49:e333–e333 Available at: http://dx.doi.org/10.1038/emm.2017.56.

Sharma K, Schmitt S, Bergner CG, Tyanova S, Kannaiyan N, Manrique-Hoyos N, Kongi K, Cantuti L, Hanisch U-K, Philips M-A, Rossner MJ, Mann M, Simons M (2015) Cell type- and brain region-resolved mouse brain proteome. Nat Neurosci 18:1819–1831 Available at: http://dx.doi.org/10.1038/nn.4160.

Shokhirev MN, Johnson AA (2022) An integrative machine-learning meta-analysis of high-throughput omics data identifies age-specific hallmarks of Alzheimer's disease. Ageing Res Rev 81:101721 Available at: http://dx.doi.org/10.1016/j.arr.2022.101721.

Silva-Spínola A, Lima M, Leitão MJ, Durães J, Tábuas-Pereira M, Almeida MR, Santana I, Baldeiras I (2021) Serum neurofilament light chain as a surrogate of cognitive decline in sporadic and familial Frontotemporal dementia. Eur J Neurol Available at: http://dx.doi.org/10.1111/ene.15058.

Sims JR et al. (2023) Donanemab in early symptomatic Alzheimer disease: The TRAILBLAZER-ALZ 2 randomized clinical trial. JAMA 330:512–527 Available at: http://dx.doi.org/10.1001/jama.2023.13239.

Singhrao SK, Neal JW, Gasque P, Morgan BP, Newman GR (1996) Role of complement in the aetiology of Pick's disease? J Neuropathol Exp Neurol 55:578–593 Available at: http://dx.doi.org/10.1097/00005072-199605000-00010.

Sirkis DW, Geier EG, Bonham LW, Karch CM, Yokoyama JS (2019) Recent advances in the genetics of frontotemporal dementia. Curr Genet Med Rep 7:41–52 Available at: http://dx.doi.org/10.1007/s40142-019-0160-6.

Snowden J, Neary D, Mann D (2007) Frontotemporal lobar degeneration: clinical and pathological relationships. Acta Neuropathol 114:31–38 Available at: http://dx.doi.org/10.1007/s00401-007-0236-3.

Son HJ, Oh JS, Roh JH, Seo SW, Oh M, Lee SJ, Oh SJ, Kim JS (2019) Differences in gray and white matter 18F-THK5351 uptake between behavioral-variant frontotemporal dementia and other dementias. Eur J Nucl Med Mol Imaging 46:357–366 Available at: http://dx.doi.org/10.1007/s00259-018-4125-x.

Spillantini MG, Murrell JR, Goedert M, Farlow MR, Klug A, Ghetti B (1998) Mutation in the tau gene in familial multiple system tauopathy with presenile dementia. Proc Natl Acad Sci U S A 95:7737–7741 Available at: http://dx.doi.org/10.1073/pnas.95.13.7737.

Spillantini MG, Yoshida H, Rizzini C, Lantos PL, Khan N, Rossor MN, Goedert M, Brown J (2000) A novel tau mutation (N296N) in familial dementia with swollen achromatic neurons and corticobasal inclusion bodies. Ann Neurol 48:939–943 Available at: http://dx.doi.org/10.1002/1531-8249(200012)48:6<939::aid-ana17>3.3.co;2-t.

Steele JC, Richardson JC, Olszewski J (1964) Progressive supranuclear palsy. A heterogeneous degeneration involving the brain stem, basal ganglia and cerebellum with vertical gaze and pseudobulbar palsy, nuchal dystonia and dementia. Arch Neurol 10:333–359 Available at: http://dx.doi.org/10.1001/archneur.1964.00460160003001.

Strang KH, Golde TE, Giasson BI (2019) MAPT mutations, tauopathy, and mechanisms of neurodegeneration. Lab Invest 99:912–928 Available at: http://dx.doi.org/10.1038/s41374-019-0197-x.

Strittmatter WJ, Saunders AM, Schmechel D, Pericak-Vance M, Enghild J, Salvesen GS, Roses AD (1993) Apolipoprotein E: high-avidity binding to beta-amyloid and increased frequency of type 4 allele in late-onset familial Alzheimer disease. Proc Natl Acad Sci U S A 90:1977–1981 Available at: http://dx.doi.org/10.1073/pnas.90.5.1977.

Swarup V, Chang TS, Duong DM, Dammer EB, Dai J, Lah JJ, Johnson ECB, Seyfried NT, Levey AI, Geschwind DH (2020) Identification of Conserved Proteomic Networks in Neurodegenerative Dementia. Cell Rep 31:107807 Available at: http://dx.doi.org/10.1016/j.celrep.2020.107807.

Taniguchi S, McDonagh AM, Pickering-Brown SM, Umeda Y, Iwatsubo T, Hasegawa M, Mann DMA (2004) The neuropathology of frontotemporal lobar degeneration with respect to the cytological and biochemical characteristics of tau protein. Neuropathol Appl Neurobiol 30:1–18 Available at: http://dx.doi.org/10.1046/j.0305-1846.2003.00481.x.

Tcw J, Goate AM (2017) Genetics of β-amyloid precursor protein in Alzheimer's disease. Cold Spring Harb Perspect Med 7:a024539 Available at: http://dx.doi.org/10.1101/cshperspect.a024539.

Teunissen CE, Elias N, Koel-Simmelink MJA, Durieux-Lu S, Malekzadeh A, Pham TV, Piersma SR, Beccari T, Meeter LHH, Dopper EGP, van Swieten JC, Jimenez CR, Pijnenburg YAL

(2016) Novel diagnostic cerebrospinal fluid biomarkers for pathologic subtypes of frontotemporal dementia identified by proteomics. Alzheimers Dement (Amst) 2:86–94 Available at: http://dx.doi.org/10.1016/j.dadm.2015.12.004.

Thal DR, Rüb U, Orantes M, Braak H (2002) Phases of Aβ-deposition in the human brain and its relevance for the development of AD. Neurology 58:1791–1800 Available at: http://dx.doi.org/10.1212/wnl.58.12.1791.

Tsai RM, Boxer AL (2014) Treatment of frontotemporal dementia. Curr Treat Options Neurol 16:319 Available at: http://dx.doi.org/10.1007/s11940-014-0319-0.

van de Veerdonk FL, Netea MG, Dinarello CA, Joosten LAB (2011) Inflammasome activation and IL-1β and IL-18 processing during infection. Trends Immunol 32:110–116 Available at: http://dx.doi.org/10.1016/j.it.2011.01.003.

van den Ameele J, Hong YT, Manavaki R, Kouli A, Biggs H, MacIntyre Z, Horvath R, Yu-Wai-Man P, Reid E, Williams-Gray CH, Bullmore ET, Aigbirhio FI, Fryer TD, Chinnery PF (2021) [^{11}C]PK11195-PET brain imaging of the mitochondrial translocator protein in mitochondrial disease. Neurology 96:e2761–e2773 Available at: http://dx.doi.org/10.1212/wnl.0000000000012033.

van der Poel M, Ulas T, Mizee MR, Hsiao C-C, Miedema SSM, Adelia, Schuurman KG, Helder B, Tas SW, Schultze JL, Hamann J, Huitinga I (2019) Transcriptional profiling of human microglia reveals grey-white matter heterogeneity and multiple sclerosis-associated changes. Nat Commun 10:1139 Available at: http://dx.doi.org/10.1038/s41467-019-08976-7.

van Dyck CH, Swanson CJ, Aisen P, Bateman RJ, Chen C, Gee M, Kanekiyo M, Li D, Reyderman L, Cohen S, Froelich L, Katayama S, Sabbagh M, Vellas B, Watson D, Dhadda S, Irizarry M, Kramer LD, Iwatsubo T (2023) Lecanemab in early Alzheimer's disease. N Engl J Med 388:9–21 Available at: http://dx.doi.org/10.1056/NEJMoa2212948.

Vega AR, Chkheidze R, Jarmale V, Shang P, Foong C, Diamond MI, White CL 3rd, Rajaram S (2021) Deep learning reveals disease-specific signatures of white matter pathology in tauopathies. Acta Neuropathol Commun 9:170 Available at: http://dx.doi.org/10.1186/s40478-021-01271-x.

Viejo L, Noori A, Merrill E, Das S, Hyman BT, Serrano-Pozo A (2022) Systematic review of human post-mortem immunohistochemical studies and bioinformatics analyses unveil the complexity of astrocyte reaction in Alzheimer's disease. Neuropathol Appl Neurobiol 48:e12753 Available at: http://dx.doi.org/10.1111/nan.12753.

Vijayaragavan K et al. (2022) Single-cell spatial proteomic imaging for human neuropathology. Acta Neuropathol Commun 10:158 Available at: http://dx.doi.org/10.1186/s40478-022-01465-x.

Vogel C, Marcotte EM (2012) Insights into the regulation of protein abundance from proteomic and transcriptomic analyses. Nat Rev Genet 13:227–232 Available at:

http://dx.doi.org/10.1038/nrg3185.

Wan Y-W et al. (2020) Meta-analysis of the Alzheimer's disease human brain transcriptome and functional dissection in mouse models. Cell Rep 32:107908 Available at: http://dx.doi.org/10.1016/j.celrep.2020.107908.

Wang D, Eraslan B, Wieland T, Hallström B, Hopf T, Zolg DP, Zecha J, Asplund A, Li L-H, Meng C, Frejno M, Schmidt T, Schnatbaum K, Wilhelm M, Ponten F, Uhlen M, Gagneur J, Hahne H, Kuster B (2019) A deep proteome and transcriptome abundance atlas of 29 healthy human tissues. Mol Syst Biol 15:e8503 Available at: http://dx.doi.org/10.15252/msb.20188503.

Wang Y, Mandelkow E (2016) Tau in physiology and pathology. Nat Rev Neurosci 17:5–21 Available at: http://dx.doi.org/10.1038/nrn.2015.1.

Wanjek C (2022) Systems Biology as Defined by NIH. Available at: https://irp.nih.gov/catalyst/19/6/systems-biology-as-defined-by-nih [Accessed November 3, 2023].

Wegmann S, Biernat J, Mandelkow E (2021) A current view on Tau protein phosphorylation in Alzheimer's disease. Curr Opin Neurobiol 69:131–138 Available at: http://dx.doi.org/10.1016/j.conb.2021.03.003.

Weingarten MD, Lockwood AH, Hwo SY, Kirschner MW (1975) A protein factor essential for microtubule assembly. Proc Natl Acad Sci U S A 72:1858–1862 Available at: http://dx.doi.org/10.1073/pnas.72.5.1858.

Wickham H (2016) ggplot2: Elegant Graphics for Data Analysis. New York: Springer-Verlag. Available at: https://ggplot2.tidyverse.org.

Wightman DP et al. (2021) A genome-wide association study with 1,126,563 individuals identifies new risk loci for Alzheimer's disease. Nat Genet 53:1276–1282 Available at: http://dx.doi.org/10.1038/s41588-021-00921-z.

Wimo A, Seeher K, Cataldi R, Cyhlarova E, Dielemann JL, Frisell O, Guerchet M, Jönsson L, Malaha AK, Nichols E, Pedroza P, Prince M, Knapp M, Dua T (2023) The worldwide costs of dementia in 2019. Alzheimers Dement 19:2865–2873 Available at: http://dx.doi.org/10.1002/alz.12901.

Wingo TS, Lah JJ, Levey AI, Cutler DJ (2012) Autosomal recessive causes likely in early-onset Alzheimer disease. Arch Neurol 69:59–64 Available at: http://dx.doi.org/10.1001/archneurol.2011.221.

Witt A, Macdonald N, Kirkpatrick P (2004) Memantine hydrochloride. Nat Rev Drug Discov 3:109–110 Available at: http://dx.doi.org/10.1038/nrd1311.

Wood EM, Falcone D, Suh E, Irwin DJ, Chen-Plotkin AS, Lee EB, Xie SX, Van Deerlin VM, Grossman M (2013) Development and validation of pedigree classification criteria for frontotemporal lobar degeneration. JAMA Neurol 70:1411–1417 Available at:

http://dx.doi.org/10.1001/jamaneurol.2013.3956.

Wood JG, Mirra SS, Pollock NJ, Binder LI (1986) Neurofibrillary tangles of Alzheimer disease share antigenic determinants with the axonal microtubule-associated protein tau (tau). Proc Natl Acad Sci U S A 83:4040–4043 Available at: http://dx.doi.org/10.1073/pnas.83.11.4040.

Woollacott IOC, Rohrer JD (2016) The clinical spectrum of sporadic and familial forms of frontotemporal dementia. J Neurochem 138 Suppl 1:6–31 Available at: http://dx.doi.org/10.1111/jnc.13654.

Wu T et al. (2019) Complement C3 is activated in human AD brain and is required for neurodegeneration in mouse models of amyloidosis and tauopathy. Cell Rep 28:2111-2123.e6 Available at: http://dx.doi.org/10.1016/j.celrep.2019.07.060.

Yokoyama JS et al. (2017) Shared genetic risk between corticobasal degeneration, progressive supranuclear palsy, and frontotemporal dementia. Acta Neuropathol 133:825–837 Available at: http://dx.doi.org/10.1007/s00401-017-1693-y.

Younes K, Miller BL (2020) Frontotemporal dementia: Neuropathology, genetics, neuroimaging, and treatments. Psychiatr Clin North Am 43:331–344 Available at: http://dx.doi.org/10.1016/j.psc.2020.02.006.

Yu Y, Herman P, Rothman DL, Agarwal D, Hyder F (2018) Evaluating the gray and white matter energy budgets of human brain function. J Cereb Blood Flow Metab 38:1339–1353 Available at: http://dx.doi.org/10.1177/0271678X17708691.

Zamanian JL, Xu L, Foo LC, Nouri N, Zhou L, Giffard RG, Barres BA (2012) Genomic analysis of reactive astrogliosis. J Neurosci 32:6391–6410 Available at: http://dx.doi.org/10.1523/JNEUROSCI.6221-11.2012.

Zhang K, Sun Z, Chen X, Zhang Y, Guo A, Zhang Y (2021) Intercellular transport of Tau protein and β-amyloid mediated by tunneling nanotubes. Am J Transl Res 13:12509–12522 Available at: https://www.ncbi.nlm.nih.gov/pubmed/34956469.

Zhang Y, Chen K, Sloan SA, Bennett ML, Scholze AR, O'Keeffe S, Phatnani HP, Guarnieri P, Caneda C, Ruderisch N, Deng S, Liddelow SA, Zhang C, Daneman R, Maniatis T, Barres BA, Wu JQ (2014a) An RNA-sequencing transcriptome and splicing database of Glia, neurons, and vascular cells of the cerebral cortex. J Neurosci 34:11929–11947 Available at: http://dx.doi.org/10.1523/jneurosci.1860-14.2014.

Zhang Y, Chen K, Sloan SA, Bennett ML, Scholze AR, O'Keeffe S, Phatnani HP, Guarnieri P, Caneda C, Ruderisch N, Deng S, Liddelow SA, Zhang C, Daneman R, Maniatis T, Barres BA, Wu JQ (2014b) An RNA-sequencing transcriptome and splicing database of glia, neurons, and vascular cells of the cerebral cortex. J Neurosci 34:11929–11947 Available at: http://dx.doi.org/10.1523/JNEUROSCI.1860-14.2014.

Zhang Y, Sloan SA, Clarke LE, Caneda C, Plaza CA, Blumenthal PD, Vogel H, Steinberg GK, Edwards MSB, Li G, Duncan JA 3rd, Cheshier SH, Shuer LM, Chang EF, Grant GA,

Gephart MGH, Barres BA (2016) Purification and Characterization of Progenitor and Mature Human Astrocytes Reveals Transcriptional and Functional Differences with Mouse. Neuron 89:37–53 Available at: http://dx.doi.org/10.1016/j.neuron.2015.11.013.

Zhang Y, Wu K-M, Yang L, Dong Q, Yu J-T (2022) Tauopathies: new perspectives and challenges. Mol Neurodegener 17:28 Available at: http://dx.doi.org/10.1186/s13024-022-00533-z.

Zhao J, Wu H, Tang X-Q (2021) Tau internalization: A complex step in tau propagation. Ageing Res Rev 67:101272 Available at: http://dx.doi.org/10.1016/j.arr.2021.101272.

Zhong Y, Wan Y-W, Pang K, Chow LML, Liu Z (2013) Digital sorting of complex tissues for cell type-specific gene expression profiles. BMC Bioinformatics 14:89 Available at: http://dx.doi.org/10.1186/1471-2105-14-89.